CRANFIELD UNIVERSITY

Qingling Liu

Supervisor: Dr. Alastair Cooke, Mr. M. Mudassir Lone

Pilot-induced-oscillation detection and mitigation

SCHOOL OF ENGINEERING
Department of Aerospace Engineering
Full Time MSc by Research

MSc THESIS
Academic Year: 2011 - 2012

December 2012

CRANFIELD UNIVERSITY

SCHOOL OF ENGINEERING
Department of Aerospace Engineering
Full Time MSc by Research

MSc THESIS

Academic Year 2011-2012

Qingling Liu

Pilot-induced oscillation detection and mitigation

Supervisor: Dr. Alastair Cooke, Mr. M. Mudassir Lone

December 2012

This thesis is submitted in fulfilment of the requirements for the degree of Master of Science

Abstract

The aim of this thesis is to develop a real time PIO detection and mitigation system that consists of a detector based on short time Fourier transform(STFT) and autoregressive model(ARX) with exogenous inputs, together with an adaptive controller based mitigation system. The system not only detects the traditional PIO characteristics but also focuses on the trend of pilot behaviour by calculating the rate of change in the open loop crossover frequency. In the detection system, a sliding windowed STFT method was applied to identify the frequency and phase characteristics of the system via processing the signal of pilot input and aircraft state. An ARX model was also applied to get the rate of change of the crossover frequency. After detection, a PIO cue was shown on the primary flight display. A scheduled gain controller was coupled to provide PIO mitigation by varying stick input gain.

Compensatory and tracking tests for the evaluation of this system were performed using a quasi-linear Boeing-747 aircraft model including nonlinear command gearing and actuator rate-limiting. Bandwidth and Gibson criteria were used to design PIO prone control laws for system evaluation experiments. Results from PIO tests conducted on desktop PCs were presented. These were analyzed and compared with those obtained from implementing the Real-time Oscillation Verifier module available in literature.

Keywords:
Pilot Vehicle System, Flight Control System, Pilot Induced Oscillation, Aircraft Pilot Coupling, Short Time Fourier Transform, ARX Model, Adaptive Controller, Pilot Modelling

Acknowledgements

This project was performed in School of Engineering, sponsored by Commercial Aircraft Corporation of China, Ltd (COMAC) and Chinese Scholarship Council. The supervisors are Dr Alastair Cooke and Mr Mudassir Lone. It is my honour to take this opportunity to express my gratitude to the following persons for their contributions to this project.

I would like to give my sincerest appreciation to my supervisor, Dr Alastair Cooke, for his great help in my research. Also, I owe my deepest gratitude to Mr Mudassir Lone, for his valuable guidance and supports in the whole period of my research. I am grateful to Dr M.V Cook and Dr James Whidborne, for their help in the flight control law design. My thanks also go to Dr Al Savvaris, for his help in my research.

I would like to acknowledge COMAC and the Chinese Scholarship Council for funding the project. I could not have the opportunity to study here in Cranfield for my further education without their support. Especially, I appreciate Xiangsheng Tan, the head of the flight test station. He gave me a lot of support in both studies and daily life during my stay in UK. I also want to give my thanks to my colleagues in the COMAC group.

It is an honour for me to get considerable supports from test pilots Vicente Payo and Neil Sheath. They provided their time to discuss and participate in the piloted tests, and gave me precious advices.

My appreciation also extends to all my friends. Their friendship companied me and encouraged me to overcome difficulties and challenges in my life.

Finally, I owe my deepest gratitude to my family for being supportive and understanding during the past year.

Contents

Contents . . . . . **vii**

List of figures . . . . . **ix**

List of tables . . . . . **xv**

Abbreviations . . . . . **.xvii**

Nomenclatures . . . . . **xix**

1 Introduction **1**

1.1 Aims and objectives 2

1.2 Project scope 3

1.3 Thesis structure 3

2 Literature review **5**

2.1 PIO theory 5

2.1.1 Definition 5

2.1.2 Causes. 6

2.1.3 Categories 7

2.1.4 Prediction and evaluation criteria 8

2.1.5 Detection methods 16

2.1.6 Mitigation Methods 24

2.2 Signal processing and system identification 28

2.2.1 STFT and wavelet 28

2.2.2 System identification 30

2.3 Pilot modelling techniques . . . 31
2.3.1 Pilot model . . . 31
2.3.2 Forcing function . . . 33
2.4 Methodology . . . 35
3 Control law design . . . 37
3.1 Longitudinal aircraft model . . . 37
3.1.1 Longitudinal equations . . . 37
3.1.2 Flight condition and actuator models . . . 38
3.1.3 Flight control law design . . . 39
3.2 Control law test and modification . . . 49
4 Detection and mitigation system design . . . 51
4.1 Characteristics detector . . . 52
4.1.1 ARX calculator . . . 53
4.1.2 Time domain calculator . . . 56
4.1.3 STFT calculator . . . 57
4.2 Tendencies indicator . . . 60
4.3 Compensator . . . 63
4.4 Off-line tests . . . 63
4.4.1 Time error during real-time detection . . . 63
4.4.2 Off-line tests . . . 65
4.4.3 Limit cycle avoidance. . . . 65
5 Pilot-in-the-loop experiments . . . 67
5.1 Experiment aims . . . 67
5.2 Compensatory and tracking training . . . 68
5.2.1 Compensatory training . . . 68
5.2.2 Discrete tracking training . . . 71
5.3 Piloted trials . . . 71
5.3.1 Experimental setup . . . 71

5.3.2 Training runs data analysis 74
5.3.3 Tracking runs data analysis 76
6 Conclusions and future work 85
6.1 Summary 85
6.2 Conclusions 86
6.3 Future work. 87
References 89
A Review test examples 95
B Boeing-747 model 99
C Limit cycle analysis 101
D ARX structure optimization results 103
E Experiment data 105

List of Figures

2.1 Structure of General Pilot Vehicle System 6
2.2 Closed loop pitch tracking model 9
2.3 Neal-Smith parameter plane 9
2.4 Bandwidth Parameters 11
2.5 Bandwidth Criterion(Flight phase category A and C) 12
2.6 Bandwidth Criterion with three added parameters 13
2.7 Bandwidth criterion corresponds to Boeing flight phase category C database 13
2.8 Gibson criterion parameters 14
2.9 Dropback Criterion boundaries advised by Gibson and Mooij 15
2.10 Gibson Phase Rate criterion 16
2.11 Gibson Phase Rate Criterion correspond to Boeing approach/landing database 17
2.12 Structure of ROVER method 18
2.13 Structure of fuzzy logic detector 19
2.14 Structure of PIO feature detector and Neural network discriminator 21
2.15 Actuator rate limiting 21
2.16 A general system considers rate limiting 22
2.17 Nichols Chart of OLOP criterion 23
2.18 Structure of feedback with bypass filter 25
2.19 SAFE-Cue gain adjustment 26
2.20 SAFE-Cue stick force feedback 26
2.21 Closed loop multi-model controller 27

2.22 STFT(Left), Wavelet(Right) 29
2.23 Single loop control behaviour system 31
2.24 Quasi linear pilot model control system 32
2.25 Bimodal Model Structure 33
2.26 Pure disturbance-rejection task 33
2.27 Pure tracking task 34
2.28 Discrete steps and ramps tracking signal 35

3.1 Root Locus of Pitch rate open loop function 39
3.2 Bandwidth Criterion evaluation - Controller 1 41
3.3 Bandwidth Criterion evaluation - Controller 2 42
3.4 Bandwidth Criterion evaluation - Controller 3 43
3.5 Gibson Criterion evaluation - Controller 1 44
3.6 Gibson Criterion evaluation - Controller 2 45
3.7 Gibson Criterion evaluation - Controller 3 46
3.8 Bandwidth Criterion evaluation of selected controllers 47
3.9 Gibson Dropback Criterion evaluation of selected controllers 47
3.10 Pitch rate and pitch angle time response 48
3.11 Simple anti-windup PI controller 50
3.12 Test setup for PI windup effect 50
3.13 Limit cycle phenomenon with PI controller C2 50

4.1 Structure of PIO detection and mitigation system 51
4.2 Regression and aggression control 52
4.3 Structure of PIO detector 53
4.4 ARX model order selection (Run No.9) 54
4.5 ARX model order validation 55
4.6 Time domain peak-to-peak calculation block as implemented in Simulink ® 56

4.7 Four different windows 58

4.8 Comparison between Different Window types and Different Window lengths 59

4.9 Procedure of STFT calculation 61

4.10 Procedure of tendencies indicator 62

4.11 Weighting factors function 63

4.12 Primary Flight Display 64

4.13 The structure of compensator 64

4.14 Off-line test 66

4.15 Comparison between simple anti-windup PI controller and reset PI controller 66

5.1 Time domain plots of compensatory training 69

5.2 RMS plot of disturbance, stick input and pitch angle 69

5.3 Frequency domain plots of stick input and pitch angle 70

5.4 Frequency domain plots of Yp, Yc and YpYc 70

5.5 Handling quality rating and tracking error results of Tracking training test 72

5.6 Structure of experimental setup and display 72

5.7 Joystick and display setup 73

5.8 Experimental tasks setup 73

5.9 Compensatory task time domain plot of the fourth subject, the fifth run . . 75

5.10 Pitch error RMS of compensatory training in piloted test 75

5.11 Cooper-Harper and PIO rating evaluation of PVS with different controllers 76

5.12 Cooper-Harper and PIO rating evaluation for PVS in different PIO detection and mitigation mode 78

5.13 PIO detection results - the second run (with PIO cue) of subject A 79

5.14 PIO detection six flags - the second run (with PIO cue) of subject A . . . 79

5.15 Relationship between PIO events and the rate of change in crossover frequency - the second run (with PIO cue) of subject A 81

5.16 The fourth run(No PIO cue) of subject B 82

5.17 The fourth run of(No PIO cue) of subject D 82

5.18 Stick input modification after mitigation for the fourth run of series one of subject B (The whole time history) 83

5.19 Stick input modification after ROVER for the fourth run of series one of subject B (The whole time history) 84

5.20 Stick input modification after mitigation system for the fourth run of series one of subject B (86s to 96s) 84

5.21 Stick input modification after ROVER for the fourth run of series one of subject B (86s to 96s) 84

A.1 ROVER detection example 95

A.2 Fuzzy variables descript membership function 96

A.3 Example of fuzzy logic detection for Boeing-747 model 96

A.4 OLOP test model and test results 97

A.5 Disturbance open loop full order system estimation using ARX and FCM 98

B.1 Linear Boeing-747 aircraft model 100

C.1 The nonlinear actuator rate limiting and saturation 102

C.2 The describing function tests of rate-limiting and saturation 102

D.1 ARX structure optimization Run No.3 103

D.2 ARX structure optimization Run No.4 104

D.3 ARX structure optimization Run No.5 104

E.1 Evaluation results of tracking training 105

E.2 Time history plot - the second run of subject 1 in tracking training task . . 106

E.3 Time history plot - the second run of subject 2 in tracking training task . . 106

E.4 Pilot trials questionnaire 107

E.5 Relationship between PIO events and the rate of change in crossover frequency - the fourth run(with PIO cue and mitigation) of subject B 108

E.6 Relationship between PIO events and the rate of change in crossover frequency - the third run (with PIO cue) of subject C 109

E.7 The third run of subject B(No PIO cue) 110

E.8 The third run of subject D(No PIO cue) 110

E.9 The third run of subject B(PIO cue) 111

E.10 The third run of subject D(PIO cue) 111

E.11 The fourth run of subject B(PIO cue) 112

E.12 The fourth run of subject D(PIO cue) 112

List of Tables

2.1 Disturbance function 34

3.1 Aircraft dynamic mode properties 49

4.1 Window properties 57
4.2 Parameters of the sum of sines input signal 58
4.3 Thresholds of PIO feature Parameters 60
4.4 System Time Error test 65

5.1 Test subject information 74

A.1 parameters of ARX model test forcing function 98

Abbreviations

APC	Aircraft Pilot Coupling
ARX	Autoregressive Model with Exogenous Inputs
COMAC	Commercial Aircraft Corporation of China, Ltd
DFT	Discrete Fourier Transform
FT	Fourier Transform
FBW	Fly-By-Wire
FCM	Fourier Coefficient Method
FCS	Flight Control System
FFT	Fast Fourier Transform
FWB	Feedback With Bypass
LAHOS	Landing Approach High Order System
LOAS	Low-order Approximate System
MMAC	Multi-Model Adaptive Controller
OCM	Optimal Controller Model
OLOP	Open-Loop Onset Point
PFD	Primary Flight Display
PI	Proportional and Integral
PIO	Pilot-Induced-Oscillation
PVS	Pilot Vehicle System
ROVER	Real-Time Oscillation Verifier
RIV	ROVER Integer Value
RMS	Root Mean Squared
SAFE-Cue	Smart Adaptive Flight Effective Cue
SAS	Stability Augmentation System
SPPO	Short Period Pitch Oscillation
STFT	Short Time Fourier Transform

Nomenclatures

A	Maximum input amplitude
A, B, C, D	State-Space System Matrix
A_d	Amplitude of Disturbance Signal
$A(q), B(q)$	Polynomials of ARX model
cov	Covariance
$c(t)$	Operator Output
D	Acquisition Time
DB	Dropback
D_p	Pure Time Delay of τ seconds
$e(t)$	Error
$E(s)$	Fourier Transform of $e(t)$
$f(t)$	Input Function
f_d	Disturbance Signal
f_t	Tracking Signal
$F_C\,(j\omega)$	Closed Loop Transform Function
$F_0\,(j\omega)$	Open Loop Transform Function
g	Gravitational acceleration, $9.81m/s^2$
$g[l]$	Window Function
G_{nm}	Neuromuscular System
h	Altitude
$H_{LF}(s)$	Transfer Function of Low Pass Filter
$H_{NF}(s)$	Notch Filter Transfer Function
$i(t)$	System Forcing Function
K_p	Gain Compensation
L	Length of Window Function
$m(t)$	System Output
M	Mach Number
Mag_{δ_s}	Magnitude of Stick Input
Mag_q	Magnitude of Pitch Rate
M_q	Pitching Moment due to Pitch Rate Derivative
M_u	Pitching Moment due to Axial Velocity and Propulsion Derivative
M_w	Pitching Moment due to Normal Velocity Derivative
$M_{\dot{u}}$	Pitching Moment due to Rate of Change of Axial Velocity Derivative
$M_{\dot{w}}$	Pitching Moment due to Rate of Change of Normal Velocity Derivative
$M_{\delta e}$	Pitching Moment due to Elevator Derivative
$M(s)$	Fourier Transform of $m(t)$
$N(j\omega)$	Rate Limit Describing Function
N_z	Normal Acceleration

N_{zc}	Load Factor Demand
N_{RL}	Describing function of rate limiter
n_a	Number of Poles of the system
n_b	Number of Zeros Plus 1 of the system
n_k	Dead Time in the System
P_p	Phase Compensation
q	Pitch Rate
q_{c0}	Maximum Magnitude of Pitch Rate Input
q_s	Static Pitch Rate after Removing Input
q_m	Maximum Pitch Rate
R	Rate Limit
r_{RL}	Rate Limiting Threshold
s	Laplace Operator
t	Time
t_γ	Flight Path Time Delay
T	Oscillation Period
T_s	Sample Time
$T_{\theta 2}$	Flight Path Angle to Pitch Attitude Lag Time Constant
T_I	Pilot Equalisation Characteristics
T_L	Pilot Equalisation Characteristics
T_N	Neuromuscular Delay
T_{P1}	Pilot Lead Compensation Time Constant
T_{P2}	Pilot Lag Compensation Time Constant
u	Linear Perturbed Velocity Along the X-axis, ft/sec
u, v, w	Perturbed Velocity Components Along the x, y and z Body Axes
U, V, W	Components of Velocity along x, y and z Body Axes
v	Linear Perturbed Velocity Along the Y-axis, ft/sec
V	Airspeed
w	Linear Perturbed Velocity Along the Z-axis, ft/sec
X_q	Axial Force Due to Pitch Rate Derivative
X_u	Axial Force Due to Axial Velocity Derivative
X_w	Axial Force Due to Normal Velocity Derivative
$X_{\delta e}$	Axial Force Due to Elevator Derivative
$X_{\dot{w}}$	Axial Force Due to Rate of Change of Normal Velocity Derivative
$X(f)$	Fourier Transform of $x(t)$
$X[k]$	Discrete Fourier Transform of $x(t)$
$X[i, k]$	Short Time Fourier Transform of $x(t)$
y, y_e	Actual system output, Output of ARX Model
$Y_C(s)$	Vehicle Transfer Function
$Y_P(s)$	Pilot Transfer Function
Z_q	Normal Force Due to Pitch Rate Derivative
Z_u	Normal Force Due to Axial Velocity Derivative
Z_w	Normal Force Due to Normal Velocity Derivative
$Z_{\delta e}$	Normal Force Due to Elevator Derivative
$Z_{\dot{w}}$	Normal Force Due to Rate of Change of Normal Velocity Derivative
ω	Frequency
ω_{180}	Neutral Stability Frequency
$2\omega_{180}$	Twice of the ω_{180}

ω_{BWE}	Equivalent Bandwidth in Time Domain Neal-Smith Criterion
ω_{BW}	Bandwidth
$\omega_{BWphase}$	Phase Bandwidth
ω_{BWgain}	Gain Bandwidth
$\omega_{BW\gamma}$	Flight Path Bandwidth
$\omega_{180\theta}$	Neutral Stability Frequency
ω_c	Crossover frequency of pilot vehicle system open loop function
ω_n	Natural Frequency
ω_{onset}	Open Loop Onset Frequency
$\bar{\omega}_{onset}$	Close Loop Onset Frequency
ω_p	Phugoid Mode Natural Frequency
ω_{pk}	Frequency defined as $3.5rad/s$
ω_s	Short Period Mode Natural Frequency
δ	Denominator
δ_c	Pilot Command
δ_e	Elevator Surface Deflection
δ_{ec}	Elevator Surface Deflection Command
δ_p	Pilot Output
δ_s	Stick Deflection
δ_t	Error Signal
δ_τ	Engine thrust
$\Delta G\,(q)$	Pitch Rate Overshoot
η	Elevator Command
δ_{ec}	Pilot Commanded Elevator Deflection
τ	Time Delay
τ_e	The Sum of all Pilot Pure Time Delays and High Frequency Lags
τ_{ph}	Pitch Attitude Phase Delay
θ_e	Tracking Error
γ	Flight Path Angle
Φ_{PD}	Phase Difference Threshold
Φ, θ, ψ	Perturbed Euler Angles
ρ	General Scheduling Parameter
$\rho_{y,ye}$	Linear Correlation between System Output and Estimated Output
σ_y/σ_{ye}	Standard Deviation of System Output/Estimated Output
Θ	Pitch Attitude
ϕ	Phase
$\phi_{2\omega 180}$	The Phase at twice the Neutral Stability Frequency
ϕ_p	Maximum Phase Shift at ω_{pk}
ζ	Damping Ratio
ζ_p	Phugoid Mode Damping Ratio
ζ_s	Short Period Mode Damping Ratio

Chapter 1

Introduction

Unintended aircraft pilot interactions that lead to unexpected oscillation motion in aircraft attitude and flight path are normally regarded as Pilot-induced oscillations, Pilot-involved oscillations or Pilot in-the-loop oscillations(PIO)[1]. PIO can happen in any kinds of aircraft, especially those with agile and high performance, such as the documented accidents of YF-22 and JAS-39 "Gripen"[2].

PIO problems are increasing due to several reasons. First is the development of new aviation technologies. In the early days, PIO mainly occurred in military aircraft. Recently, many visible PIOs occurred in civil aircraft tests and commercial aircraft service, such as several Boeing-777 PIOs during flight test in 1995 and the Airbus-321 PIO on April 27, 1995[2]. Most civil aircraft PIOs occurred at the aircraft with high advanced digital Fly-By-Wire(FBW) flight control systems. The FBW technology is widely used in fighters and modern large transport aircraft. This new technology provides enormous advantages to aircraft design, such as good handling quality, high performance, weight reductions and operational flexibility[2]. However, the following characteristics of FBW technology also increase the potential possibilities of PIOs: (1) pilot cannot receive the actuator rate-limiting signal directly through cockpit control device, (2) pilot control authority is reduced since the software control functions of FBW control system share the same effectors with pilot and, (3) FBW system has multi redundant control modes, which may cause unexpected changes to flight dynamics when the flight control mode is switched. If not implemented carefully, the FBW can "detach" the pilot from the aircraft and thus deny access to critical cues necessary for safe flight.

Second, atmospheric disturbance due to congested airspace resulted by busy air traffic today is also increasing the possibilities of PIOs. Air traffic over East Asia is expected to rise dramatically in the next 10 to 20 years and it will eventually reach the high densities currently seen over Western Europe[3]. Consequent effects are not only important at the air traffic management level, but also for flight control system design where atmospheric disturbance effects must be considered, such as upsets due to wake vortex encounters. A number of recent studies have shown that gust profiles from wake vortices can be triggering events for PIO[4]. Such work has emphasised the necessity to develop a deeper understanding of PIOs and to design detection and mitigation techniques.

Third, it is hard to eliminate PIO by control law design though almost all the designs of modern aircraft take PIO effects into consideration. The US Air Force did considerable research in PIO in mid-1990 and announced that the reduction of PIO should be 80%, 99% and 99.95% via criteria, evaluation and compensation methods respectively[5]. Variable factors such as improper pilot operation, adverse weather, system malfunction, rate-limiting and flight mode switching contribute to PIOs, although handling qualities criteria and PIO criteria attempt to ensure PIO does not occur and the pilot is always in control. These criteria tend to be based on low order equivalent system representations of the aircraft and rely on either linear systems theory or describing function methods. These are effective for Categories I and II PIO. Yet it should be noted that by their nature, PIOs will occur as long as the human pilot is in the loop. Therefore, detection and mitigation techniques will be necessary as long as the pilot is in the cockpit.

A great deal of research has been done on PIO detection and mitigation. Over the last 30 years, various techniques have been developed. Detection methods like Real time Oscillation Verifier(ROVER)[5][6], fuzzy logic detector[7], neural network detector[8][9], and Open loop onset point(OLOP) method[10] were established. Mitigation methods can be roughly categorized into three approaches: (1) use of filters to remove exacerbating inputs during PIO[6], (2) use of adaptive controllers [11][12] to shape pilot input and, (3) use of visual[13] and tactile[14] cues to influence pilot decision making. Usually, an experienced pilot will let go of the stick when he realizes that a PIO has occurred. He may "freeze" the control stick in the central point to avoid PIO when the aircraft encounters continuous disturbance. However, it is hard for the pilot to recognize PIO and decide when to take over the stick again during PIOs. An economic and simple way to attenuate PIO tendencies is to develop PIO detection and mitigation system which can be coupled to the existing flight control systems without affecting their performance unless PIO occurs.

1.1 Aims and objectives

The aim of this thesis is to develop a real time PIO detection and mitigation system that consists of a detector based on short time Fourier transform(STFT) and autoregressive model(ARX) with exogenous inputs, together with an adaptive controller based mitigation system.

The following objectives should help to achieve the above aim:

1. Review state-of-the-art of PIO detection and mitigation techniques.
2. Develop control laws of Boeing-747 aircraft model for PIO system evaluation.
3. Design PIO detection system using STFT, peak-to-peak calculation method and ARX model.
4. Design PIO mitigation system using adaptive controller.
5. Design tracking tasks for piloted trials.
6. Conduct piloted trials.

7. PIO detection and mitigation system evaluation.

1.2 Project scope

The scope of this project is limited to:

- Longitudinal dynamics of Boeing-747 model with nonlinear command gearing and rate-limiting.
- Desktop based piloted trials.

1.3 Thesis structure

The following shows the thesis structure:

Chapter 1 Introduction of the background, aims and objectives and scopes of this project.

Chapter 2 Review of PIO theory, detection and mitigation methods, Fourier transform method, autoregressive model and pilot modelling techniques.

Chapter 3 Boeing-747 model control law design for detection and mitigation system evaluation tests.

Chapter 4 PIO detection and mitigation system design.

Chapter 5 Pilot-in-the-loop experiments and analysis.

Chapter 6 Conclusions and future work.

Chapter 2

Literature review

PIO appeared a long time ago and it persists to threaten flight safety of modern aircraft. During the last decade, almost every military and civil aircraft design has encountered PIO. It is inevitable to consider PIO avoidance in modern aircraft design. This chapter first gives a brief introduction to PIO theory including definition, causes, categories, detection and mitigation methods, then introduces the STFT signal processing method and ARX system identification method, finally presents some basic knowledge of pilot modelling techniques.

2.1 PIO theory

2.1.1 Definition

An accurate definition of PIO is required to understand, detect and mitigate PIO. `MIL-STD-1797` demonstrates a general PIO definition described as following:

> *There shall be no tendency for pilot-induced oscillations, that is, sustained or uncontrollable oscillations resulting from efforts of the pilot to control the aircraft*[15].

Pilot is driven by the oscillation and forced to terminate current tasks during a PIO event. A great deal of research has been done to distinguish different PIO categories and establish an accurate definition of PIO. Ten definitions of PIO were summarized in Mitchell's report[16]. Based on deep research into the PIO phenomenon, another definition is presented by Mitchell and Klyde - PIO is an unintentional oscillation caused by Pilot Vehicle System(PVS) interactions, during the oscillation, the aircraft attitude, angular rate, normal acceleration, or other characteristics derived from these states, are approximately 180 degrees out of phase against the pilot's control inputs[5].

2.1.2 Causes

PIO occurs in different aircraft during different flight phases, especially when tight control is attempted and is often seen during both Category A and Category C type manoeuvres[6]. Category A and category C manoeuvres are described as following:

> Category A: *those non-terminal flight phases that require rapid manoeuvring, precision tracking, or precise flight-path control*[15].
>
> Category C: *terminal flight phases that are normally accomplished using gradual manoeuvres and usually require accurate flight-path control*[15].

Three main factors contribute to the PIO events[17][18]: some triggering events occurred, the original aircraft dynamics had a small stability margin, and finally the pilot was trying to control the aircraft. According to these three main factors, numbers of PIO variables in PVS can be categorized into three major elements, which are triggering events, aircraft dynamics and pilot behaviour. General structure of PVS is shown in Fig. 2.1.

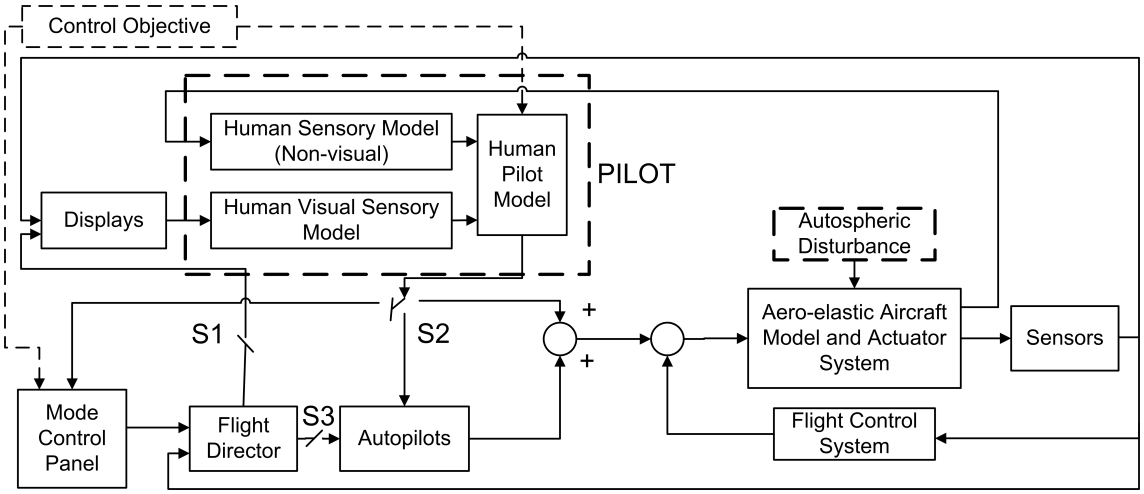

Figure 2.1: Structure of General Pilot Vehicle System (modified from[19])

Triggering events

The triggering events may cause sudden change to aircraft dynamics and pilot reactions, which induce corrective inputs that start PIO events. The external triggers mainly contain collision avoidance, wind-shear, gusts, vortex, icing and clean air turbulence. Vehicle system triggering events mainly include control surface malfunction, control law switching, configuration modifications and control power system failures[17].

Aircraft dynamics

The aircraft dynamics contains Stability Augmentation System(SAS), actuators, airframe, inceptors and artificial feeling system. Pilot control inputs will be changed by the aircraft dynamics subsystems. These changes are due to two major reasons: (1) the linear

characteristics of the SAS like second-order or equivalent second-order pre-filters will cause phase delay to the aircraft responses, (2) the nonlinear contributions which mainly include actuator saturation, rate-limiting, dead zone, hysteresis/backlash, jump resonance and nonlinear gearing/shaping[20], will cause constraints in control gain and lead to phase lag. If the phase lag became excessive, for example, nearly 180 degrees, PIO may happen.

Pilot

The pilot is the most unpredictable element in flight control. However, the experienced flight data has shown that the spectrum of pilot behavioural patterns are alike in controlling flight vehicle systems[1][17]. Basically, pilot behavioural types can be described as compensatory, pursuit and precognitive behaviour[21]. Compensatory behaviour is a basic reaction to keep the aircraft stable by reducing the system error between desired track and random appearing disturbance signal. The only information displayed to the human controller is system error[21]. Pursuit behaviour joins the compensatory behaviour when the command inputs and system outputs can both be recognized by virtue of the display or preview[21]. Precognitive behaviour is a higher control level with predictable compensation based on the familiarity of the control task. It is an open loop control action.

2.1.3 Categories

PIOs can be classified into four categories[22][23]:

- Category I: Linear PVS oscillations. This type of PIO is mainly due to the excessive time lag and phase loss caused by filters and improper control/response sensitivity. It is well understood and easy to be mitigated.
- Category II: Quasi-linear events with some nonlinear contributions like rate-limiting. This kind of PIO can be modelled as linear elements adding separated nonlinear contributions. It is the most common PIO in modern aircraft.
- Category III: Nonlinear PIOs with transients. They are very rare but significantly dangerous. Usually, this category of PIO is caused by sharp change of dynamics properties such as control mode switching or control system malfunction. It is believed that improper response to the category I or category II PIO will finally lead to nonlinear PIO. Once nonlinear PIO happened, it is hard to be stopped.
- Category IV: Aero-elastic PIO. This PIO is usually caused by the complexity of the PVS or the interactions between pilot and aircraft structural modes. It is not so common but should be carefully treated, especially in large transport aircraft.

Category I has been well understood after many years research. Detection and mitigation method was developed and proven to be effective for category I, such as ROVER[5][6]. Category II is mainly caused by rate-limiting. It is very common but still not fully understood and controlled. Category III is a fully developed divergent aircraft pilot coupling(APC) event. The best way to control this type of PIO is to detect and stop category I and II before they fully develop into the onset of category III. Category IV is mainly due

to the large aircraft elastic and the long distance between pilot and the centre of gravity of the aircraft. It can be alleviated by increasing airframe stiffness. In consideration of the above reasons, this thesis will develop detection and mitigation methods for the common category II and category I PIOs.

2.1.4 Prediction and evaluation criteria

A number of analysis criteria have been established to evaluate handling qualities and PIO severities. Most of these criteria are based on experimental data of certain type of aircraft. Using criteria derived from one type of aircraft to design and evaluate other types of aircraft turns out to be dangerous. Moreover, the flight dynamics of PVS is getting more complex with the development and widely use of modern FBW control systems. In this section, five mainly used criteria which are frequency domain Neal-Smith, time domain Neal-Smith, Bandwidth, Gibson Dropback and Gibson Phase Rate will be discussed.

A. Frequency domain Neal-Smith Criterion

The frequency domain Neal-Smith Criterion was established based on the data of precise pitch tracking tasks and it was developed particularly for the handling qualities requirements of fighter aircraft[24]. It was established by modelling the pilot-vehicle control loop as a unity feedback system with a pilot model in the forward path. Considering real pilot characteristics, the pilot model should contain a tunable gain, a pure time delay, the ability to introduce lead compensation and lag compensation[25]. A simple pilot model is described using transfer function[25]:

$$F_p(s) = K_p e^{-\tau s}\left(\frac{1+sT_{p_1}}{1+sT_{p_2}}\right) = K_p D_p(s) P_p(s) \tag{2.1}$$

where

K_p - pilot gain

T_{p_1} - pilot lead compensation time constant

T_{p_2} - pilot lag compensation time constant

$D_p(s)$ - pure time delay of τ seconds

$P_p(s)$ - phase compensation

The pilot keeps the aircraft under control by adjusting K_p, τ, T_{p_1} and T_{p_2}. The pure time delay range is limited as $0.2 \leq \tau \leq 0.4$ seconds. For the purposes of present application the delay is assumed to remain constant at 0.3 seconds[25]. Positive phase angle means pilot lead compensation. This happens when the pilot is doing an aggressive control to override the aircraft. Negative phase angle means pilot lag compensation. This occurs when the pilot is performing regressive control to follow flight tasks smoothly.

The pitch tracking task is described by a unity feedback PVS model as shown in Fig.2.2. The pilot model of this closed loop system is described by Eq. 2.1. The aircraft model

mainly consists of bare airframe dynamics, flight control system dynamics and sensors dynamics.

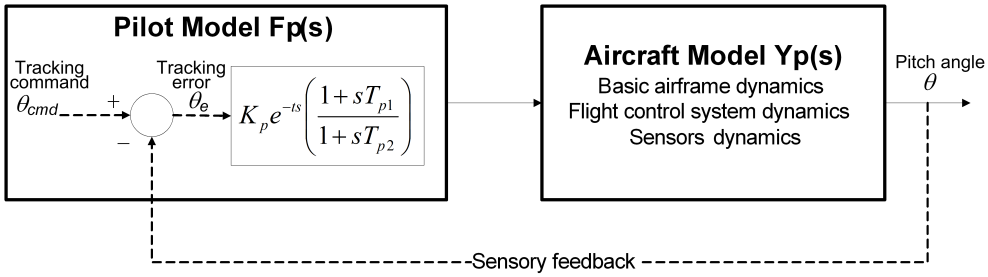

Figure 2.2: Closed loop pitch tracking model (modified from[25])

The criterion assumes that the pilot imposes a performance standard in the feedback control loop during a flight task. This performance standard is calculated at a closed loop bandwidth frequency of ω =3.5rad/s referred to phase angle at -90deg and a closed loop droop of -3dB. The outputs of this criterion are pilot compensation angle and the maximum closed loop resonance. The criterion then quantifies the pitch tracking handling performance and PIO tendencies of the aircraft as a function of the closed loop resonance and the required pilot phase compensation, as shown in Fig. 2.3. The performance boundaries of level 1, level 2 and level 3 correspond to the Cooper-Harper pilot ratings[15] of lower than 3.5, between 3.5 and 6.5, and higher than 6.5 respectively.

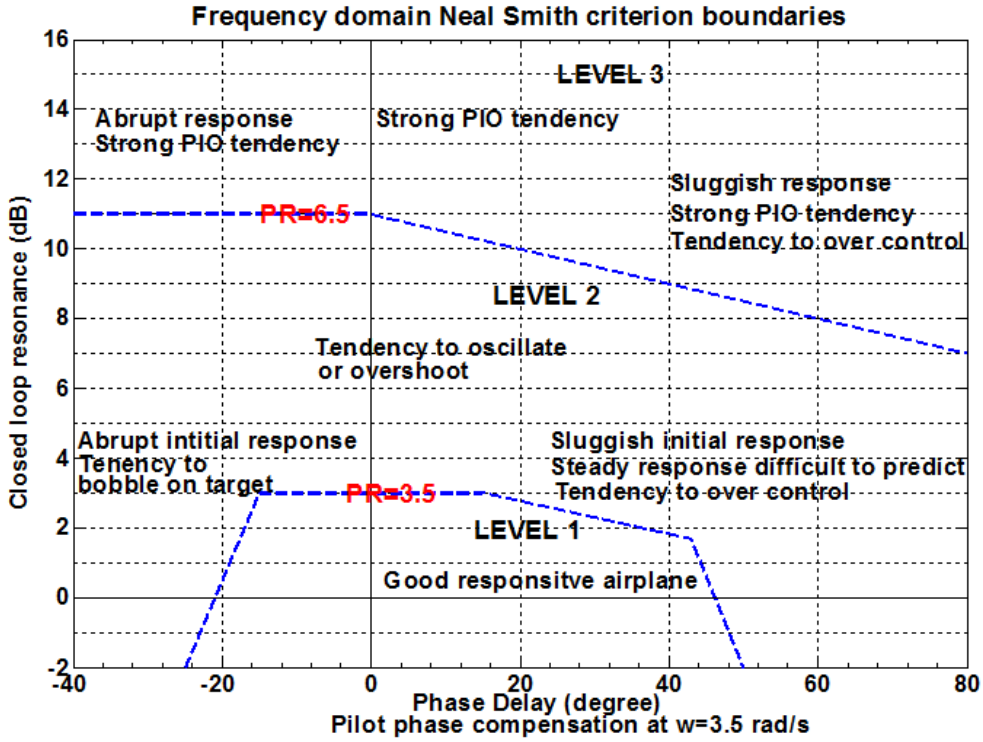

Figure 2.3: Neal-Smith parameter plane(modified from [25])

The advantage of this criterion is that it takes pilot model into account. When pilot delay

or task demands increases, the close loop resonance will increase or more pilot compensation will be required, which can be directly evaluated from this criterion. The disadvantages of this criterion are: (1) it is hard to determine which is the best pilot model for handling quality and PIO tendencies rating, (2) this criterion is based on the data of combat aircraft, (3) the minimum bandwidth is fixed to $3.5rad/s$, (4) this criterion uses transfer function models to calculate the outputs, rather than frequency-response plots, which makes it is not so convenient in real flight test data analysis.

B. Time domain Neal-Smith Criterion

The time domain Neal-Smith Criterion was developed by CALSPAN among the projects efforts in developing criteria to deal with nonlinear causes of PIO[26]. This criterion utilizes the frequency domain Neal-Smith Criterion and time domain Step Target Tracking Criterion. It is based on a closed loop pitch tracking task which is divided into an acquisition task and a fine tracking task.

There are two major outputs in time domain Neal-Smith Criterion. One is acquisition time D, which is defined as the time at which the pitch attitude error becomes less than the allowable pipper error after the pitch attitude command input at 0.25 seconds. It reflects the system ability to catch up an attitude change. The other is Root Mean Squared(RMS) pitch tracking error θ_e after the acquisition time. It directly measures the closed-loop stability. D is related to the equivalent bandwidth ω_{BWE} in frequency domain Neal-Smith Criterion. Assume that the ideal open loop transfer function of the tracking system is obtained as $\frac{Kp}{s}$ by using a simple gain pilot model and assume the pipper error is $\frac{1}{40}$ times the tracking command. The relationship is described by[26]:

$$\omega_{BWE} = -\frac{1}{D - 0.25}\ln(\frac{1}{40}) \tag{2.2}$$

Some similarities and differences between the frequency domain and time domain Neal-Smith criterion are generalized in reference [27]. Larger D means pilot has enough time to control aircraft smoothly, and makes the θ_e small. Smaller D means pilot has to operate quickly to catch the attitude, which may cause abrupt inputs and APC in low frequency. One reasonable θ_e is assumed to be $100deg/s^2$ based on the data from `Neal-Smith`, `LAHOS`, and `TIFS` databases[26][27]. Handling quality evaluation in time domain is more ocular and direct compared to frequency domain method. The major shortcoming of this criterion is the lack of a workload or pilot compensation measure. It is currently composed of only performance measures[27].

C. Bandwidth Criterion

The original Bandwidth Criterion was established by Hoh, Mitchell and Hodgkinson in 1982[1]. The purpose of this criterion is to evaluate the handling qualities and PIO tendencies of highly-augmented aircraft. The Bandwidth Criterion is an evolutionary development of the Neal-Smith Criterion[25]. It calculates the open loop pitch attitude frequency response to make an assessment of the control quality with system bandwidth ω_{BW} and pitch attitude phase delay τ_{ph}. The ω_{BW} is the frequency at which the phase margin $\omega_{BWphase}$ is $45deg$ or the gain margin ω_{BWgain} is $6dB$, whichever frequency is lower. Definitions of gain and phase margin are shown in Fig. 2.4.

The $45deg$ phase margin is an assumption that a pilot would introduce a phase lag to the aircraft. This additional phase lag would increase the overall PVS phase lag. Thus, 45 degrees are introduced as a buffer to accommodate the pilot in the system. The additional $6dB$ corresponds to the gain of two times of pilots input. It means that the Bandwidth Criterion allows the pilot to give input as much as twice of intended amplitude. The reason for this margin is that the aircraft response to the input is slower than what was expected, which makes the pilot tend to give larger input amplitude.

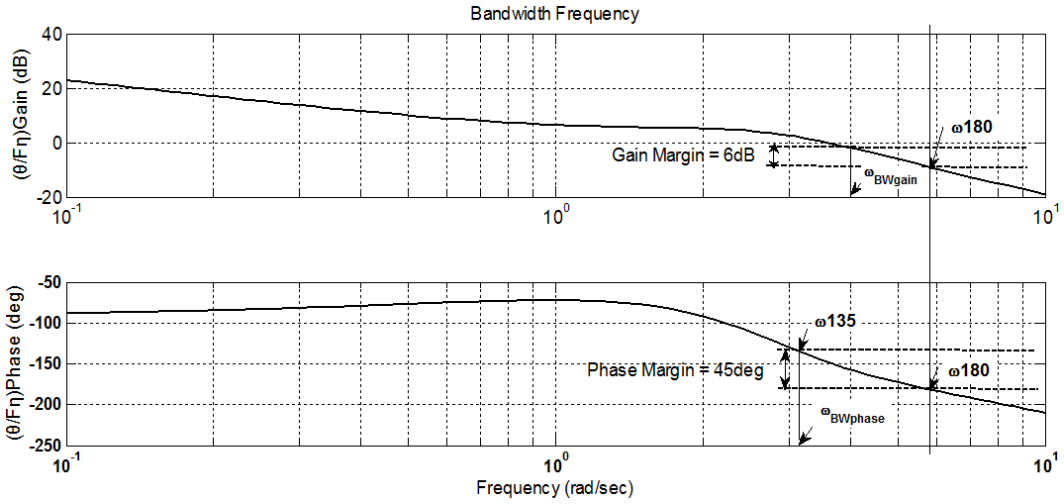

Figure 2.4: Bandwidth Parameters (modified from [25])

It is found that the result of handling quality and PIO assessment of Bandwidth Criterion does not show identical results to the Neal and Smith database[22]. Other three parameters were added to the original Bandwidth Criterion to give more accurate handling quality and PIO tendencies evaluation. These three parameters are flight path bandwidth $\omega_{BW\gamma}$, pitch rate overshoot $\Delta G\left(q\right)$ and neutral-stability frequency ω_{180}[22]. Corresponding parameters definitions are shown as following:

ω_{BW}, frequency at which phase margin is $45deg$ or gain margin is $6dB$, whichever is lower.

ω_{180}, frequency at which phase is $-180deg$.

τ_{ph}, the phase delay at the frequency of ω_{180}, calculated by $\tau_{ph} = \frac{-\left(\Phi_{2\omega_{180}}+180°\right)}{(57.3\times 2\omega_{180})}$, $\Phi_{2\omega_{180}}$ is the phase at twice ω_{180}.

$\omega_{BW\gamma}$, the frequency at which the phase margin of the flight path to stick force response is $45deg$.

$\Delta G\left(q\right)$, a frequency domain measure of overshoot referenced to the high frequency pitch mode response of the pitch rate response transfer function.

Flight control quality and PIO severity can be evaluated by plotting the corresponding parameters on the Bandwidth Criterion diagrams. Handling quality boundaries are different for different types of aircraft in different flight phases. As shown in Fig. 2.5, there

are three levels of handling quality regions according to parameter ω_{BW} and τ_{ph}[28]. Level 1 means good handling quality with high bandwidth and low phase delay while level 3 means bad handling quality with low bandwidth and large phase delay, level 2 is in the middle. The bandwidth and phase delay requirements of high manoeuvre combat task(flight phase category A) is more restrictive than approach and landing task(flight phase category C).

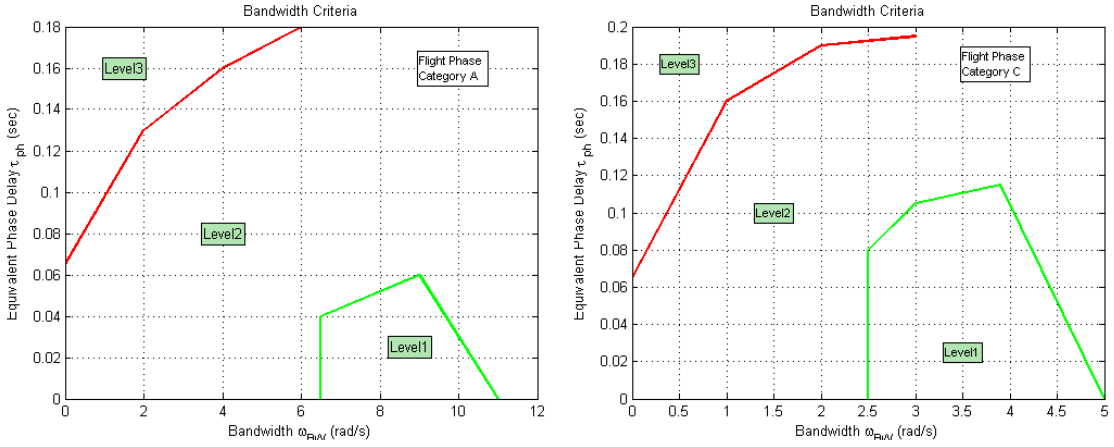

Figure 2.5: Bandwidth Criterion(Flight phase category A and C)(modified from [28])

The Fig. 2.6 shows the PIO susceptibility prediction Bandwidth Criterion diagram with added parameters ω_{BW_γ} and $\Delta G\,(q)$. This modified Bandwidth Criterion diagram shows detail PIO regions. The possibility of encountering PIO can be reduced if the gain and phase bandwidth characteristics are properly constrained according to the criterion. The Fig. 2.7 shows that although the results are conservative in the PIO tendencies evaluations of level 2 and level 3, the evaluation results of this criterion are reliable while applying to the Boeing approach and landing task database[29].

The Bandwidth Criterion can be applied to different types of aircraft and different flight phases. It is a criterion for PIO avoidance rather than response shaping for good handling quality[25]. The open loop transfer function of PVS can be calculated using real data frequency response method, which means that the phase and gain margin can be calculated easily. Thus, this criterion will be selected to design control laws for PIO experiments in this thesis.

D. Gibson Dropback Criterion

The Gibson Dropback Criterion is a time domain criterion. It is a criterion developed for handling quality evaluation rather than PIO criterion. It is known that traditional handling quality criteria are based on the assumption that the short term response behaviour of the aircraft is essentially governed by short period mode dynamics, thus, the concerned short term dynamics can be described by the reduced order transfer functions derived from the short period approximation equations of motion[25]. The pitch attitude response to elevator transfer function and flight path angle to elevator transfer function are given in Eq. 2.3 and 2.4 respectively[25], where $T_{\theta 2}$ represents the flight path angle to pitch attitude

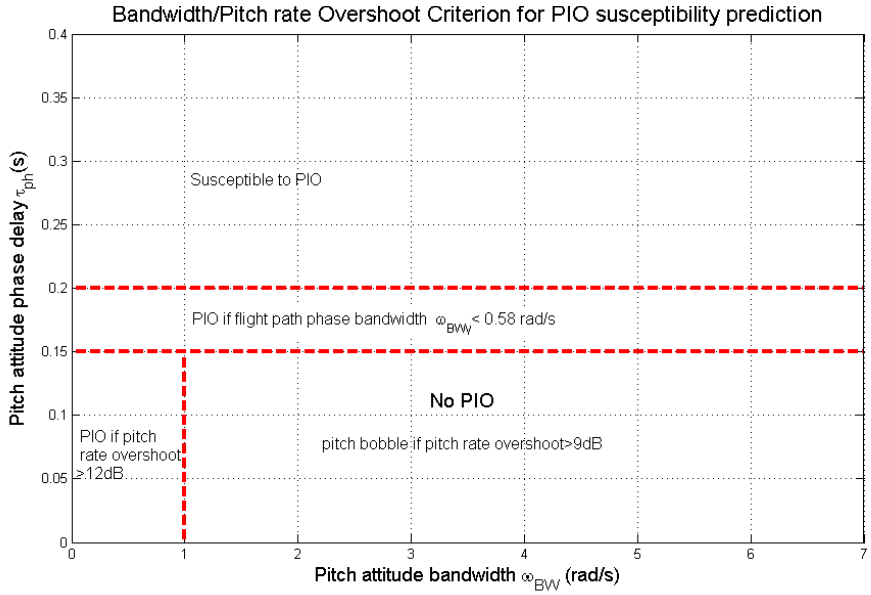

Figure 2.6: Bandwidth Criterion with three added parameters (modified from [25])

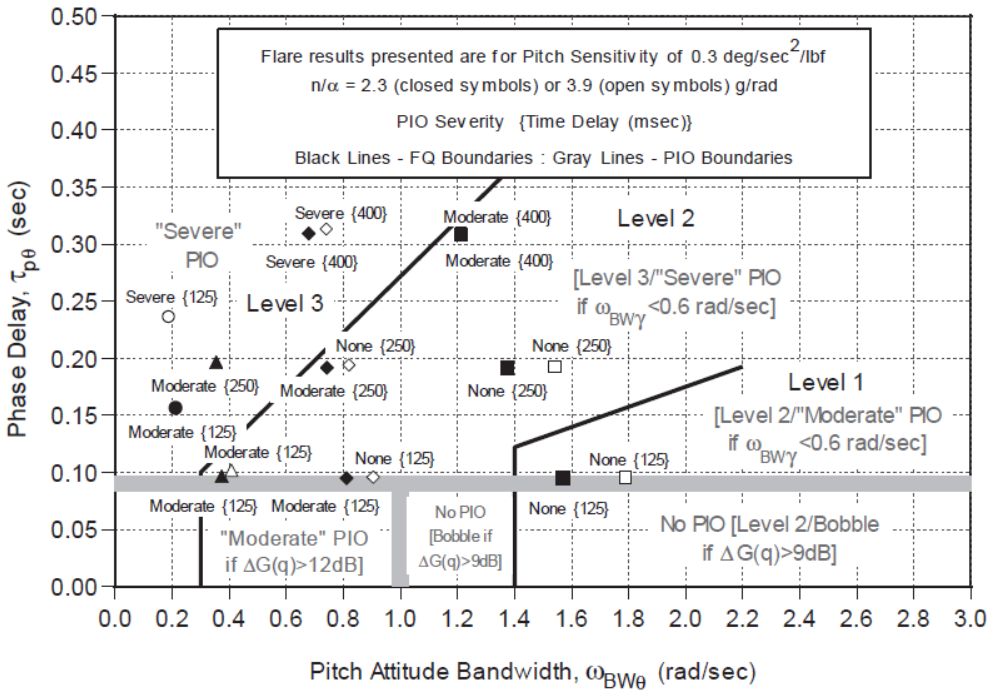

Figure 2.7: Bandwidth criterion corresponds to Boeing flight phase category C database (adapted from[29])

lag. The Dropback Criterion discloses the relationship between these two parameters. It is not only expressed in the understandable terms of the classical aircraft, but also applicable to highly augmented aircraft with high order system[28].

$$\frac{\theta(s)}{\eta(s)} \simeq \frac{k_q(s+1/T_{\theta_2})}{s(s^2+2\zeta_s\omega_s s+\omega_s^2)} \tag{2.3}$$

$$\frac{\gamma(s)}{\eta(s)} \cong \frac{k_q}{T_{\theta_2} s\left(s^2 + 2\zeta_s \omega_s s + \omega_s^2\right)} \tag{2.4}$$

Dropback is where the pitch attitude drops back or decreases to a lower steady value after removing the input and overshoot is defined as maximum pitch rate over the steady pitch rate[25]. As shown in Fig. 2.1.4, the actual dropback value is represented as *DB*, q_s is the static pitch rate after removing inputs, t_γ is the flight path delay. Thus, the time lag from flight path angle to pitch attitude is represented by $T_{\theta 2}$, calculated by Eq. 2.5. The Dropback Criterion was defined on limiting values of pitch rate overshoot ratio $\frac{q_m}{q_s}$ and the ratio of attitude dropback to steady state pitch rate $\frac{DB}{q_s}$.

$$T_{\theta_2} = \frac{DB}{q_s} + t_\gamma \tag{2.5}$$

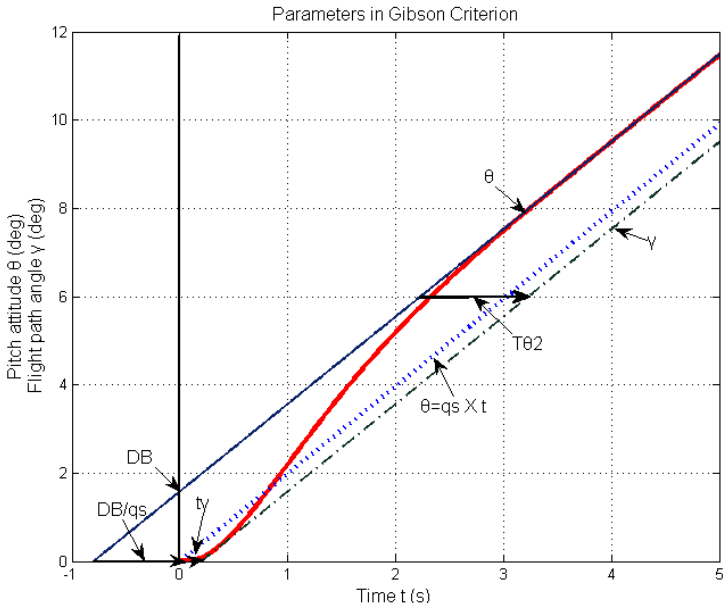

Figure 2.8: Gibson criterion parameters (modified from [25])

To achieve good handling quality and avoid PIO evens, the following requirements should be satisfied.

- Pitch rate overshoot ratio $\frac{q_m}{q_s} \leq 1.0$ will lead to unsatisfactory handling qualities.
- Zero dropback only is acceptable, if the $\frac{q_m}{q_s}$ is not in the satisfactory region.
- The acceptable value of pitch rate overshoot lies in the range $1.0 \leq \frac{q_m}{q_s} \leq 3.0$.

Gibson Dropback Criterion is an effective method in assessing pitch attitude longitudinal quality for tracking tasks. The dropback criterion diagram with boundaries proposed by Gibson[28] and Mooij[30] is shown in Fig. 2.9. Flight handling quality and PIO tendency can be evaluated by plotting $\frac{DB}{q_s}$ and $\frac{q_m}{q_s}$ in the diagram. Gibson boundary is derived from

fighter aircraft and Mooij boundary is derived from large transport aircraft data. It can be seen that large transport aircraft with $\frac{DB}{q_s}$ and $\frac{q_m}{q_s}$ located between $0 \sim 1.5$ and $0 \sim 2.5$ has good handling quality. The Gibson Dropback Criterion has the evaluation boundary derived from transport aircraft. Furthermore, it is a time domain criterion which is capable of nonlinear analysis. Thus, the Dropback Criterion is selected to design the flight control law for PIO tests.

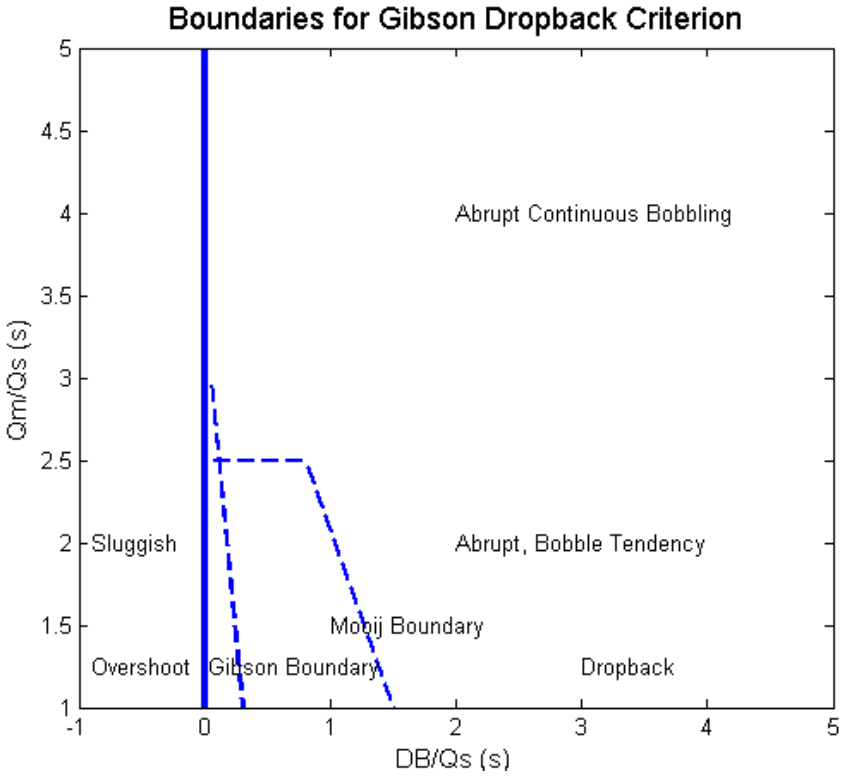

Figure 2.9: Dropback Criterion boundaries advised by Gibson and Mooij (modified from[28][30])

E. Gibson Phase Rate Criterion

The probability of PIO is generally determined by the level of gain and phase compensation introduced by the pilot during flight. The pilot introduced compensation can be determined by the open loop gain and phase characteristics of the aircraft at frequencies close to the resonant frequency of the human pilot[25]. The Gibson Phase Rate Criterion was developed to ensure good closed loop PVS performance without the threat of PIO[1].

The criterion is similar to the frequency domain Neal-Smith Criterion but without a pilot transfer function model. It deals with the open loop pitch attitude frequency response of the augmented aircraft in the region where the phase first reaches $-180deg$ as the frequency increases. The neutral stability frequency ω_{180} is defined as the frequency at which the phase of open loop transfer function first passes through $-180deg$[28]. Phase rate is a measure of the slope of the phase curve for frequencies near the crossover frequency, calculated by Eq. 2.6. It is also the direct equivalent of phase delay defined by

the Bandwidth criterion.

$$PR = \frac{\varphi_{2\omega_{180}} - \varphi_{\omega_{180}}}{2\omega_{180} - \omega_{180}} \text{deg/Hz} \tag{2.6}$$

where

$\varphi_{2\omega_{180}}$ represents the phase when the frequency at twice of ω_{180}

As shown in Fig. 2.10, the experienced data indicate that in consideration of avoiding PIO, the PIO crossover point at which the frequency is estimated to be no less than $1Hz$, and that the average phase rate should be less than $100deg/Hz$[25]. As shown in Fig. 2.11, the boundaries correspond to the Boeing approach and landing database[29] show that the published Gibson boundaries are too restrictive, although they do follow the form of the data. The reason is that the boundaries are derived from fighter aircraft data.

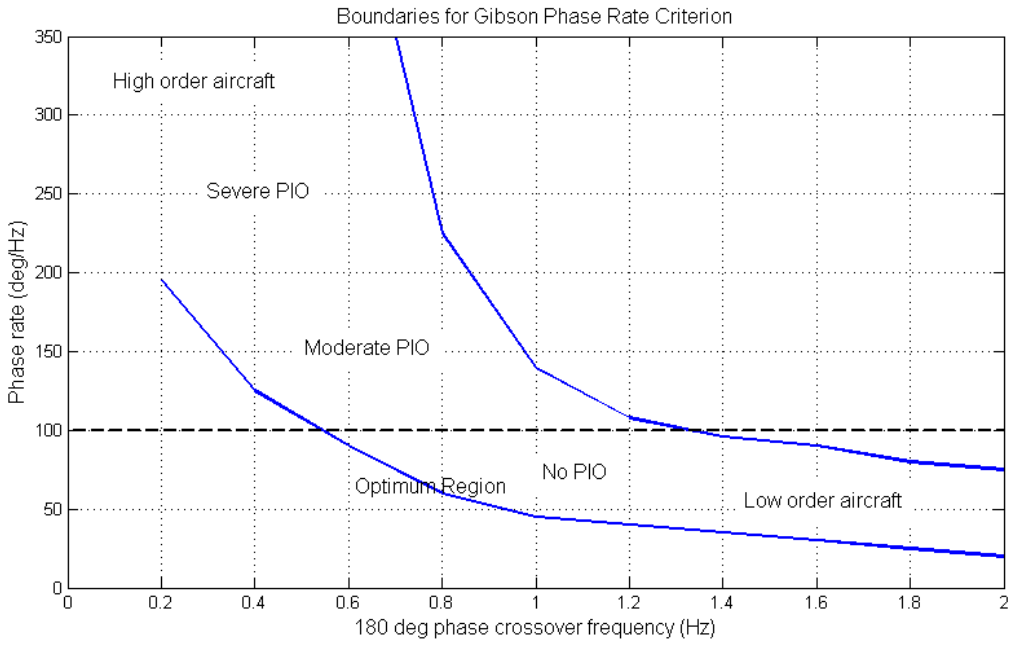

Figure 2.10: Gibson Phase Rate criterion (modified from [28])

The disadvantage of this criterion is that it attempts to ensure suitable margins for the pilot to make gain and phase compensation to get rid of PIO without affecting the aircraft stability[31].

2.1.5 Detection methods

Thanks to many years of experience and research, Category I PIOs are now very well understood. Detection and mitigation methods based on linear assumptions have been shown to be effective for incidents in this particular category[32]. After some high profile incidents, efforts to suppress Category II PIOs have resulted in the utilisation of methods

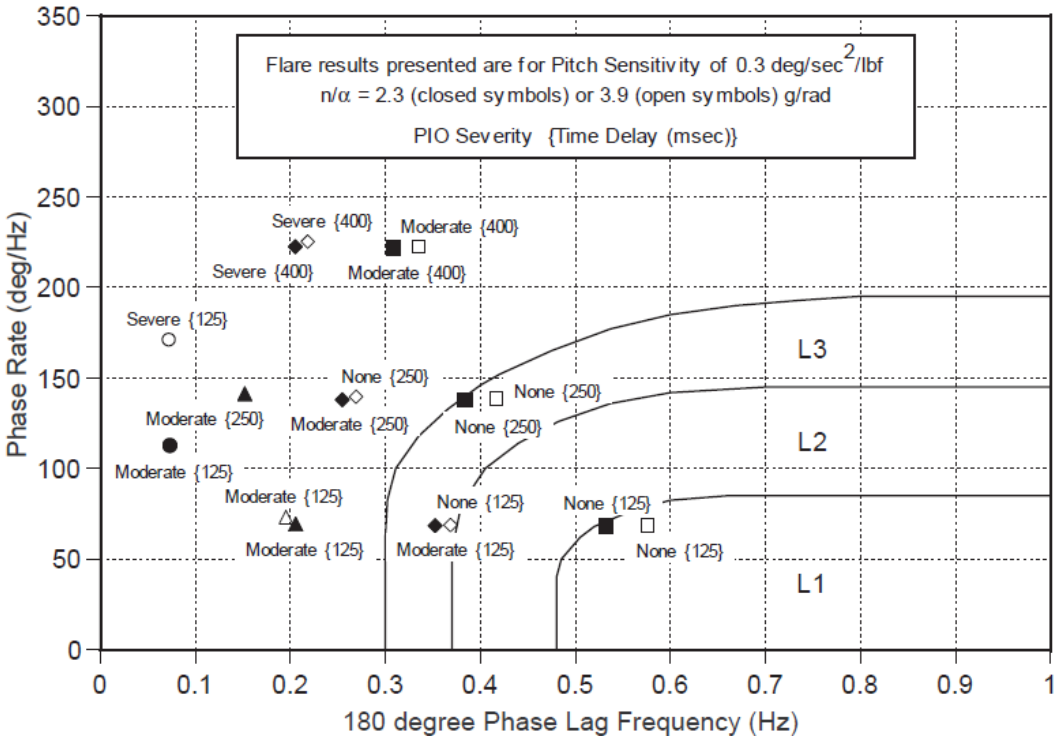

Figure 2.11: Gibson Phase Rate Criterion correspond to Boeing approach/landing database (adapted from [29])

based on describing function theory during the FCS design process[20]. So far almost all severe PIOs have featured some form of rate-limiting[16]. The nonlinear and divergent nature of Category III PIOs has meant that the only suppression method available is to detect and stop category I and II PIO before they fully develop. Category IV PIOs on the other hand, can be alleviated by increasing the aircraft's structural stiffness. Mitchell and Klyde[33] have reviewed and summarised some methods in this area. This section builds on their review and very briefly discusses some relevant state-of-the-art methods. First step towards avoiding PIO is at the Flight Control System(FCS) design stage where a number of criteria are available to assess handling qualities and PIO tendencies. For example the Neal-Smith, Gibson, Bandwidth and OLOP criteria. Some detection methods have been developed based on these criteria and PIO experience.

A. ROVER

Mitchell's research at Hoh Aeronautics, Inc. established a PIO detection and mitigation schemes called ROVER[6]. This scheme collects the pilot input and aircraft pitch rate response and makes a comparison of the characteristics between these two sets of signals. The severity prediction is based on monitoring four parameters: aircraft pitch rate magnitude and frequency, magnitude of pilot input and phase lag between pilot input and aircraft pitch rate. The structure of ROVER is shown in Fig. 2.12. It can be seen from the figure that a ROVER Integer Value(RIV) is used as a labelled sum of four detected flags. When RIV equals four, means a PIO occurred, a notch filter inside the ROVER will be activated to remove high-frequency noise and data spikes. The notch filter works as a

low pass filter activated at a PIO situation to minimize the input of pilots. Thus the PIO susceptibility can be suppressed. Detailed discussion of this notch filter will be performed in section 2.1.6.

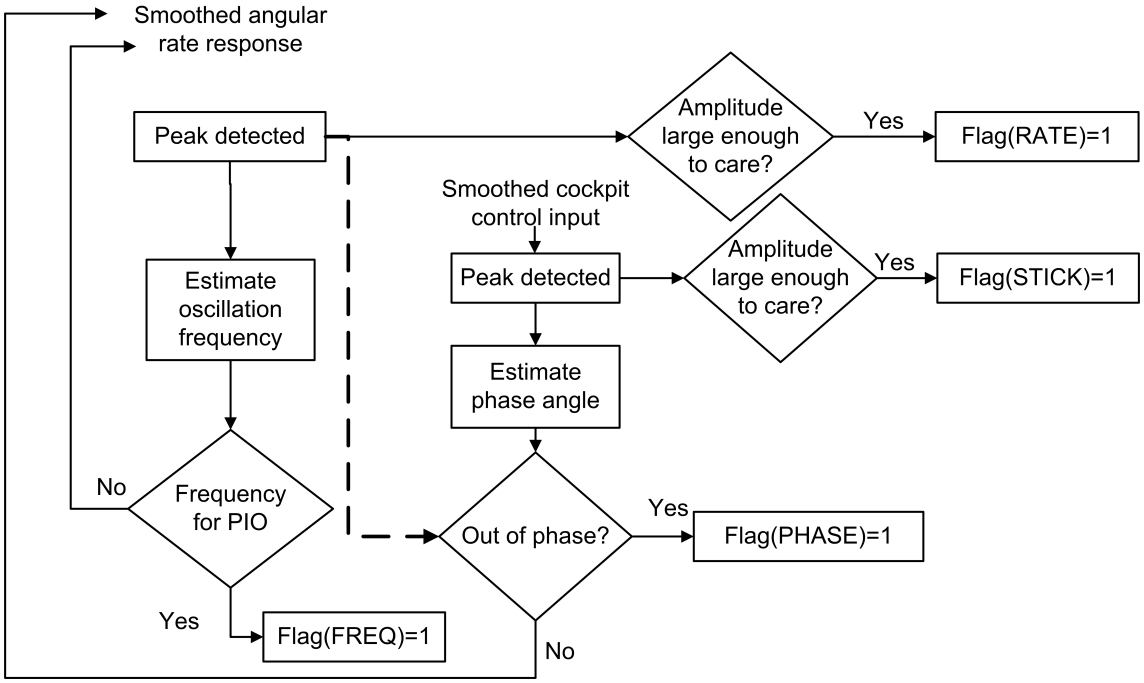

Figure 2.12: Structure of ROVER method (modified from [5])

ROVER is mainly designed for the prediction and mitigation of Category I PIO. Although nonlinear dynamics are not considered in its formulation, rate-limiting which effectively introduces a phase lag into the closed-loop system, can be detected during the phase lag estimation process. Therefore, Category II PIOs can be suppressed as shown by Mitchell and Klyde[32]. One simulated PIO detection for a tracking task performed in Boeing-747 model is shown in Appendix A. It can be seen that the detection results for PIO tendencies are about one oscillation circle lag. PIO is true at 45, 78, 90, 112 and 118 seconds when oscillations occurred. The detection sensitivity can be improved by reducing the thresholds of the four flags, but this will lead to a problem of misjudgment of normal oscillation. Thus, the most difficulty of adapting this detection method is the thresholds setting.

ROVER is simple and effective. It can be adapted to various kinds of aircraft by varying the threshold settings of the four flags. The disadvantage of ROVER is that it is mainly designed for the prediction and mitigation of category I PIO. Category I PIO events usually designed out in early flight control system design work. Common PIO events happened in modern aircraft are associated with rate-limiting, this factor is not directly considered in ROVER.

B. Fuzzy logic detector

A fuzzy logic based PIO detector was proposed by Jeram and Prasad[7]. The detector detects pilot signals and aircraft responses, then uses fuzzy logic system to assign values

between 0 and 1 to the aircraft PIO tendencies. The structure of fuzzy logic detector is shown in Fig. 2.13. Detection steps of this method are: (1) detect pilot signals and aircraft responses and calculate PIO feature variables using Fourier Transform, (2) predict PIO tendency using PIO criteria derived from experienced PIO data in the fuzzy logic analysis system. The PIO tendency prediction is based on four criteria described in the following[7],

- Attitude phase lag is about 180 degrees
- Pilot stick input has a large magnitude
- Main Coupling frequency is approximately $0.3 \sim 1.5Hz$
- Control actuator limiting and saturation happened

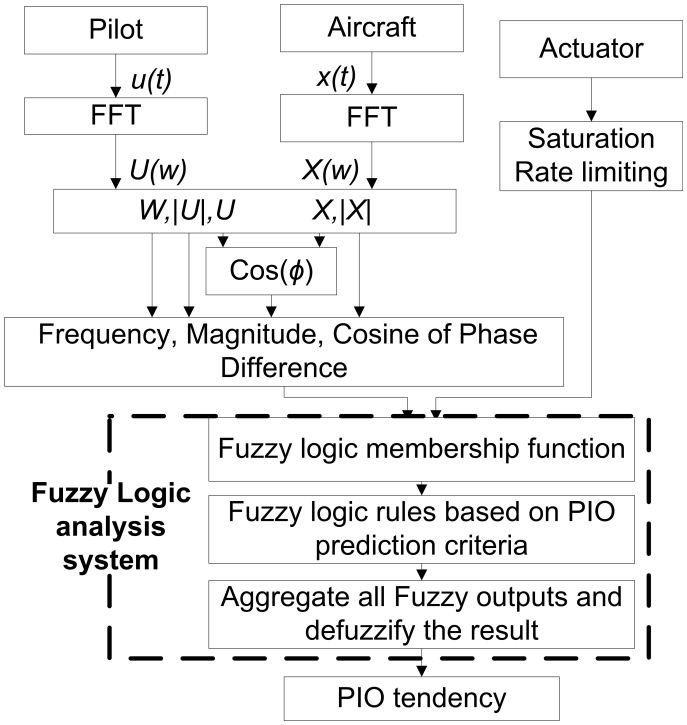

Figure 2.13: Structure of fuzzy logic detector (modified from[7])

As shown in Fig. 2.13, the fuzzy logic analysis system receives the PIO feature variables and determines the degree to which they belong to each of the appropriate fuzzy sets via membership functions. Generally, the PIO feature variables are main frequency, magnitude of pilot input, cosine of phase delay between pilot input and aircraft attitude response and actuator rate-limiting. The bell-shaped membership function and trapezoidal-shaped membership function is usually selected to assign values between 0$\sim$1 to these variables. The bell-shaped membership function is described by Eq. 2.7, and the trapezoidal-shaped membership function is described by Eq. 2.8. The shape of these two function is controlled by the parameters of $\{a, b, c\}$ and $\{a, b, c, d\}$ respectively. These four parameters can be estimated by PIO data clustering method and experience. An example of using fuzzy logic detector is shown in Appendix A. The input signal was the same as that in

ROVER test. It can be seen that by choosing membership function and PIO fuzzy logic rules, PIO tendencies prediction can be obtained.

$$f(x,a,b,c) = \frac{1}{1+\left|\frac{x-c}{a}\right|^{2b}} \tag{2.7}$$

$$f(x,a,b,c,d) = \left\{ \begin{array}{ll} 0 & x \leq a \\ \frac{x-a}{b-a} & a \leq x \leq b \\ 1 & b \leq x \leq c \\ \frac{d-x}{d-c} & c \leq x \leq d \\ 0 & d \leq x \end{array} \right\} \tag{2.8}$$

The advantage of this detection method is that it can be coupled to different types of aircraft by varying the membership functions. The design of membership function based on the characteristics of pilot and aircraft responses when PIO happens. The fuzzy logic rules are dependent on the knowledge of PIO theories. Hence, the disadvantage of this method is that it requires clustering and analysis of enormous PIO data and deep understanding of PIO theories.

C. PIO feature detector and Neural network discriminator

Another PIO detection and compensation approach was introduced by Cox and Lewis[8], as shown in Fig. 2.14. The detector includes a PIO feature calculator and a PIO tendency discriminator. The feature calculator receives pilot signals(stick, column and pedal force/deflection) and aircraft states(attitudes of pitch, roll and yaw) sensed by respective sensors of the aircraft, and uses these signals to create PIO feature parameters. The PIO feature parameters include magnitudes of pilot inputs and aircraft attitudes, the average frequency and the phase difference between pilot inputs and aircraft states. Four types of PIO feature calculators were introduced in [8]. Each of them uses different calculation methods such as time domain differentiation, fast Fourier transform(FFT), polynomial data fitting and error function minimization. After calculation, PIO feature signals are passed to a neural network discriminator to predict whether or not a PIO occurred[8]. The neural network detector uses a gradient descent-like process to adapt itself to PIO detection function. Thus, PIO and non-PIO are grouped with quantitative judgments[9].

The advantage of neural network detector is that it can be adapted to different PVS to make more precise PIO tendency judgment if it has perfect database. The difference between neural network detector and fuzzy logic detector is that neural network detector compares the features of real time input signal with exist data in the database to make PIO tendencies detection, while fuzzy logic detector uses prediction criterion derived from experience data and simulation data to make PIO discrimination. The disadvantage of neural network method is that it needs a large database for training.

D. Open Loop Onset Point Method

The Open Loop Onset Point(OLOP) was developed by DLR(Deutsches Zentrum f$\ddot{u}$r Luft- und Raumfahrt), German Aerospace[10]. The OLOP is a kind of method using describing function techniques and stability regions on the Nichols chart to predict PIO caused by

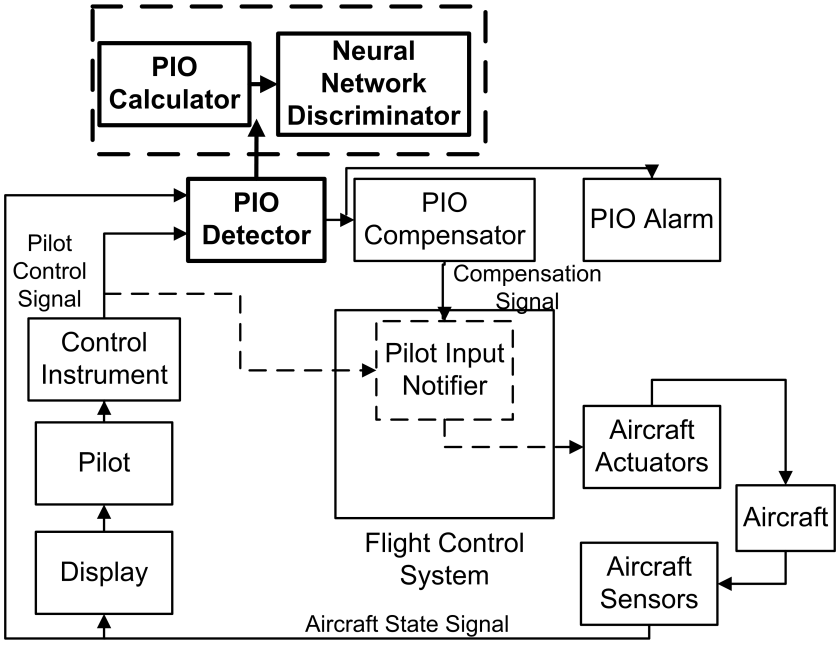

Figure 2.14: Structure of PIO feature detector and Neural network discriminator (modified from [8])

varies kinds of rate-limiting. The rate limiting has two major effects on PVS when the commanded deflection rate is greater than the rate-limiting: (1) It causes phase delay between pilot inputs and system outputs, which will lead to an unstable oscillation of the PVS and make pilot to do fast compensatory reaction, (2) it reduces gain, which causes inadequate control effect leading pilot to increase command inputs. Both effects will increase the PIO tendencies. The phase margin of current FBW aircraft is around 45 degrees, which can be exceeded quickly by the phase lag caused by rate-limiting[34].

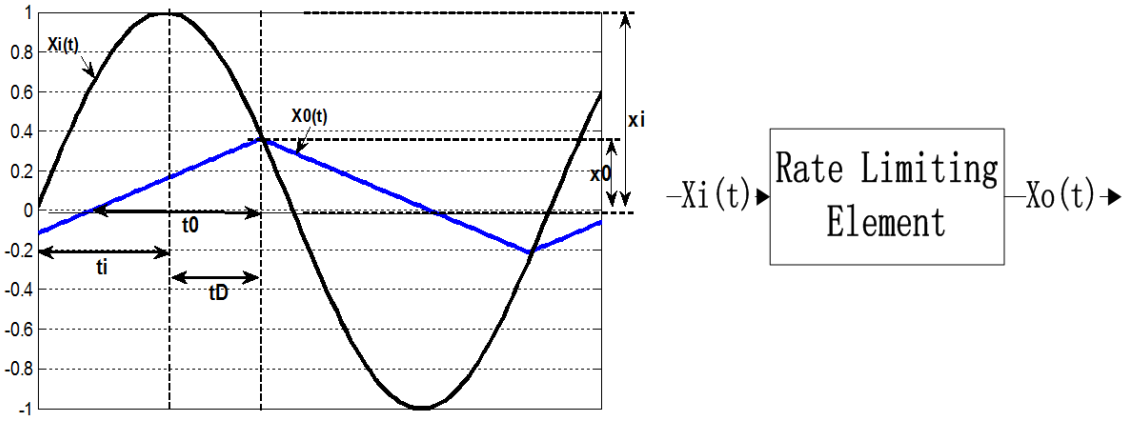

Figure 2.15: Actuator rate limiting (modified from [35])

From Fig. 2.15, relative parameters definition and describing function are described as following[35].

The input signal is described by

$$x_i(t) = x_i \sin(wt) \tag{2.9}$$

So the input rate is calculated by

$$\dot{x}_i(t) = x_i w \cos(wt) \tag{2.10}$$

The signal frequency $\omega = \frac{2\pi}{T}$, where $T = 4t_i$, then the maximum input rate is

$$\dot{x}_{i\max} = \frac{\pi}{2}\frac{x_i}{t_i} \tag{2.11}$$

The output rate is equal to the slope of the output which is described as

$$\dot{x}_0 = \pm\frac{x_0}{t_0} \tag{2.12}$$

thus,

$$\frac{\dot{x}_0}{\dot{x}_{i\max}} = \frac{x_0}{t_0}\frac{2t_i}{\pi x_i} \tag{2.13}$$

Consider that t_0 equals to t_i , the output/input magnitude ratio $K = \frac{x_0}{x_i}$ can be given as

$$K = \frac{x_0}{x_i} = \frac{\pi}{2}\frac{\dot{x}_0}{\dot{x}_{i\max}} = \frac{\pi}{2}\frac{R}{wx_i} \tag{2.14}$$

The Fourier fundamental mode for a triangle wave with magnitude x_0 is $\frac{8x_0}{\pi^2}$, so the describing function can be described as $|N(jw)| = \frac{8x_0}{\pi^2}\frac{1}{x_i} = \frac{8K}{\pi^2}$, and the onset frequency is defined as $\omega_{onset} = \frac{R}{x_i}$, this is the frequency where the actuator saturation first occurs. Finally the complete describing function for the limiting element in terms of ω and ω_{onset} can be obtained as

$$N_{\sin}(jw, w_{onset}) = \frac{4}{\pi}\frac{w_{onset}}{w}e^{-j\cos^{-1}(\frac{\pi}{2}\frac{w_{onset}}{w})} \tag{2.15}$$

valid for $\omega \geq \frac{1}{2}\sqrt{\pi^2 + 4\omega_{onset}}$.

The OLOP point is defined as the frequency response value of the open-loop system at the closed-loop onset frequency $\bar{\omega}_{onset}$. Thus it is easy to calculate the frequency of the

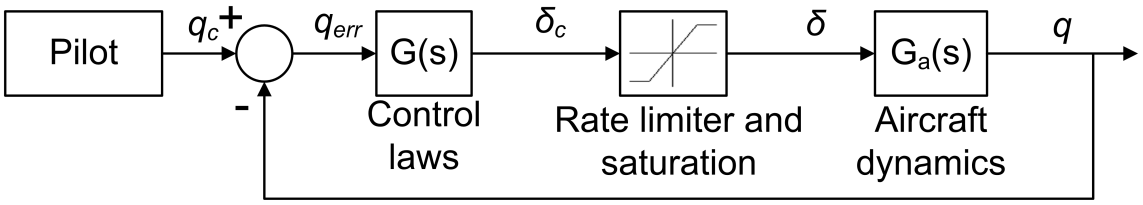

Figure 2.16: A general system considers rate limiting

onset point with Fig. 2.16 and the equation below.

$$q_{c0}\left|\frac{\delta_c}{q_c}(j\bar{w}_{onset})\right| = \frac{R}{\bar{w}_{onset}} \tag{2.16}$$

where q_{c0} is the maximum magnitude of input, R is the rate limit.

The onset point is at the intersection of the magnitude of closed loop system frequency response from pilot to the input of rate limiter and a straight line with slope *-20 dB/decade* that crosses the *0 dB* line at the rate-limiting R [34]. With this onset point, open loop phase and gain in the Nichols chart can be achieved and determined to be stable or has the PIO susceptibility according to existed data. The Nichols chart of OLOP criterion is shown in Fig. 2.17.

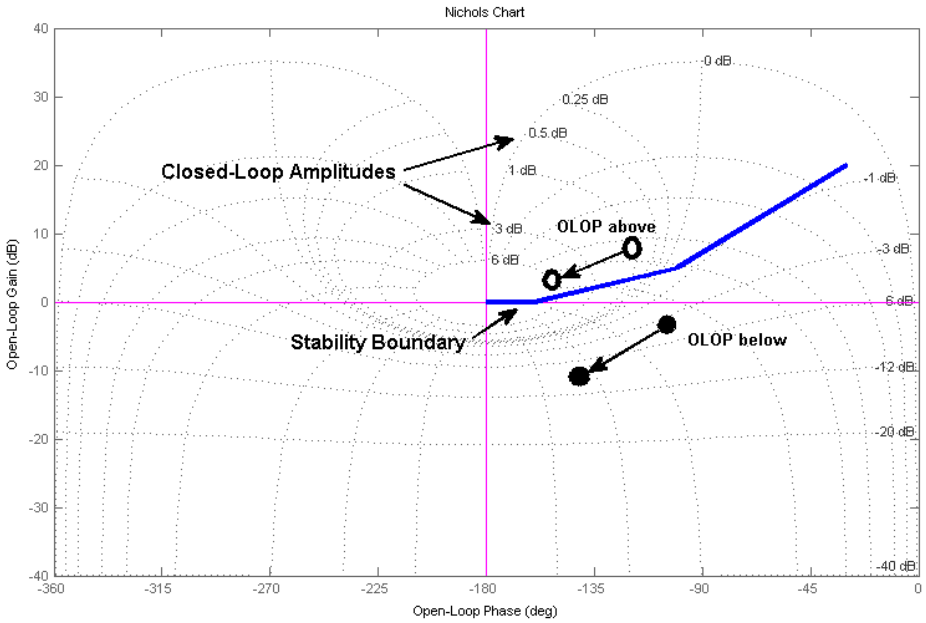

Figure 2.17: Nichols Chart of OLOP criterion (modified from [34])

The OLOP analysis and calculation process[10] is shown below:

- Define a simple gain pilot model.
- Use maximum stick amplitude to calculate the closed loop response from pilot input to rate limiter input $\left|\frac{\delta_c}{q_c}(j\bar{w}_{onset})\right|$.
- Determine the closed-loop onset frequency $\bar{\omega}_{onset}$ by solving Eq. 2.16.
- Determine the open loop transform function $F_0\left(j\omega\right)$ of the system. This function is calculated with $F_0\left(j\omega\right) = \frac{Fc(j\omega)}{(1-Fc(j\omega))}$ refers to close loop function $Fc(jw)$. Thus, the required open-loop frequency response and magnitude $A\left(j\omega\right)$ and phase $\Phi\left(j\omega\right)$ can be obtained.
- Determine where the OLOP parameter is on the Nichols chart in relation to the stability boundary and estimate the PIO tendency.

An example is carried out to display the effect of rate-limiting in Appendix A. It can be seen from the figure that different maximum stick magnitude will lead to different onset

point frequency. For maximum input 0.02, onset frequency is calculated as $5.1rad/s$. The input of magnitude of 0.02 and frequency of $4.5rad/s$ has a good result but when the input increases to 0.028, rate limiting and divergence happened. Another input of magnitude of 0.02 and frequency of $5.1rad/s$ also causes divergence because the frequency is at the onset point. Thus, the OLOP method has limitation in using as a prediction tool, but it is very useful for PIO evaluation in the design stage.

E. Summary of detection methods

There are still other PIO prediction approaches such as wavelet transform method[36], probabilistic neural network detection method[37], detection of power spectral density of pilot input signals[38], special PIO cases like limit cycle oscillations[39]. Most of these detection methods detect the oscillation level of the control input and aircraft state and the relationship between them. By comparison with these detection methods, this thesis presents an idea to detect trend of pilot movement. The moving trend is a sign of pilot awareness of PIO during oscillations. The aggressiveness and regressiveness of pilot movement is assumed to indicate whether the PIO is getting stronger or weaker. This detection method aims to identify the pilot effects during oscillations and to reduce the PIO false detection by detecting pilot's moving trend.

2.1.6 Mitigation Methods

PIO mitigation methods are roughly categorized into three approaches: (1) different kinds of filters are used to compensate or suppress pilot inputs when PIO happens, (2) adaptive controller are used to decrease the stick gain or to increase the damping of aircraft and, (3) visual or tactile cues are given for pilot to reduce take active actions. These mitigation methods can be combined or used separately. Several kinds of filters and adaptive controllers are introduced in this section.

A. Notch filter

In a control system, filter is generally used to pass or stop certain range of signals to make the system operation run smoothly and efficiently. When a PIO happens, the control rate and acceleration will increase rapidly, then the filter can be activated to provide suppression to the stick inputs. Thus, the PIO tendency can be attenuated.

Notch filter is a kind of filter which passes all frequencies except at a fundamental frequency. In fact, a notch filter usually acts as a low-pass filter cascaded with high-pass filter. ROVER system contains a notch filter which is able to remove high-frequency noise and data spikes. When a pilot is unable to control the aircraft or is unaware of a developing PIO, the notch filter will be activated to decrease or stop pilot inputs over a limited frequency range, but very low frequencies commands are remain unaffected. This filter is only activated when a severe PIO is detected. Pilot still owns low frequency authority even when the filter is activated. The transfer function of the notch filter inside

ROVER is described by Eq.2.17[6].

$$H_{NF}(s) = \frac{(s+2.5)^2(s+8)^2}{(s+0.6)^2(s+33)^2} \tag{2.17}$$

This filter is simple and effective but it will cause a phase delay of $50deg$ near the frequency of $1rad/s$. This will affect the control quality of large transport aircraft since the large transport aircraft usually has low short period oscillation frequency ranged from 1 to $3rad/s$.

B. Feedback With Bypass filter

SAAB JAS-39 was designed with relaxed longitudinal static margin technique. Two prototype aircraft were destroyed due to PIO caused by rate limiting[40]. The Feedback-With-Bypass(FWB) filter was designed in response to the loss of these two aircraft. The structure of the filter is shown in Fig. 2.18. It can be seen that the signal difference between the output and bypass of the "rate limiter 1" goes through a second low pass filter. This signal is negative, it will add phase lead to the pilot input when it feeds back. Thus, the phase lag caused by rate-limiting can be suppressed.

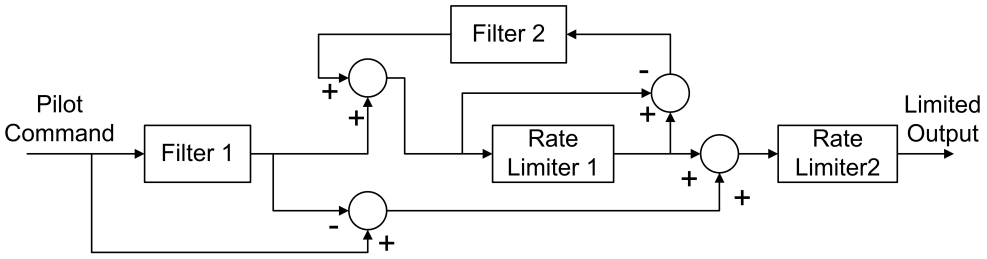

Figure 2.18: Structure of feedback with bypass filter (modified from [40])

This type of filter is mainly designed to suppress category II PIO. The disadvantage of this filter is that it will not modify the low frequency signal which may cause category I PIO.

C. Adaptive controller-Smart Adaptive Flight Effective Cue(SAFE-Cue)

Adaptive control is a technique of building a model based on the input-output experiments of the system and using this model to design an adaptive controller which can be adjusted to appropriate values during the operation of the system as the system parameters vary. The adaptive controller can be adapted to time or space varying systems.

One way to reduce the PIO tendency is to provide the pilot with cueing that what has been changed during the flight and what should be done during or after the changes. Thus, visual display, warning voice or adaptive force feedback can be selected according to different conditions to guide the action of pilots. This concept led to the SAFE-Cue system which was introduced to solve the APC problems[12]. This system can provide guidance to pilots via force feedback cues and appropriate commands. These cues and

commands are calculated from an active control inceptor with command gain adjustments when the adaptive control system is activated.

The calculation of system error is a key function in this system. Generally, the system error can be computed between the adaptive system response and a model based nominal system response. The difference of the selected signals between these two systems is the system error. The structure of force feedback and command path gain adjustment based on the computation of pitch rate error is shown in Fig. 2.19 and 2.20.

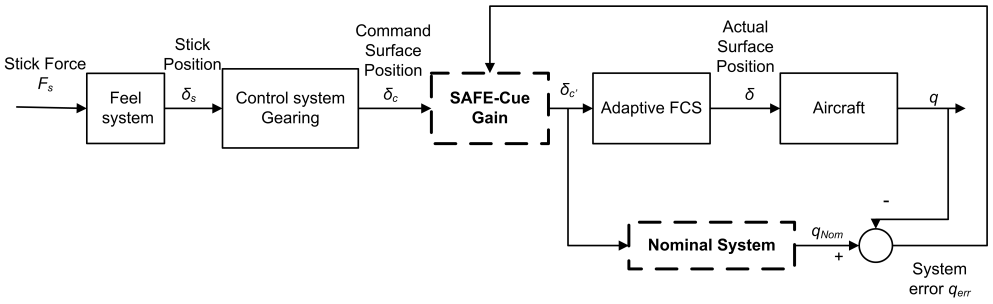

Figure 2.19: SAFE-Cue gain adjustment (modified from [12])

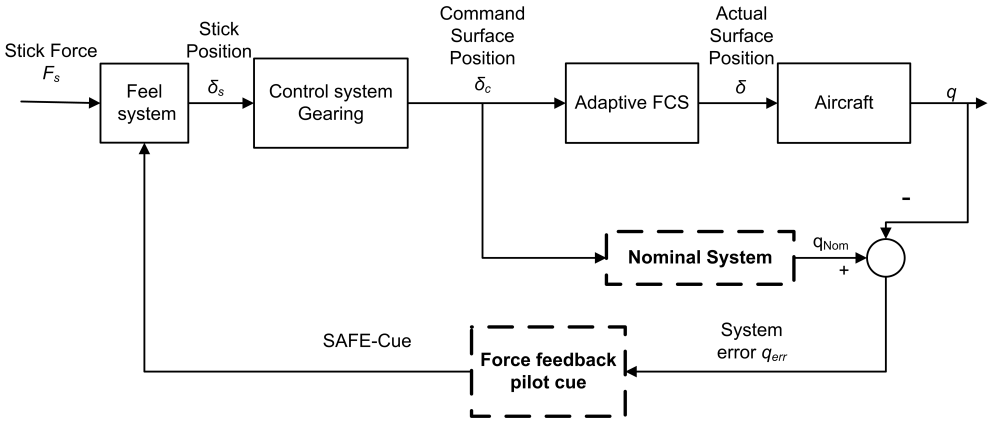

Figure 2.20: SAFE-Cue stick force feedback (modified from [12])

When a malfunction or damage happens, the actual adaptive system will experience sudden fierce change in dynamics and lead to abrupt pilot control, thus, the rate limiting may happen and the pitch rate system error will exceed a preset threshold. At this moment, the SAFE-Cue will be activated. It will provide visual and aural cue and stick force feedback to the pilot. The system can also provide a self tune gain to attenuate the oscillations. This kind of adaptive controller is effective for PIO mitigation, but it is much complicated than the notch and FWB filter. The establishment of nominal system requires deep understanding of the aircraft flight dynamics.

D. Adaptive controller-Multi-Model Adaptive Controller(MMAC)

A real time MMAC for PIO prevention is introduced in[11]. Pilot command system is treated as feedback transfer function from aircraft responses. Based on the analysis of

PVS stabilities, a set of pilot response model is developed as a pilot model library. Thus a serial of pilot response models would be established. After that, true output of pilot control will be monitored and compared with the output from suitable simulated nominal pilot control model. When difference between these two compared signals happens, PIO susceptibility can be obtained and compensation can be performed to reform the dynamics of real PVS. Usually, pilot control gain is selected to be compared and controlled. Structure of this kind of PIO controller is shown in Fig. 2.21. It can be seen that the gain pilot input δ_s is compared with preset nominal pilot gain model, after comparison and calculation, the pilot gain K_{pr} will be modified by K_{pm}. This method can be easily coupled to the aircraft system. However, it modelled pilot as a simple gain, which may ignore the lead and lag compensation of pilot operations. Moreover, it does not consider the aircraft response in real time detection, which may misjudge the normal control into PIO.

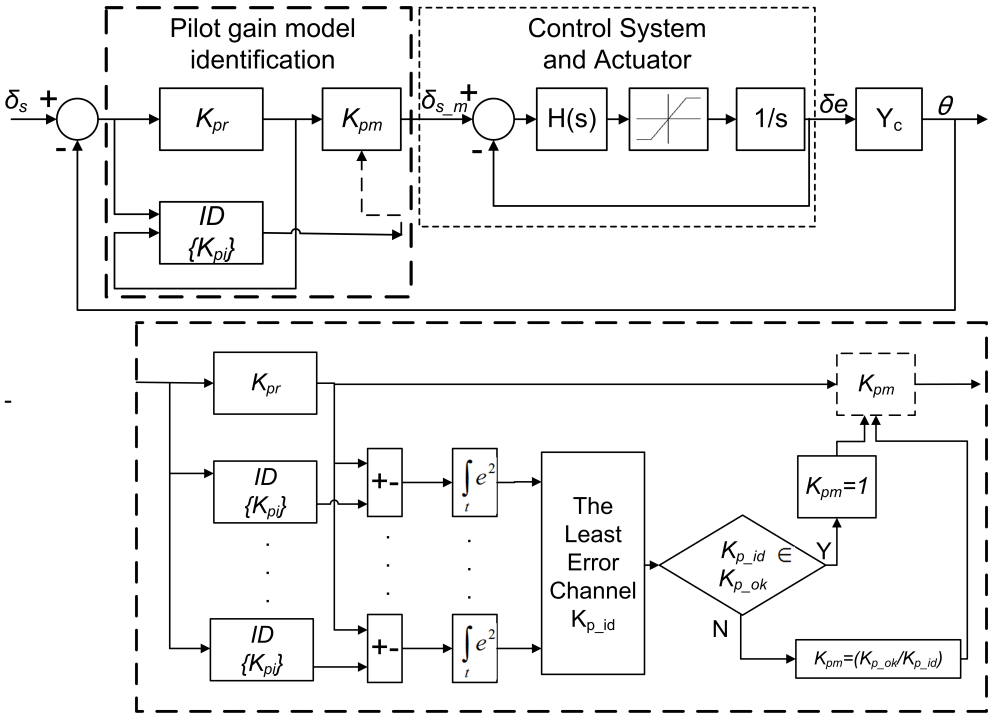

Figure 2.21: Closed loop multi-model controller (modified from [11])

E. Summary of mitigation methods

The PIO mitigation methods were to reduce the stick input gain or to provide PIO cue for the pilot. Using filter to mitigate PIO will more or less cause phase lag to the control signal. To avoid phase distortion, an scheduled gain controller is selected to mitigate PIO in this thesis. This adaptive controller is simple. However, the weighted gains should be carefully selected.

2.2 Signal processing and system identification

2.2.1 STFT and wavelet

PIO characteristics parameters including magnitude and frequency of pilot and aircraft state, and phase lag between them. The first step of PIO detection and mitigation is to obtain these parameters accurately. The signals from pilot control and aircraft state are non-stationary. Generally, signals can be divided into two types, stationary and non-stationary. The characteristics of stationary signal remain the same pattern when time or space varies, while non-stationary signal means that the characteristics of signals change when time or space changes[41]. STFT and wavelet transform are effective in getting frequency and time domain characteristics from real time signals.

The STFT theory can be explained as following[42]. For a continuous signal $x(t)$ with bounded energy on a finite time interval $[0 \quad T]$, its Fourier Transform function $X(f)$ can be described by:

$$X(f) = \int_0^T x(t)e^{-j2\pi ft}dt \tag{2.18}$$

or

$$X(\omega) = \int_0^T x(t)e^{-j\omega t}dt \tag{2.19}$$

where, $\omega = 2\pi f$.

When $x(t)$ is sampled in evenly discrete time intervals Δt, the finite Fourier Transform can be approximated as

$$X(f) = \Delta t \sum_{i=0}^{N-1} x_i e^{-j2\pi ft_i} \tag{2.20}$$

where $t_i = i\Delta t, \quad x_i = x(i\Delta t), \quad \Delta t = \frac{T}{N}, \quad i = 0, 1, 2, 3..., N$. The equation 2.20 uses the first N points of the signal $x(t)$.

The Discrete Fourier Transform(DFT) is defined by:

$$X[k] = \sum_{i=0}^{N-1} x[i]e^{-j2\pi f_k t_i} = \sum_{i=0}^{N-1} x[i]e^{-j2\pi ik/N} \tag{2.21}$$

where, $f_k = \frac{k}{N\Delta t} = \frac{k}{T}, \quad k = 0, 1, 2, ..., M-1$, and

$$M = \begin{cases} N/2 & for\ N\ even \\ \frac{N+1}{2} & for\ N\ odd \end{cases} \tag{2.22}$$

The values M represent the limitation that the frequencies contained in the sample time history should locate inside the band $[0 \quad f_n]$, where f_n is defined as the Nyquist frequency by

$$f_n = \frac{1}{2\Delta t} \tag{2.23}$$

The equation 2.21 is used to analyze stationary signal. However, Signals come from pilot and aircraft are non-stationary. Both frequency and time should be observed and analyzed. Thus, STFT is introduced[41]:

$$X[i,k] = \sum_{l=0}^{M-1} x[i+l]g[l]e^{-j2\pi lk/N} \tag{2.24}$$

where, $k = 1, 2, 3, ..., N$.

The window function $g[l]$ is designed to keep the sampling signal stationary over the duration of observation time. As i increases, each part of the signal can be observed through the window. For a certain window, the frequency resolution in terms of the sampling period T is $\Delta f = \frac{1}{TL}$, where L is the length of the window. Once the window length is selected, STFT step is fixed. A shorter window will increase time resolution but decrease frequency resolution, while a longer window has an adverse result. Thus, the window length should be carefully selected when using STFT. The Heisenberg inequality $\Delta t \Delta f \geq \frac{1}{4\pi}$ gives a general principle in selecting reasonable time and frequency resolution.

The basic difference between wavelet and STFT is that the window length can be changed for different frequencies in wavelet transform. Wavelet is able to remain orthogonal when it is stretching along time or magnitude. Comparing to STFT, it can perform multi resolution analysis to signals, as shown in Fig. 2.22.

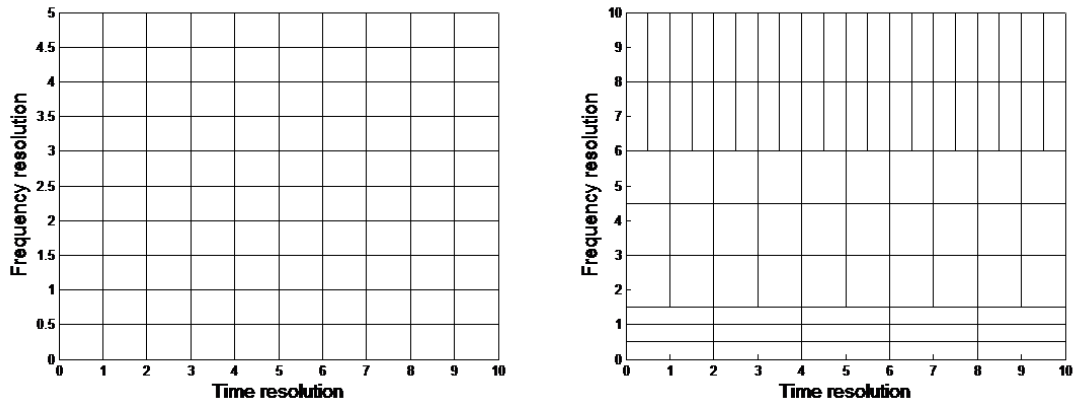

Figure 2.22: TFT(lLeft), Wavelet(Right)

Wavelet can fit signals well both in high frequency and low frequency over time. However, since wavelet transform is more complicated than STFT, it requires longer calculation time in signal processing. PIO frequency is usually $0.1 \sim 3.5Hz$, the period is about $0.33 \sim 10s$. PIO frequency bandwidth is narrow and PIO frequency is low, signals can be assumed to be stationary within a short period of time. Thus, in consideration of real time detection speed and the PIO features, STFT is selected to do the PIO detection.

2.2.2 System identification

To determine the influence of pilot dynamics to the whole PVS dynamics and get the relationship between open loop crossover frequency and PIO tendencies, system identification is performed using the Fourier Coefficient Method(FCM) and an ARX model. The frequency response functions obtained from these two methods are compared. The FCM will be used to estimate the PVS order to give more accurate orders for the ARX model, which will be used in the real time detection.

A. FCM

The FCM method uses fast Fourier transform to process the signal at certain number of frequencies. The signals can be represented by a serials of sine signals. By using fast Fourier transform to the system input and system output, the frequency response can be calculated, hence the system transfer function can be estimated through the frequency response. However, the FCM can only perform system identification at a certain number of frequencies. Thus, using this method to determine crossover frequency in real time is difficult. The FCM can be a complementary method for ARX model. It can provide a more accurate ARX model order by comparing the frequency response result of experiment data between FCM and the ARX method.

B. ARX model

ARX model can be described as an autoregressive model with exogenous inputs, which means that the current output of the ARX model corresponds to the past outputs as well as the current and past exogenous inputs. It is a kind of linear system identification model using least mean square method to estimate the parameters of the system. The ARX model can be described by:

$$y(t)+a_1y(t-1)+...+a_{n_a}y(t-n_a) = b_1u(t-n_k)+...+b_{n_b}u(t-n_b-n_k+1)+e(t) \quad (2.25)$$

where,

$y(t)$ - system output at time t

n_a - number of poles

n_b - number of zeros plus 1

n_k - number of input samples that occur before the input affects the output, also called *dead time* in the system

$y(t-1)...y(t-n_a)$ - previous outputs on which the current output depends

$u(t-n_k)...u(t-n_k-n_b+1)$ - previous and delayed inputs on which the current output depends

$e(t)$ - white noise disturbance

A more compact way to write the difference equation is as:

$$A(q)y(t) = B(q)u(t-n_k) + e(t) \quad (2.26)$$

where, q is the delay operator, and

$$\begin{aligned} A(q) &= 1 + a_1 q^{-1} + ... + a_{n_a} q^{-n_a} \\ B(q) &= b_1 + b_2 q^{-1} ... + b_{n_b} q^{-n_b+1} \end{aligned} \tag{2.27}$$

The ARX model uses least mean square method to fit the parameters of the polynomials to the time signals of input and output, resulted in a continuous transfer function in the frequency domain. Thus, it is very convenient to use ARX to get the open loop crossover frequency though the accuracy of system identification will be influenced by the order of the selected polynomials $A(q)$ and $B(q)$. An system identification example using the FCM and ARX method is shown in Appendix A.

2.3 Pilot modelling techniques

2.3.1 Pilot model

The pilot model is a modelling of human operator skill-based control behaviour. It is used to understand the pilot control actions, to predict and explain the PVS behaviour by integrating the pilot dynamics into the vehicle dynamics. If the control tasks are precisely designed, the pilot model can be described using a linear response function and a remnant signal to represent non-linearities[43]. The remnant contains the nonlinear peaks of pilot control and distractions to the pilot. Single-loop control behaviour with visual displays is a general way to develop pilot model[44][45], as shown in Fig. 2.23. The forcing function usually is a sum-of-sine time variable function with different frequencies and random phases. Operator aims to minimize system error $e(t)$.

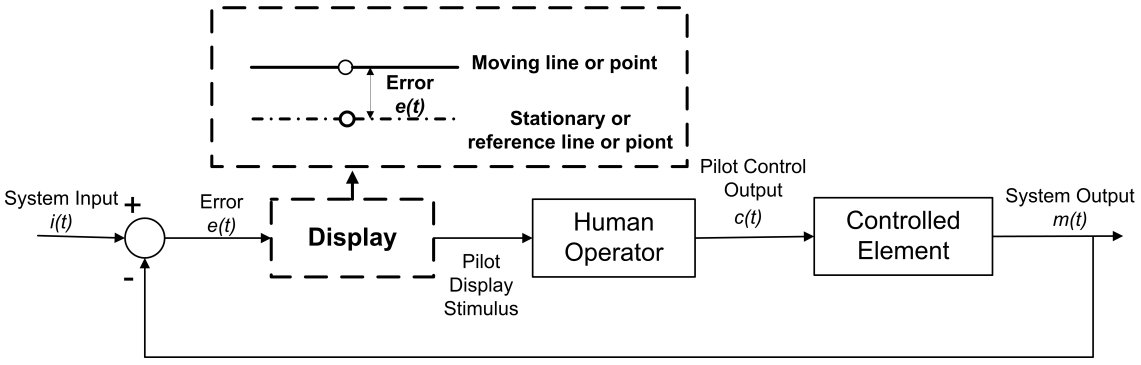

Figure 2.23: Single loop control behaviour system (modified from [46])

According to the Fig. 2.23, the frequency response of the open loop system can be calculated through Eq. 2.28. The crossover frequency then can be obtained from the frequency response.

$$Y_p(s)Y_c(s) = \frac{M(s)}{E(s)} \tag{2.28}$$

where,

$Y_p(s)$ - the transfer function of pilot

$Y_c(s)$ - the transfer function of aircraft

$M(s)$ - the Fourier transform of output $m(t)$

$E(s)$ - the Fourier transform of error $e(t)$

A. Crossover model

It assumed that the system shown in Fig. 2.23 is time stationary. An appropriate pilot model is presented in [46] by McRuer, using a quasi-linear system to describe the characteristics of non-linear PVS as shown in Fig. 2.24. The quasi-linear model now can be

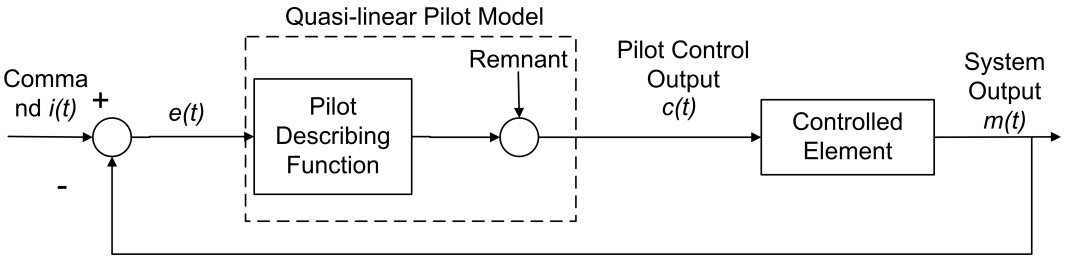

Figure 2.24: Quasi linear pilot model control system (modified from [46])

described as

$$Y_p(s) = K_p \frac{T_L s + 1}{T_I s + 1} \frac{e^{-\tau s}}{T_N s + 1} + \mathrm{R}emnant\_function \tag{2.29}$$

T_L and T_I are pilot characteristics, τ and T_N are pilot's reaction time and muscular delay, remnant function represents pilot non-linear behaviour including pilot's adaptive non-linear reaction and experiments noise. Random inputs and remnant descriptions are the most important of quasi-linear models. Random forcing functions represent the different classes of pilot tasks. The unpredictability of the tasks prevents the pilots getting used to the tasks.

McRuer presented an crossover model that accounts for the important open-loop data trends in the proper crossover frequency region[46]. The assumption was that the pilot's linear behaviour dominates near the crossover frequency. It is a model of the combined pilot/vehicle open-loop behaviour. The crossover model is described as following[46].

$$Y_P(s)Y_C(s) = \frac{\omega_c e^{-\tau_e s}}{s} \tag{2.30}$$

where $Y_P(s)$ is the pilot transfer function, $Y_C(s)$ is vehicle transfer function, ω_c is the crossover frequency, the pilot's adaptive compensation for the controlled element gain[46], τ_e is the sum of all pilot's pure time delays and high frequency lags[45].

B. Bimodal model

A pilot model called bimodal model was presented in [47]. This model assumes that the pilot is a finite capacity single-channel information processor with multiple sensory

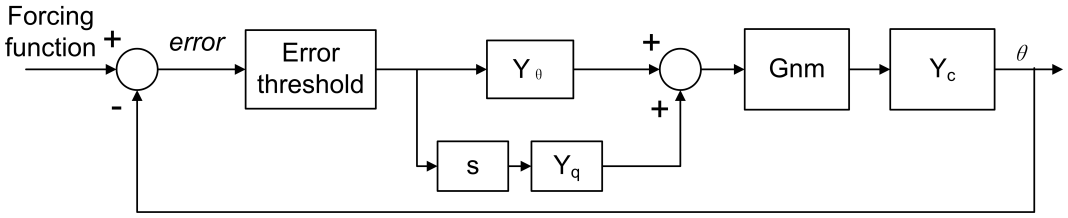

Figure 2.25: Bimodal Model Structure (modified from [47])

inputs. The bimodal model uses both attitude error and error rate feedback paths, as shown in Fig. 2.25. The model can be described by

$$Y_p(s) = (K_{p\theta}\frac{T_{L\theta}s+1}{T_{I\theta}s+1} + K_{pq}s\frac{T_{Lq}s+1}{T_{Iq}s+1})e^{-\tau s}G_{nm}(s) \tag{2.31}$$

where

$K_{p\theta}$ - pilot gain to tracking error.

$K_{p\theta}$ - pilot gain to tracking error rate.

$T_{L\theta}, T_{I\theta}$ - time constant of pilot lead and lag compensation to tracking error.

T_{Lq}, T_{Lq} - time constant of pilot lead and lag compensation to tracking error rate.

$G_{nm}(s)$ - neuromuscular system.

2.3.2 Forcing function

The experiments in this thesis include two tasks, a pure disturbance-rejection task and a pure tracking task as shown in Fig. 2.26 and 2.27.

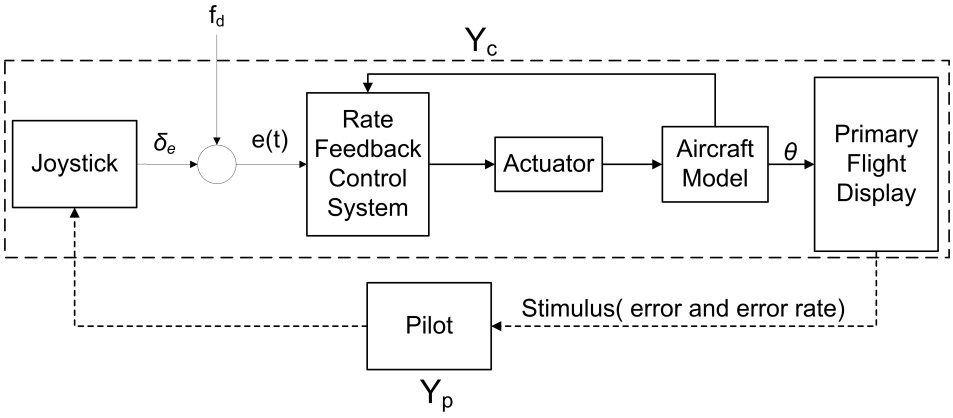

Figure 2.26: Pure disturbance-rejection task

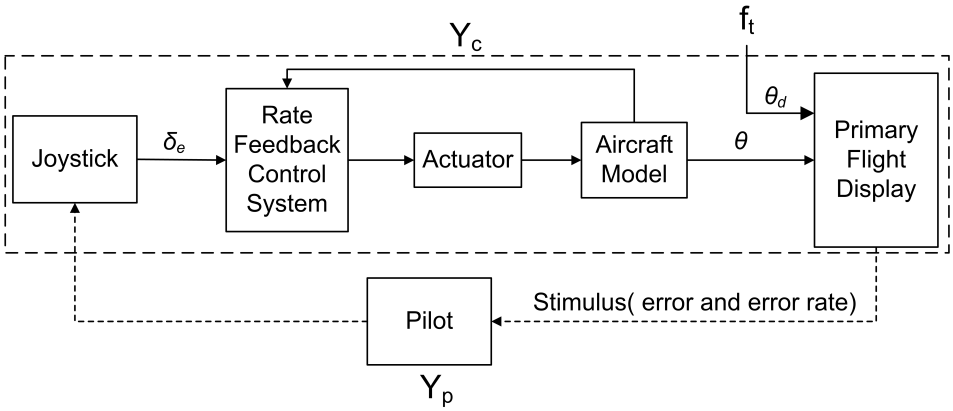

Figure 2.27: Pure tracking task

The disturbance-rejection signal f_d was designed as a quasi-random sum-of-sines defined by

$$f_d(t) = \sum_{k=1}^{N_d} A_d(k) \sin(\omega_d(k)t + \phi_d(k)) \tag{2.32}$$

where the $A_d(k)$, $\omega_d(k)$ and $\Phi_d(k)$ represent the amplitude, frequency and phase of the k_{th} sine term of f_d. The symbol N_d is the number of sine terms, which the disturbance forcing function consists. The Φ_d is a random function to avoid pilot getting familiar with the task. The $A_d(k)$ is chosen to limit the energy of the signal to control the variance of f_d. In order to improve the accuracy of PVS identification, especially for the FCM which is used to analyze the signal at particular identification frequencies. The fundamental sine frequency ω_m should be related to the tests measurement time T_m as $\omega_m = \frac{2\pi}{T_m}$[43]. For the disturbance-rejection training experiment, the run time was set to be $90s$. The data of the first $8.08s$ was discarded since the PVS needs time to stabilize. Thus the fundamental frequency is $\omega_m = \frac{2\pi}{90-8.08} = 0.0767rad/s$. Ten integer multiples of ω_m were selected to form the f_d to ensure no spectral leakage occurs when using the FCM to analyze the measured signals, as shown in Table 2.1.

Table 2.1: Disturbance function

k	n_d	ω_d *(rad/s)*	A_d *(deg)*	k	n_d	ω_d *(rad/s)*	A_d *(deg)*
1	5	0.383	0.048	6	71	5.446	0.684
2	11	0.844	0.175	7	101	7.747	0.866
3	23	1.764	0.381	8	137	10.508	1.152
4	37	2.838	0.502	9	171	13.116	1.496
5	51	3.912	0.581	10	226	17.334	2.212

The tracking task is a discrete signal formed by a combination of steps and ramps over a period of 120 seconds as shown in Fig. 2.28. This discrete task requires the pilot to perform high gain inputs which is suitable for PIO evaluation.

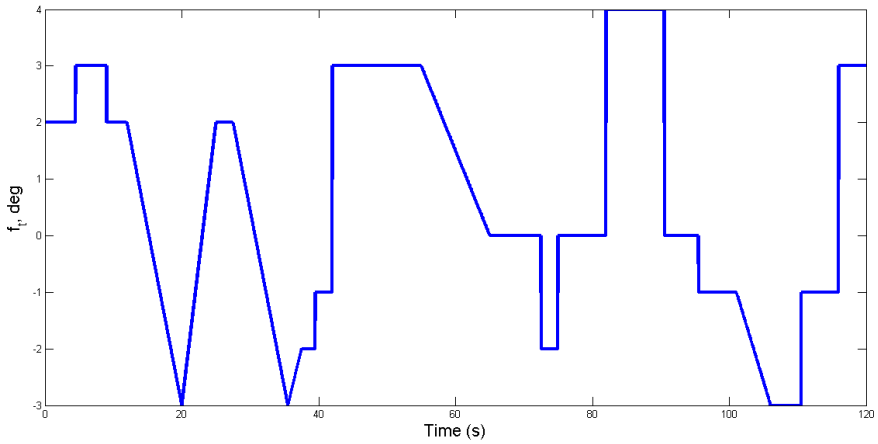

Figure 2.28: Discrete steps and ramps tracking signal (modified from [48])

2.4 Methodology

In this literature review, relevant PIO evaluation criteria, PIO detection and mitigation methods were introduced. After the review, this thesis presents a real time PIO detection system focuses on the trend of pilot behaviour besides other traditional PIO characteristics, together with a mitigation system using adaptive controller. This PIO detection system predicts the trend of pilot movement to reduce false PIO detection during oscillations.

This PIO detection and mitigation system consists of three main parts, which are detector, indicator and compensator. In the detector, a sliding window STFT method, a peak-to-peak time domain calculation method and an ARX model were selected to calculate PIO characteristics. The STFT method was selected for the reason of increasing the real time calculation speed. The ARX system identification model was used to identify the open loop transfer function of PVS. This ARX model considers the PVS as a black box to avoid complicated modelling of the pilot model. The rate of change in crossover frequency can be calculated after the system identification. This rate of change in crossover frequency was selected as a new PIO feature parameter since it reflects the moving trend of pilot stick input gain during PIOs.

A Boeing-747 aircraft model was established for the simulation tests. Since Boeing-747 is well damped even without SAS. Three longitudinal classical pitch rate attitude control laws were designed to make the model PIO prone. Bandwidth and Gibson Criterion were used to assess the control laws.

Related research in [49], [19] and [50] show the influence of forcing function, pilot model, the nonlinear command gearing and actuator rate-limiting effect on PIO events during piloted tests. Such results were used directly in this thesis to avoid the duplication of work. Thus, the pilot modelling techniques and nonlinear effects of the system will only be introduced briefly.

In the piloted trials, a primary flight display(PFD) interface was modified to give the PIO cue warning. First, disturbance-rejection training tasks were performed by engineering students in Boeing-747 model. These disturbance-rejection tests were performed to tune the aircraft model and detection and mitigation system, to prepare suitable tasks for piloted trials. Second, the detection and mitigation system was evaluated in a discrete piloted tracking tests. Results from PIO tests conducted on desktop PCs were presented and compared with those obtained from implementing the ROVER module.

Chapter 3

Control law design

This control law design exercise is done to present the subject with vehicle dynamics that have different PIO tendencies according to the Bandwidth and Gibson Dropback Criteria. Since the purpose of the piloted trials is to evaluate the PIO detection and mitigation system, such control law modifications ensure a higher likelihood that PIOs can be triggered during a tracking task.

3.1 Longitudinal aircraft model

3.1.1 Longitudinal equations

Since this thesis focuses on the longitudinal PIO events, only the longitudinal dynamics are studied. Without the atmospheric disturbance, the longitudinal dynamics of the aircraft can be written as following[19]:

$$[\mathbf{M}_{long}(\rho)]\begin{bmatrix}\dot{u}\\ \dot{w}\\ \dot{q}\\ \dot{\theta}\\ \dot{h}\end{bmatrix} = [\mathbf{A}_{long}(\rho)]\begin{bmatrix}u\\ w\\ q\\ \theta\\ h\end{bmatrix} + [\mathbf{B}_{long}(\rho)]\begin{bmatrix}\delta_e\\ \delta_\tau\end{bmatrix} \tag{3.1}$$

where

$$\mathbf{M}_{long}(\rho) = \begin{bmatrix}1-X_{\dot{u}} & X_{\dot{w}} & 0 & 0 & 0\\ Z_{\dot{u}} & 1-Z_{\dot{w}} & 0 & 0 & 0\\ M_{\dot{u}} & M_{\dot{w}} & 1 & 0 & 0\\ 0 & 0 & 0 & 1 & 0\\ 0 & 0 & 0 & 0 & 1\end{bmatrix} \tag{3.2}$$

$$\mathbf{A}_{long}(\rho) = \begin{bmatrix} X_u & X_w & X_q - W & -g\cos\Theta & 0 \\ Z_u & Z_w & Z_q + U & -g\sin\Theta & 0 \\ M_u & M_w & M_q & 0 & 0 \\ 0 & 0 & 0 & 1 & 0 \\ \sin\Theta & -\cos\Theta & 0 & U\cos\Theta + W\sin\Theta & 0 \end{bmatrix} \tag{3.3}$$

$$\mathbf{B}_{long}(\rho) = \begin{bmatrix} X_{\delta_e} & X_{\delta_\tau} \\ Z_{\delta_e} & Z_{\delta_\tau} \\ M_{\delta_e} & M_{\delta_\tau} \\ 0 & 0 \\ 0 & 0 \end{bmatrix} \tag{3.4}$$

The ρ represents the scheduling parameters. These parameters are unknown a priori but are continuous in time. The matrices described in Eq.3.2$\sim$3.4 vary linearly with Mach number and altitude. The altitude is also an explicit state variable where as Mach number is an implicit variable in the state basis. Since the scheduling parameters are part of the state basis, the model presented here can be categorised as a quasi linear parameter varying system[19].

3.1.2 Flight condition and actuator models

A quasi-linear parameter varying Boeing-747 longitudinal aircraft model was used to evaluate the PIO detection and mitigation system using Eq.3.1$\sim$3.4. PIOs usually occur in approach and landing because of the influence of disturbance, wind shear and vortex, together with the high accurate track demand in this flight stage. Thus, a flight altitude of $20000ft$ and a Mach number of $0.5M$, is selected to simulate the low speed approach condition for the piloted trials. The longitudinal dynamics can be described by the equations shown in Appendix B[19][51].

The control surface actuators and throttle actuator are modelled as second order transfer function with actuator rate limits and saturation in the aircraft model. The elevator actuator model has a rate limit of 37 degrees/s and a saturation of 25 degrees[52]. It is described by

$$\frac{\delta_e(s)}{\delta_{ec}(s)} = \frac{450}{s^2 + 30s + 450} \tag{3.5}$$

The throttle actuator transfer function is described by

$$\frac{\delta_\tau(s)}{\delta_{\tau c}(s)} = \frac{10}{s + 10} \tag{3.6}$$

3.1.3 Flight control law design

The original aircraft model was supplied by in-house code. A linear model was established as shown in Appendix B. The pitch rate open loop transfer function of the aircraft can be obtained as following:

$$\frac{q(s)}{\delta_{ec}(s)} = \frac{-489.5s(s+0.01578)(s+0.4002)}{(s^2+0.0055s+0.0063)(s^2+0.9283s+1.157)(s^2+30s+450)} \tag{3.7}$$

The root locus of the pitch rate open loop transfer function is shown in Fig. 3.1.

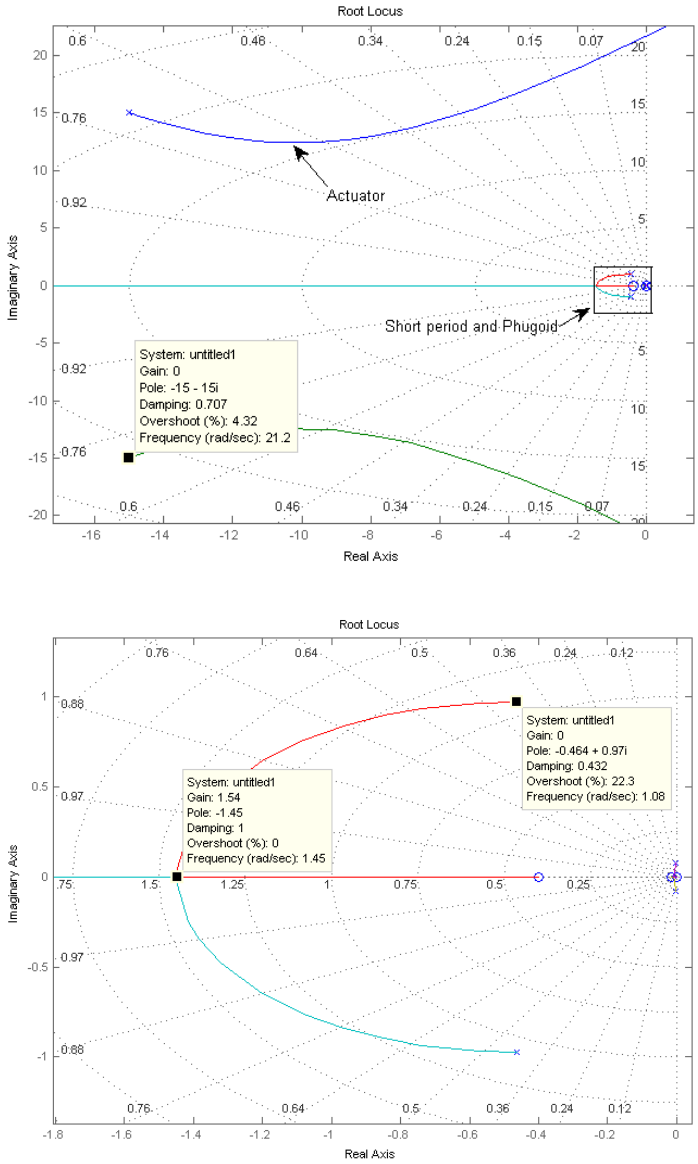

Figure 3.1: Root Locus of Pitch rate open loop function

It can be seen that the short period damping can be increased to 1 by varying the feedback gain but the short period pitch oscillation(SPPO) frequency does not change too much. Thus, classical Proportional and Integral(PI) controllers were introduced. These controllers were designed to relocate the zeros and poles of the transfer function. Thus, the aircraft handling qualities can be designed to have moderate or severe PIO tendencies for the piloted tests.

Three different pitch rate attitude hold PI controllers were evaluated using the Gibson Dropback Criterion and Bandwidth Criterion in different flight conditions, the results are shown in Fig. 3.2∼3.7. The control law design aimed to find suitable controller in certain flight condition or vice versa to put the handling qualities in different PIO regions.

It can be seen from Fig. 3.2∼3.4 that the bandwidth of the three controllers decreased as either the altitude or the Mach number increased. The Fig. 3.5∼3.7 show that the dropback and overshoot increased slightly as the speed and altitude increased. A high proportional gain leads to a large change in the output for a given input, but oscillations will happen if the proportion gain is too large. Increasing integral gain will reduce the control error but will increase the overshoot. It can be seen from these tests that the proportional gain has to be decreased to get better control quality when the speed and the altitude increase.

Another phenomenon shown in these six figures was that the selected three control laws were separated into three PIO regions in Bandwidth Criterion but the differences were small in Gibson Criterion. Such phenomenon indicates that both frequency domain and time domain criterion should be considered during flight control law design.

The following three PI controllers were selected in flight condition *M=0.5, Alt=20000ft*. The Bandwidth and Gibson Criteria evaluation of these three controllers are shown in Fig. 3.8 and 3.9. The aircraft is located in level 2 PIO region with C2 controller and is located in level 3 PIO region with C3 controller.

Controller 1 is defined by

$$C1 = -3.5(1 + \frac{2}{s}) \tag{3.8}$$

Controller 2 is defined by

$$C2 = -1.2(1 + \frac{5}{s}) \tag{3.9}$$

Controller 3 is defined by

$$C3 = -0.2(1 + \frac{5}{s}) \tag{3.10}$$

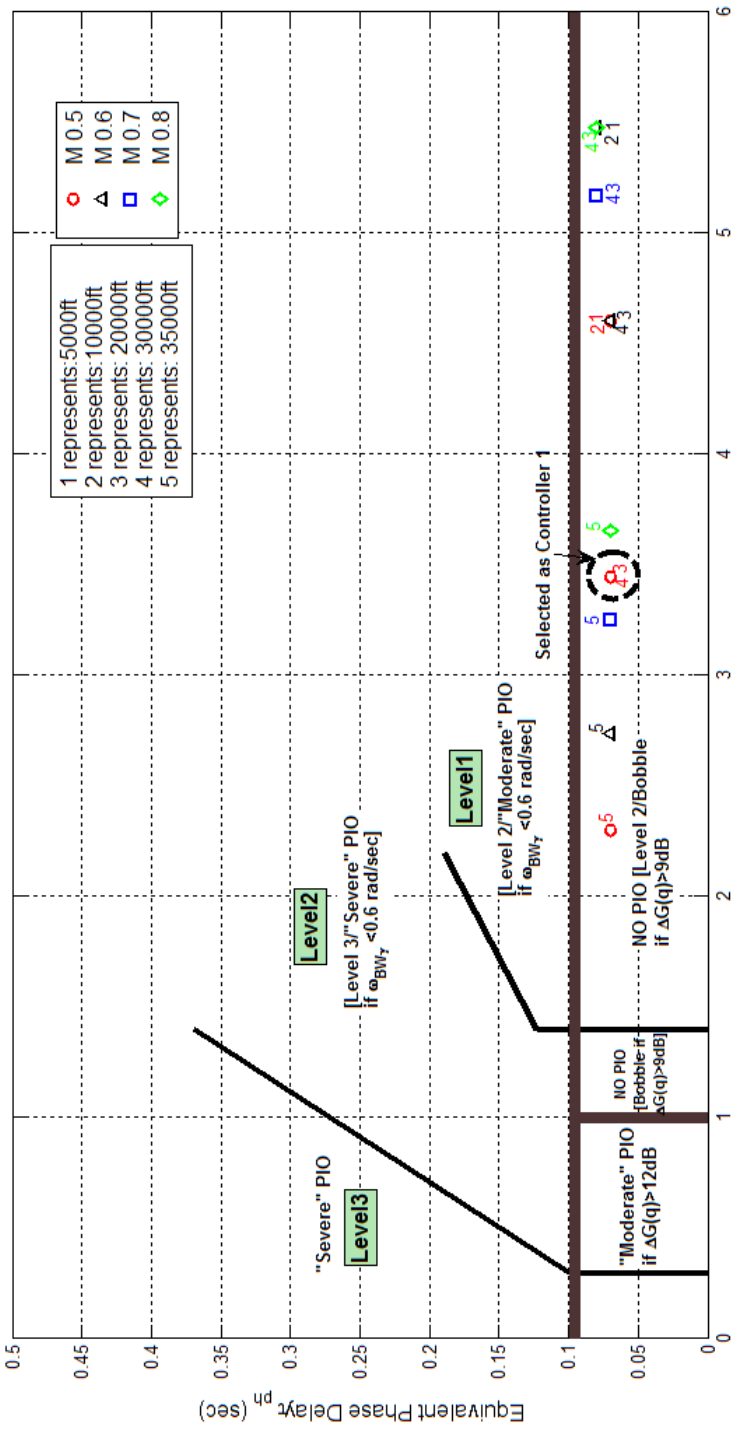

Figure 3.2: Bandwidth Criterion evaluation - Controller 1

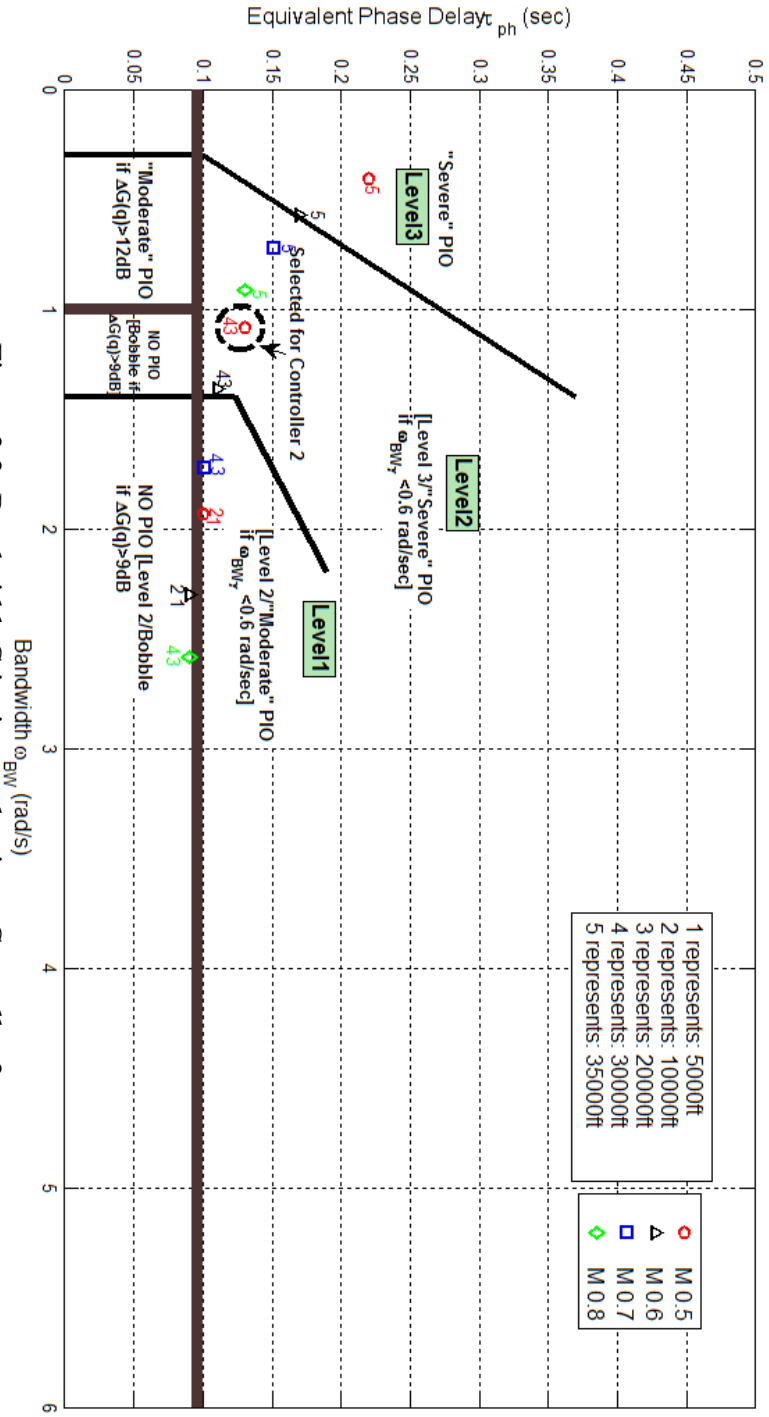

Figure 3.3: Bandwidth Criterion evaluation - Controller 2

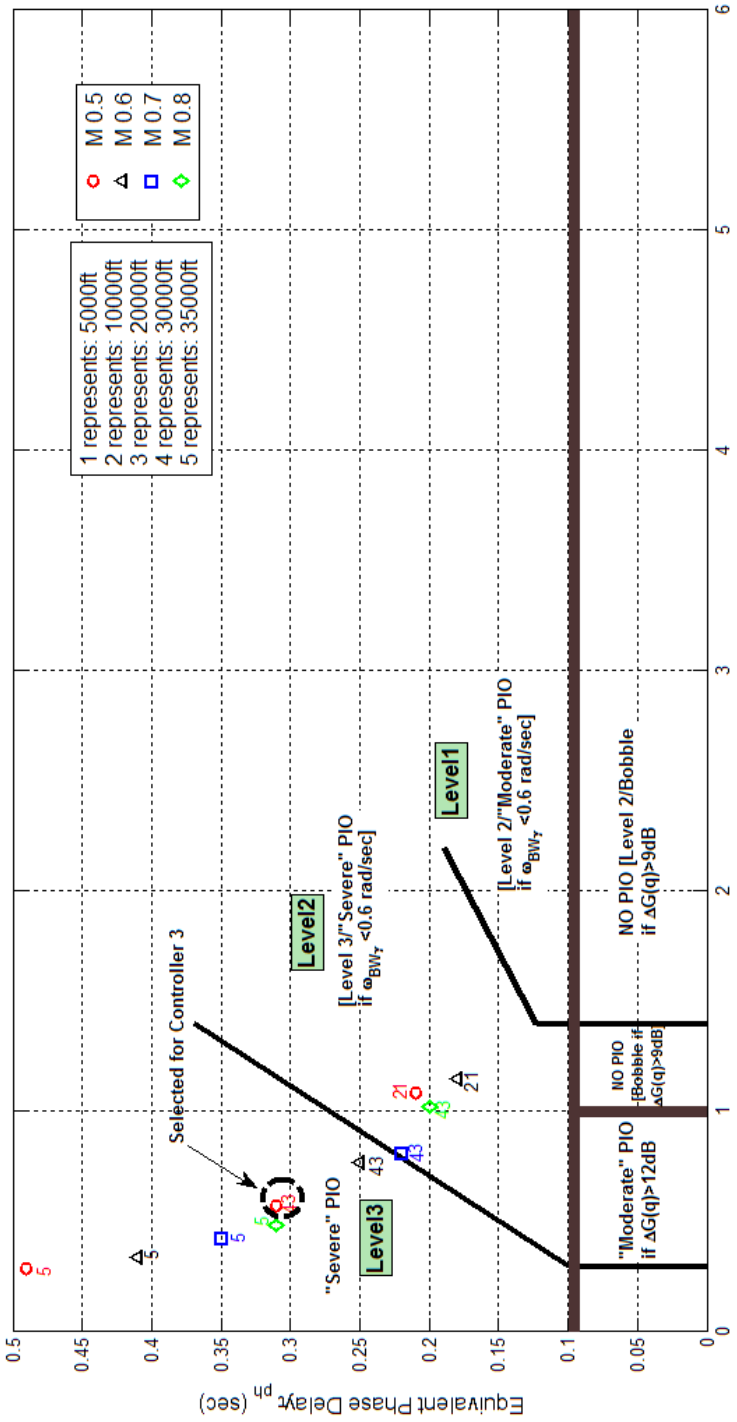

Figure 3.4: Bandwidth Criterion evaluation - Controller 3

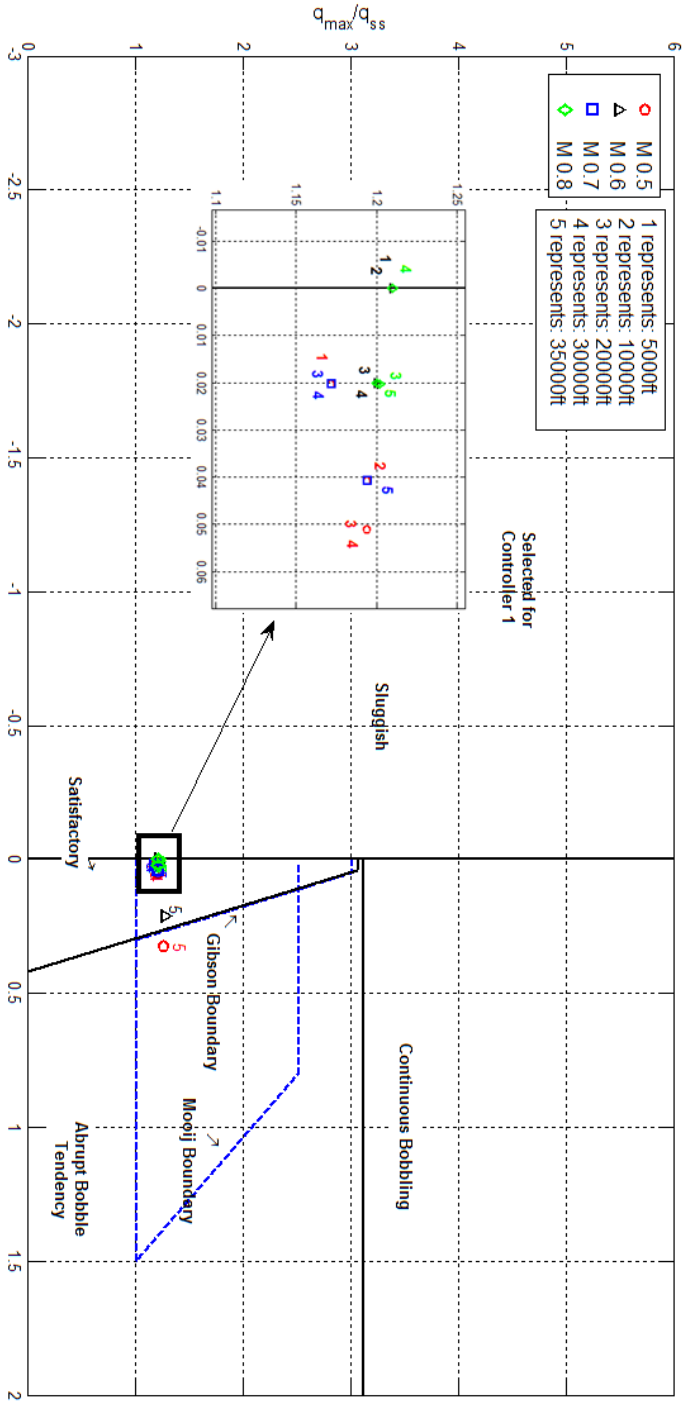

Figure 3.5: Gibson Criterion evaluation - Controller 1

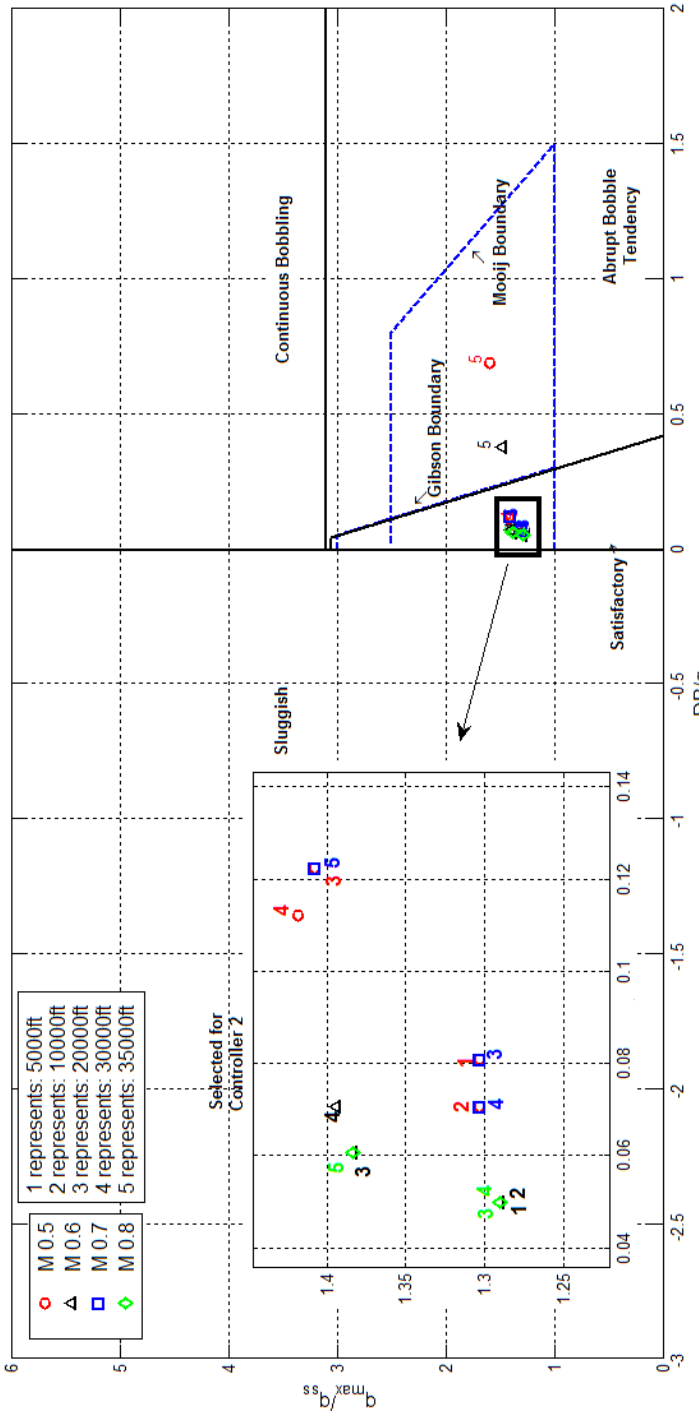

Figure 3.6: Gibson Criterion evaluation - Controller 2

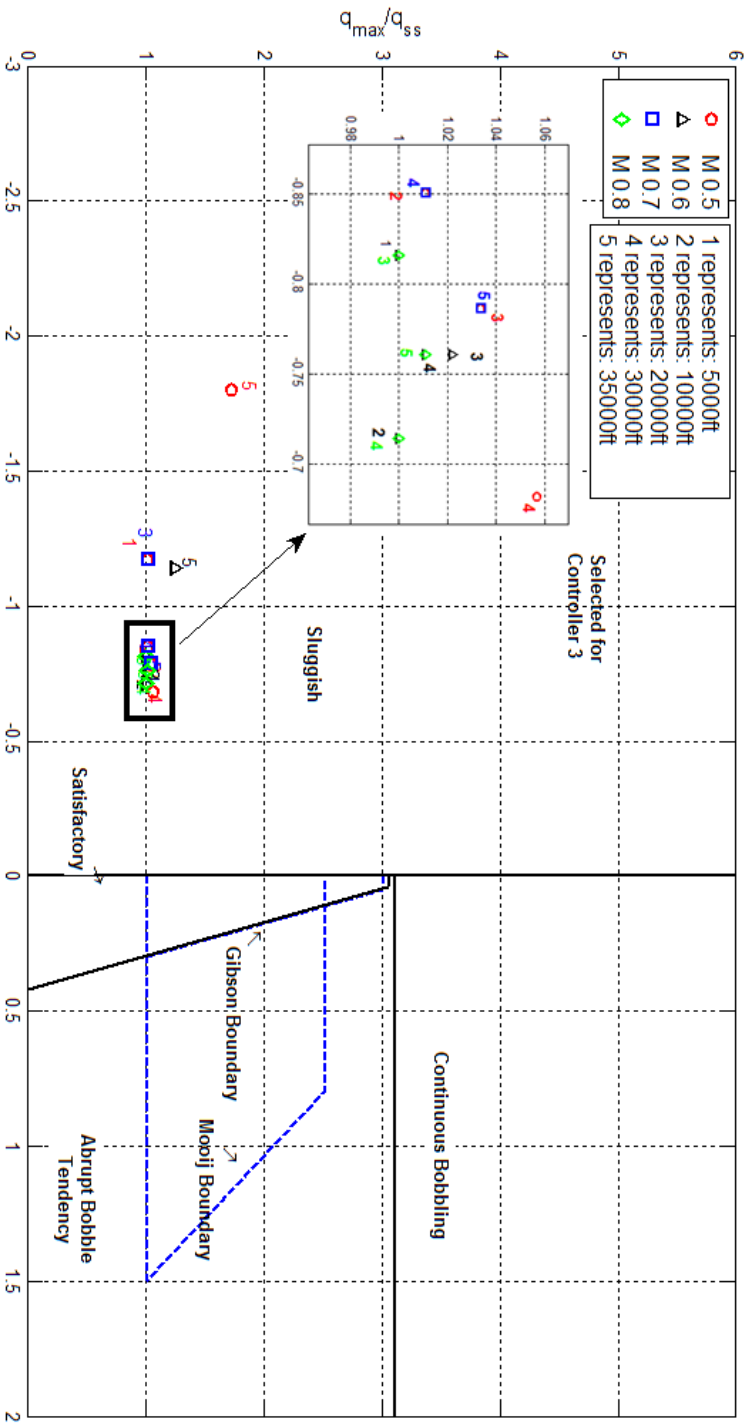

Figure 3.7: Gibson Criterion evaluation - Controller 3

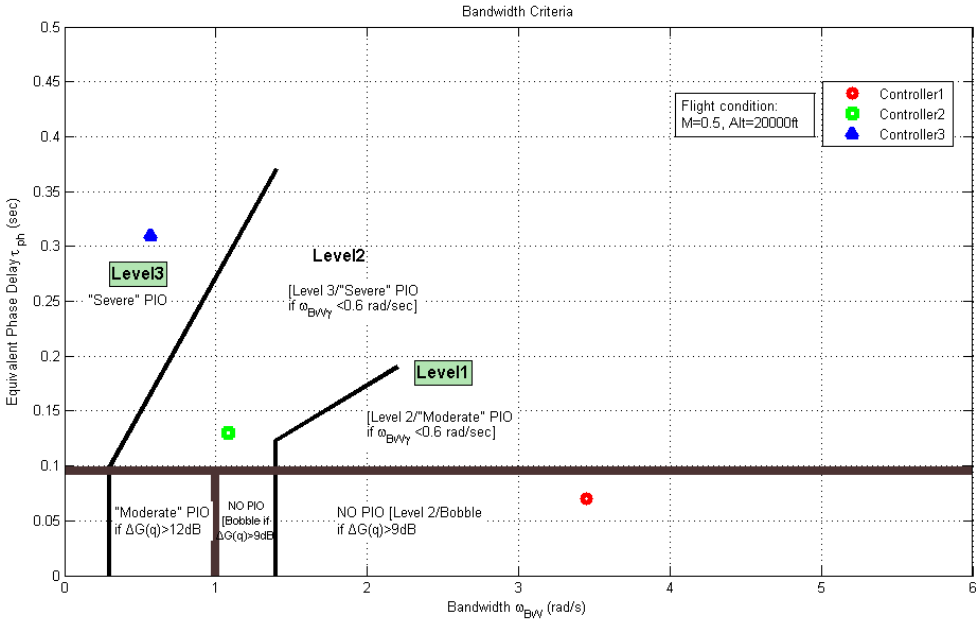

Figure 3.8: Bandwidth Criterion evaluation of selected controllers

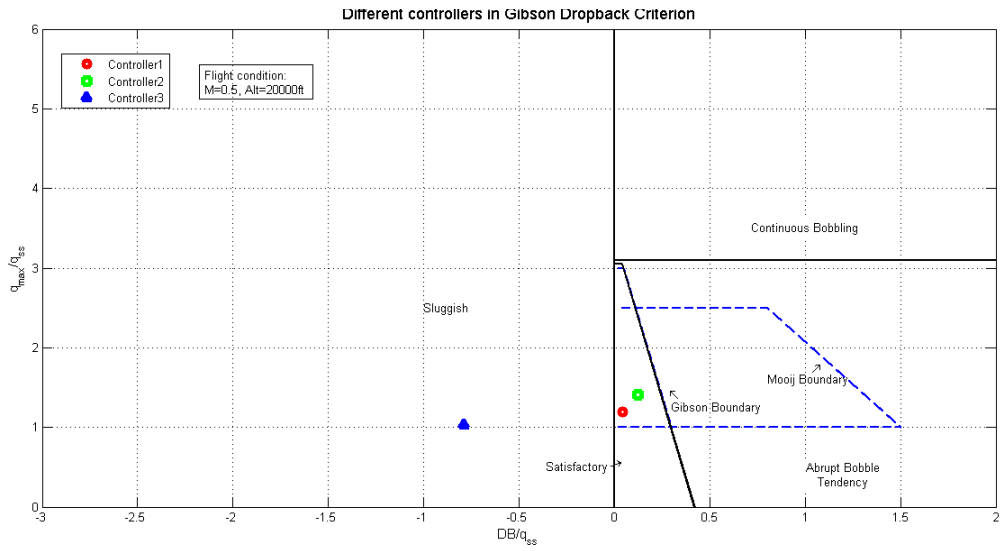

Figure 3.9: Gibson Dropback Criterion evaluation of selected controllers

The pitch rate to elevator command closed loop transfer functions with the three PI controllers can be obtained as follows:

C1:

$$\frac{q(s)}{q_c(s)} = \frac{1713.3679s(s+2)(s+0.4002)(s+0.01578)}{s(s+0.3447)(s+0.01835)(s^2+5.224s+12.17)(s^2+25.35s+323.5)} \frac{rad/s}{rad/s} \tag{3.11}$$

C2:

$$\frac{q(s)}{q_c(s)} = \frac{587.4411s(s+5)(s+0.4002)(s+0.01578)}{s(s+0.3428)(s+0.01877)(s^2+1.532s+8.156)(s^2+29.04s+415.5)} \frac{rad/s}{rad/s} \tag{3.12}$$

C3:

$$\frac{q(s)}{q_c(s)} = \frac{97.9068s(s+5)(s+0.4002)(s+0.01578)}{s(s+0.1795)(s+0.03708)(s^2+0.8696s+2.15)(s^2+29.85s+444.4)} \frac{rad/s}{rad/s} \tag{3.13}$$

The aircraft pitch rate and pitch angle time response are shown in Fig. 3.10. It can be seen that system with C1 has better handling quality than C2 and C3. The overshoot of C1 is only 1.18. The pitch rate time response settled down within $2.5s$ without oscillations. The system with C2 experiences slight oscillations, while the system with C3 has sluggish response. The dynamic mode properties are shown in Table 3.1. The system with C1 has a short period damping of 0.749 and a short period natural frequency of $3.49rad/s$. The system with C2 or C3 has low short period damping near 0.3. The C2 and C3 drive the aircraft into PIO prone tendencies. This is suitable for the assessment of the PIO detection and mitigation system.

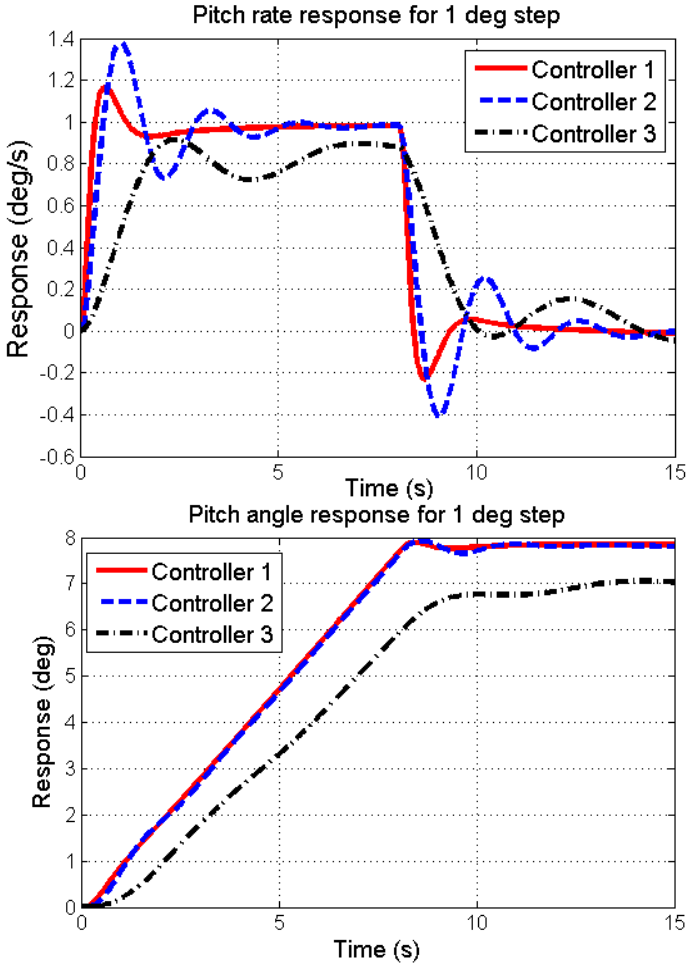

Figure 3.10: Pitch rate and pitch angle time response

Table 3.1: Aircraft dynamic mode properties

	NO SAS	C1	C2	C3
SPPO mode(ω_n(rad/s), ζ)	1.08,0.432	3.49,0.749	2.86,0.268	1.47,0.297
Phugoid mode(τ_p(s))	79.3	2.9,54.5	2.9,53.3	5.57,26.97

3.2 Control law test and modification

When a linear PI control system is designed for the control of plant with nonlinearities like rate-limiting and saturation, the integral part may become very large due to saturation and the integration lasts for a long time, this is called windup effect. Windup represents an undesirable transient in the process output caused by nonlinearities like saturation when a controller with integrators is used[53]. Such effect may lead to big oscillations or limit cycle phenomenon. Anti-windup represents precautions in the controller to keep it from winding up[53]. One simple anti-windup method is to keep the integrator output value within limits when differences occur between the pre saturation signal and post saturation signal.

A simple back-calculation method was used to alleviate the windup effect. As shown in Fig. 3.11, a saturation has the same saturation limit as actuator was added after the conventional PI controller. The difference between post and pre saturation signals feeds back to the input of the PI controller. The feedback will reduce the input when saturation happens. Thus, the oscillations caused by the integrator can be suppressed. The windup problem can not be eliminated by this method since the integrator can still keep accumulating the error caused by the actuator saturation or rate-limiting. One way to solve this problem is to reset the integrator. However, the aim of this thesis is to detect and mitigate PIO. Mild windup effect can be helpful for the PIO detection tests.

Fig. 3.12 shows a test setup for the system integrated with C1 controller and simple back-calculation units. The command gearing is described by Eq. 3.14[50]. The windup effect can be seen from Fig. 3.13. The stick input δ_{stick} is -0.6, the inceptor gain is -1.5, then the input to the command gearing is 0.9, which is one of the turning points of the command gearing. The nonlinear gain changing caused by the command gearing will increase the rate of change in stick input, this change may trigger the rate-limiting, finally leads to the limit cycle. It is clear that when the magnitude hits the saturation of the actuator, the integrator resets to zero and starts integrate again periodically. The frequency of the limit cycle is about $1.8rad/s$. A simple analysis of this limit cycle phenomenon is introduced in Appendix C.

$$\frac{\delta_{NZ}}{\delta_s} = \begin{cases} -4 & -1 \leq \delta_s \leq -0.5 \\ -1 & -0.5 < \delta_s \leq 0.9 \\ -16 & 0.9 \leq \delta_s \leq 1 \end{cases} \tag{3.14}$$

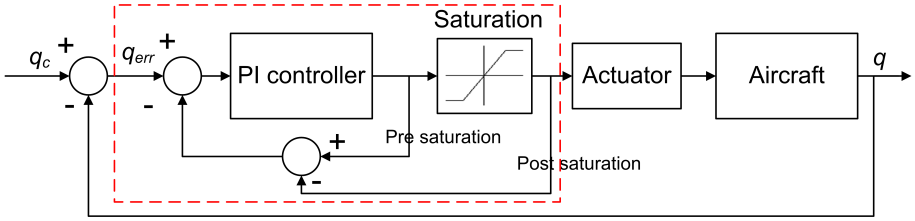

Figure 3.11: Simple anti-windup PI controller

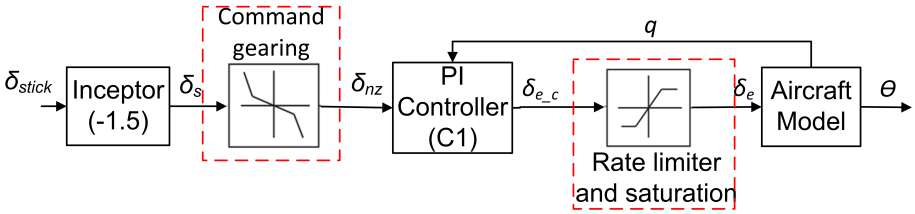

Figure 3.12: Test setup for PI windup effect

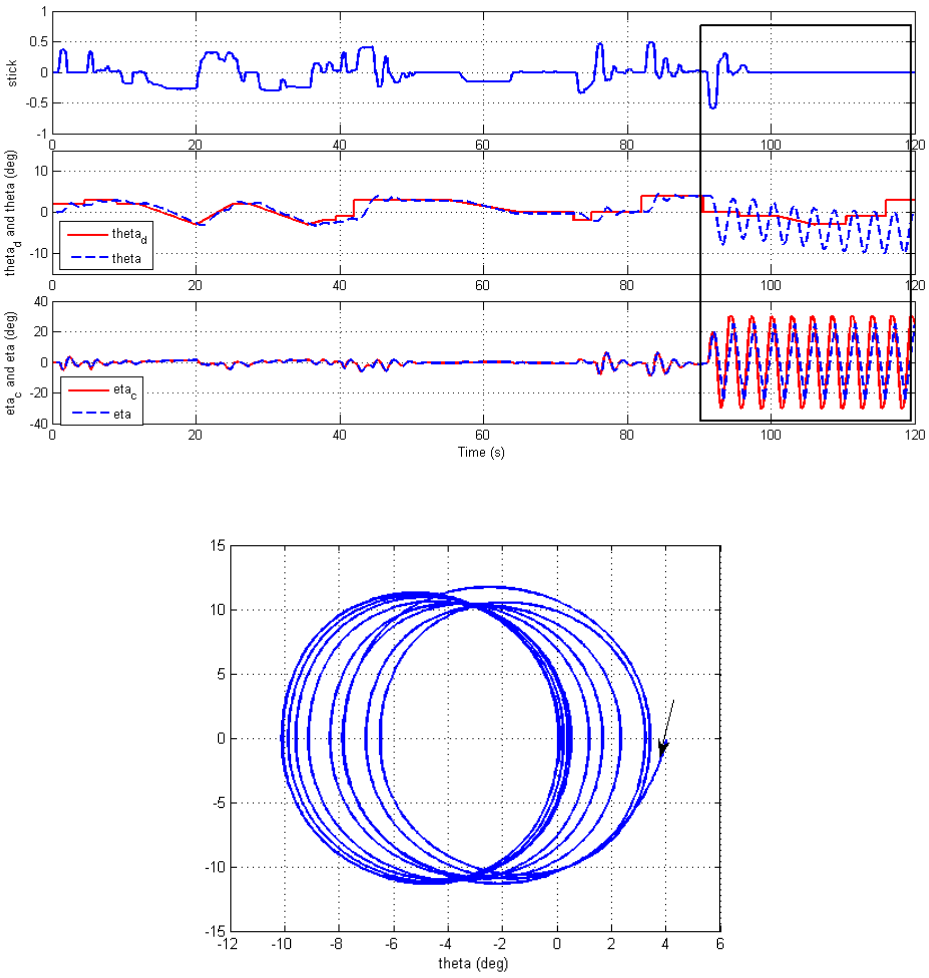

Figure 3.13: Limit cycle phenomenon with PI controller C2

Chapter 4

Detection and mitigation system design

A PIO online detection and mitigation system is presented in this chapter. The system contains three main parts which are PIO characteristics detector, tendencies indicator and compensator. The detector is based on STFT, ARX and time domain peak-to-peak calculation methods. The indicator contains a PIO tendencies logic algorithm and a PIO visual cue. The compensator is designed to adjust the stick input gain. The structure of the detection and mitigation system placement within the overall PVS is shown in Fig. 4.1.

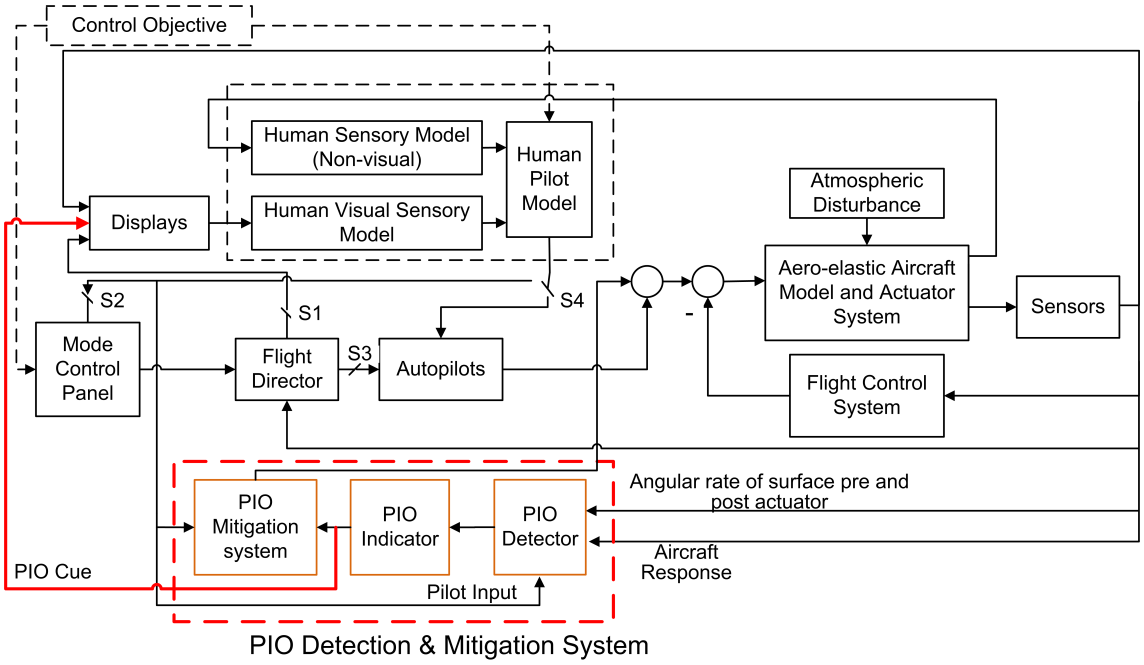

Figure 4.1: Structure of PIO detection and mitigation system

4.1 Characteristics detector

With reference to Chapter 2, six PIO feature parameters were selected: the rate of change in crossover frequency, magnitudes of stick input and pitch rate, the difference between the pre and post actuator signal, main frequency of the oscillation and phase difference between stick input and pitch rate.

Flying qualities can generally be categorized into "unattended", large amplitude manoeuvring and "closed-loop" control[21]. "Closed-loop" control means that pilot's operations are more or less affected by the differences between aircraft's desired and actual outputs[21]. The pilot is always trying to follow the control task or to reduce the control error caused by disturbances. For instance, when the aircraft encounters oscillations caused by a vortex or a gust during the approach or landing, the instinct response of the pilot is to increase his gain to eliminate the oscillations or tracking error. This operation will increase the crossover frequency of the PVS system. If the pilot realizes that his inputs are making the oscillations worse, he will reduce his gain or even let go of the inceptor to avoid the amplification. As shown in Fig.4.2, the crossover frequency of the open loop PVS is affected by the control effort of pilot. During oscillations, intensive control drives the crossover frequency towards aggression area.

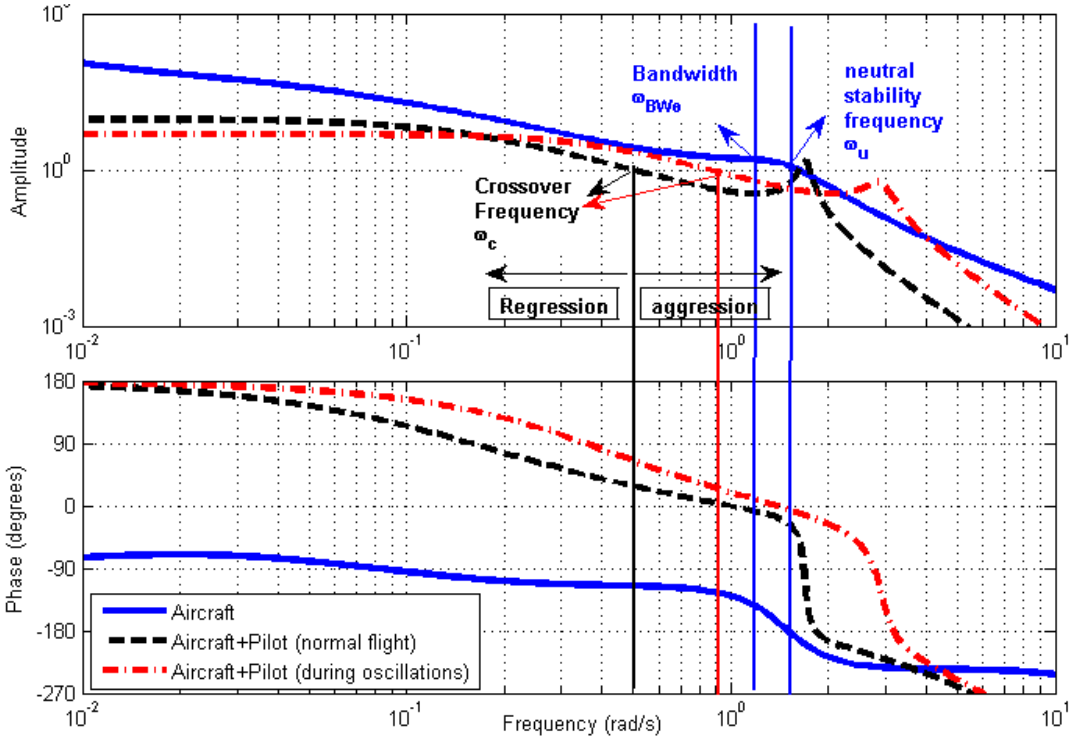

Figure 4.2: Regression and aggression control

Several models have been developed to present pilot behaviour as accurately as possible,

such as the crossover model[44], the bimodal and the precision model[45], the optimal controller model(OCM)[21] and the multi-channel model[54]. The crossover model has been proven to be reasonably accurate in describing pilot behaviour[44]. It can provide a clear statement of the relationship between pilot adaptation and the aircraft near the crossover frequency. However, it is still hard to describe the pilot separately and accurately during a real flight since the pilot control is affected by many factors, such as visual and motion cues. In order to predict the crossover frequency more accurately in real time, a linear ARX model was used for system identification. It was based on the assumption that the aircraft is linear except for the actuator and command gearing and pilot behaviour is linear except for the white noise remnant. After system parameter estimation, the rate of change in crossover frequency can be calculated. When this rate of change is positive, it means the pilot is moving towards aggressive control, which is an indication of PIO trend. Hence, the rate of change in crossover frequency gives a sign of potential PIO tendency.

The structure of detector is shown in Fig. 4.3. The inputs of the detector consist of six signals. These signals are filtered and transferred to the ARX calculator, the time domain calculator and the STFT calculator. After calculation, six PIO feature parameters are output to the indicator.

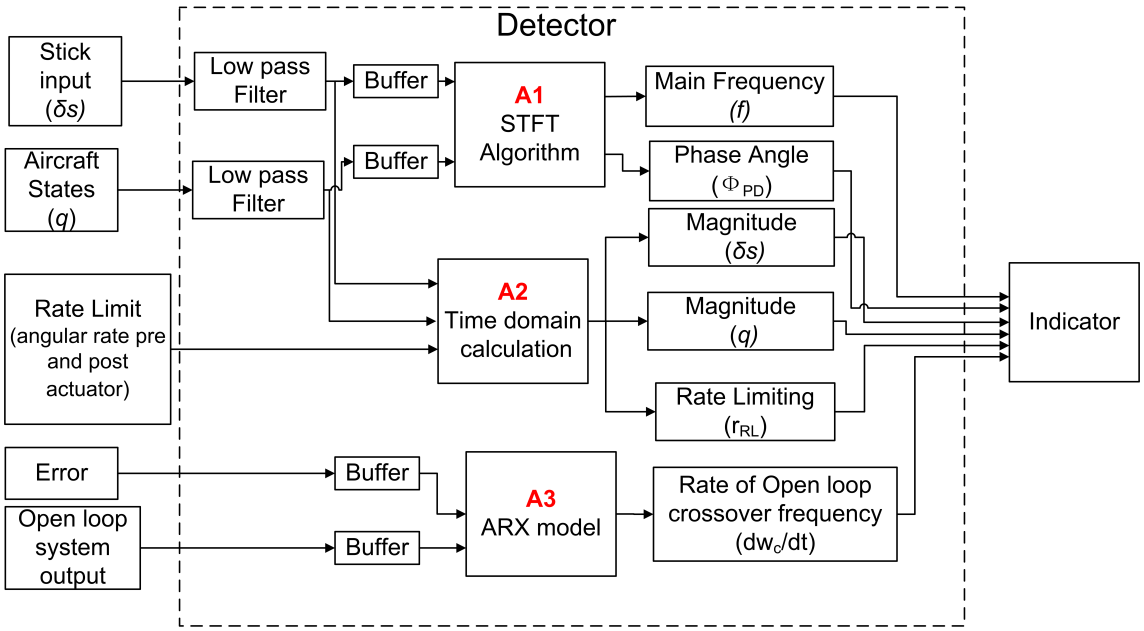

Figure 4.3: Structure of PIO detector

4.1.1 ARX calculator

The ARX based calculator calculates the system open loop frequency response. As shown in Block A3, Fig. 4.3, the inputs of the ARX model are tracking error and pitch angle. The ARX calculator includes a buffer and a processor. The buffer is coupled to receive

and store system input and output data. The processor is adapted to the buffer and is coupled to output characteristics parameters to the indicator. First, the buffer receives the system input and output data at successive time increment Δt and stores them over a predetermined time interval which is initialized as 2.56 seconds. The stored data in the buffer will be updated every 0.32 seconds. Second, the ARX model processor performs system identification to get the system open loop transfer function. Third, the crossover frequency is obtained by calculating the frequency response of the transfer function. The rate of change in crossover frequency can be calculated by dividing the difference of the crossover frequency between the present and the previous over 0.32 seconds. The Matlab function ARX is used to form the ARX processor. The structure of ARX model including the orders $[n_a \;\; n_b]$and time delay $[n_k]$ is optimized using Matlab function $struc$, $arxstruc$, and $selstruc$. The parameters n_a and n_b denote the dominator and numerator orders of the ARX model, and n_k denotes the delay of the system. By using the buffer to change the sample data into frame data, the ARX can be used to perform PVS identification. This ARX model can help to get the crossover frequency of the open loop transfer function without complicated modelling of pilot model. This simplification can increase the calculation speed and detect the PIO characteristics in real time.

Ten series of Off-line data obtained from compensatory training and tracking training was selected to do the ARX structure optimization. There are two reasons for selecting ten series data to perform the optimization. First, the author did not get enough data from different test pilots. Second, it was found that the results of the ARX model structure were similar during these ten off-line optimization tests. Thus, the author deemed that ten optimization tests were enough. For the compensatory task, the optimization results are shown in Fig. 4.4. It can be seen that the unexplained output variance decreases when the order of the structure(Number of par's) increases. However, the variance remains unchanged when the ARX order reaches 7. The ARX structure of $[na \;\; nb \;\; nk] = [6 \;\; 6 \;\; 17]$ has the best fit. The structure of $[na \;\; nb \;\; nk] = [4 \;\; 3 \;\; 30]$ has similar result but with a much lower order. In consideration of increasing the real time processing speed of the detector, the latter one is selected.

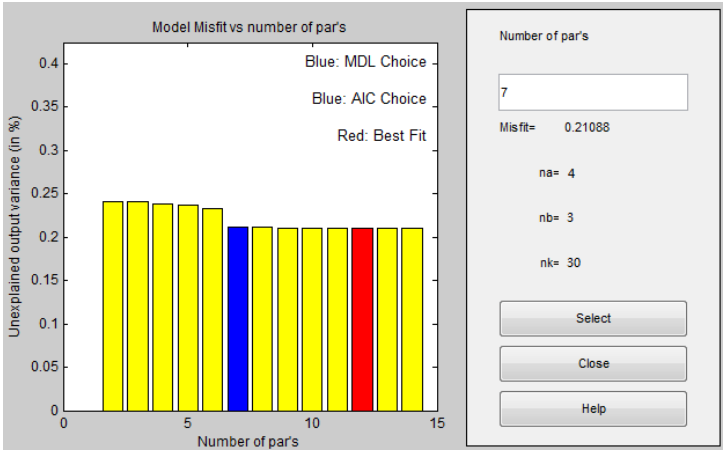

Figure 4.4: ARX model order selection (Run No.9)

The selected ARX structure was validated through two methods. First, the raw time domain data was converted into frequency domain using FCM. The frequency response results were compared with the ARX results. Second, the estimated system output was compared to the actual system. The results are shown in Fig. 4.5. It can be seen that the frequency response of ARX model and FCM are consistent below $3rad/s$. The crossover frequency is about $0.5rad/s$. The frequency response results from ARX and FCM are similar. This indicates that the system can be assumed to be linear. The results from FCM experienced oscillations after the frequency of $5rad/s$. It disclosed the pilot's nonlinear control at which the frequency was out of the crossover frequency region.

The ARX model output and real output has a linear correlation of 76.485%. This correlation was calculated by Eq. 4.1. The error was probably due to the nonlinearities of the system. As can be seen from the figure, the ARX output deviate from the real output during nonlinear peaks and high frequency oscillations. Other test data show similar results, see Appendix D. It should be noticed that during these optimization tests and the piloted tests, no boundary noise was included in the input signal. The noise sensitivity will be evaluated in the future work.

$$\rho_{y,ye} = \frac{\mathrm{cov}(y, ye)}{\sigma_y \sigma_{ye}} \tag{4.1}$$

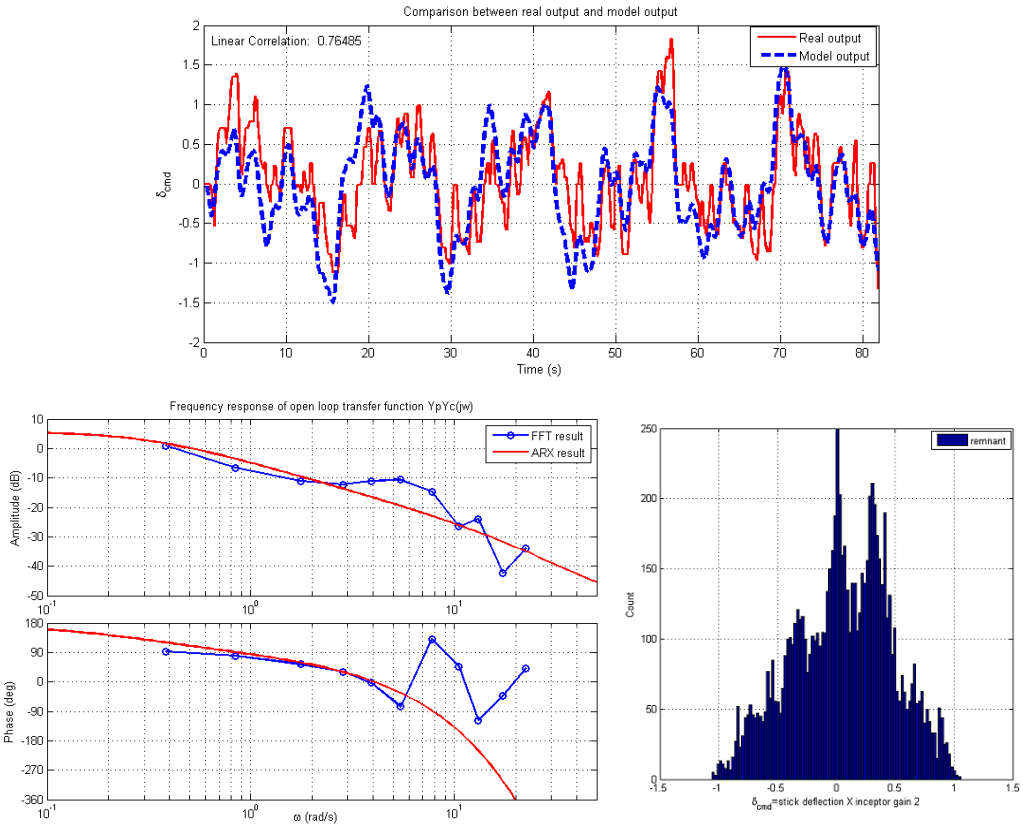

Figure 4.5: ARX model order validation

4.1.2 Time domain calculator

Peak-to-peak calculator

Magnitudes of stick input and pitch rate were calculated using a peak-to-peak method in the time domain, as shown in Block A2, Fig. 4.3. The calculation method for maximum command/pitch rate is described as following. If $g[T(k-1)] - g[T(k-2)] > 0$ and $g[T(k)] - g[T(k-1)] < 0$, then outputs $g[T(k-1)]$, else outputs the former peak value. Here T represents the time step, k represents the integers larger than 2, and $g[kT]$ represents the value of command/pitch rate in time kT. The calculation method for minimum command/pitch rate is similar but with an adverse judgment, which is $g[T(k-1)] - g[T(k-2)] < 0$ and $g[T(k)] - g[T(k-1)] > 0$. Relevant Simulink Blocks were used to build the calculator which can realize time domain peak-to-peak calculation methods. This peak-to-peak calculator can roll forward to detect the newest maximum/minimum oscillation peaks in real time. Oscillation magnitudes of command and pitch rate can be obtained by the newest maximum and minimum peaks.

The structure of the peak-to-peak calculator is shown in Fig. 4.6.

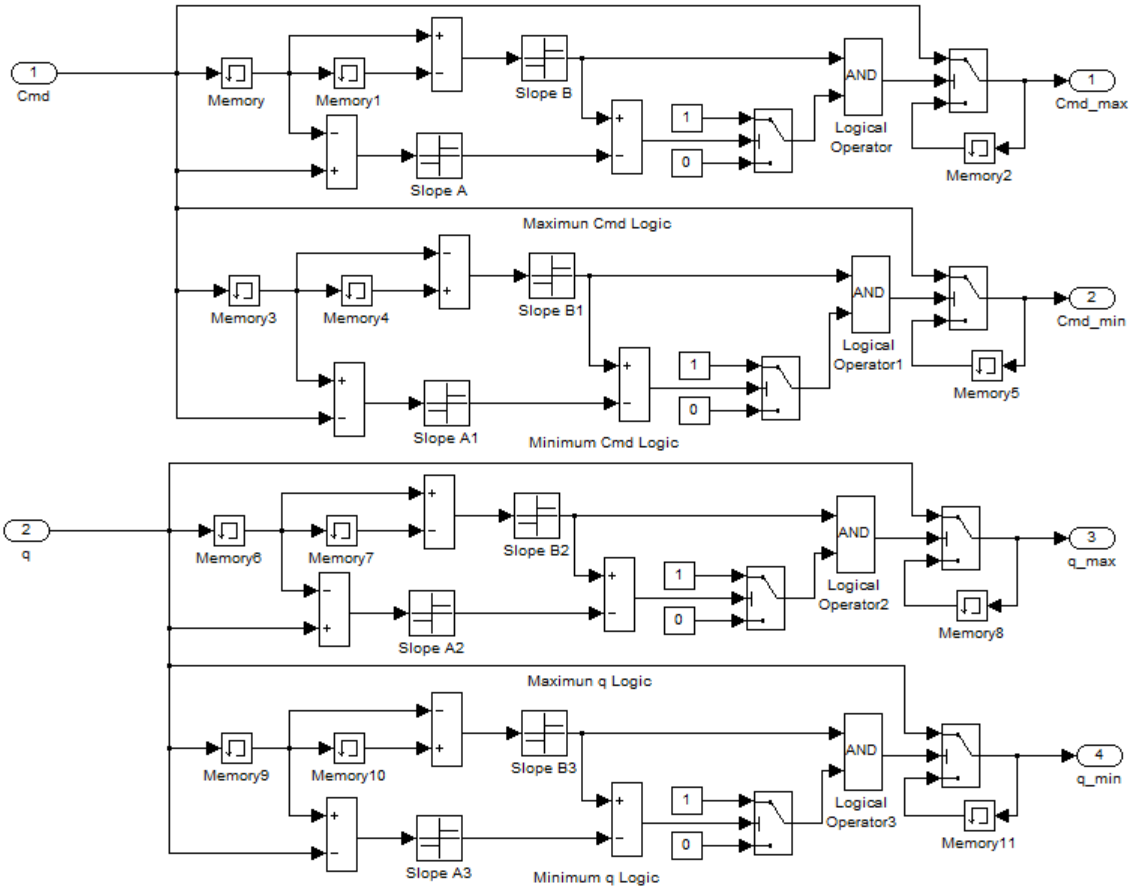

Figure 4.6: Time domain peak-to-peak calculation block as implemented in Simulink ®

The peak-to-peak method is sensitive to noise. In order to eliminate high frequency noise

effects, a low-pass filter was used before the input signal of command and pitch rate. The transfer function of the filter is described by Eq. 4.2. After the filter, the phase of the signal will be distorted up to $-45deg$ at a frequency of $20rad/s$. The phase distortion is smaller than $15deg$ in the range $1 \sim 5rad/s$, which was considered acceptable for signal processing.

$$H_{LF}(s) = \frac{20}{s + 20} \tag{4.2}$$

Rate-limiting subtractor

Another PIO feature parameter r_{RL} is calculated by subtracting the signal pre and post the actuator. This parameter was selected to give a PIO flag when rate-limiting occurred.

4.1.3 STFT calculator

The STFT calculator calculates the main frequency and phase difference between stick input and pitch rate, as shown in Block A1, Fig. 4.3.

STFT window selection

The purpose of the STFT calculator was to detect the frequency and phase of PIO signals in the range from 0.2 to $3.5Hz$. The window type and window length should be selected to reduce signal aliasing and obtain good frequency resolution within this frequency range. Proper window overlap should be selected to give suitable time resolution for real time detection.

Four kinds of window Hann, Bartlett, Blackman and Chebyshev were chosen to make a comparison, as shown in Fig. 4.7, the window length here is $5.12s$ while the sampling frequency is $100Hz$. Window property parameters represented in the frequency domain are shown in Table 4.1. It should be noticed that the window with lower side lobes can reduce energy leakage but increase the bandwidth of main lobe. The window with narrow main lobe has small frequency resolution but a relative high side lobe attenuation, which is not perfect for noise suppression. The purpose of this windowing is to distinguish different frequency components inside the PIO frequency range, which indicates that the bandwidth of the main lobe is the most critical parameter in selecting the window type. Thus, the Bartlett window with the narrowest main lobe of 0.24 was selected.

Table 4.1: Window properties

	Hann	Bartlett	Blackman	Chebyshev
Side lobe attenuation(dB)	-31.5	-26.5	-58.1	-100.0
Main lobe width (Hz)	0.27	0.24	0.32	0.34
Fall off(dB/Hz)	-66	-46	-85	-128

Another test was carried out to compare the window lengths. The test was also performed to validate that the Bartlett window was suitable for the PIO signal processing. A sum-of-sine function designed as PIO signal as shown in Eq. 4.3 and Table 4.2 was analyzed by

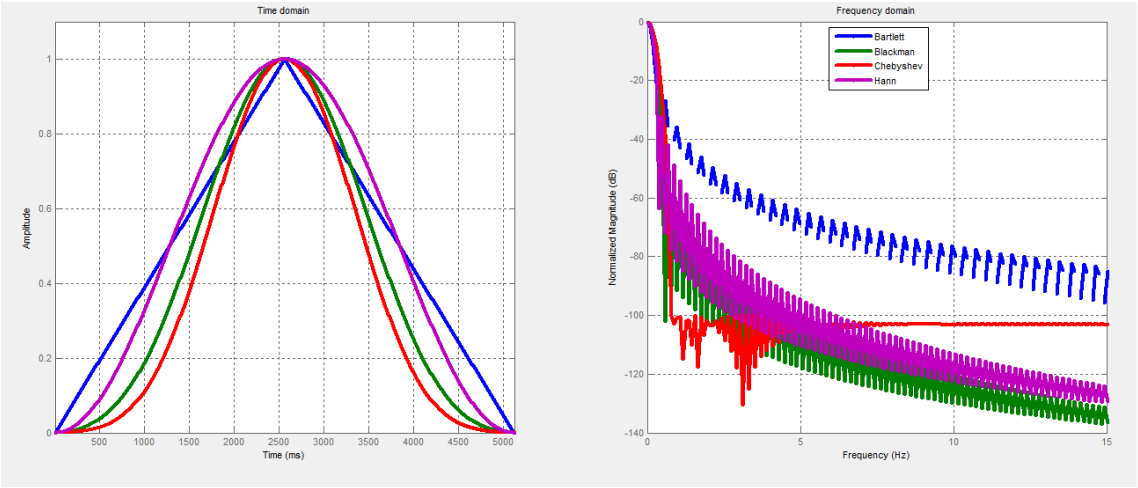

Figure 4.7: Four different windows

these four windows with window length of 2.56, 5.12 and $10.24s$. The sampling frequency remained $100Hz$. The window overlap was selected as 50% of window length.

$$f(t) = \sum_{k=1}^{12} A_k \sin(w_k t + \varphi_k) \tag{4.3}$$

Table 4.2: Parameters of the sum of sines input signal

k	*A(k) (deg)*	*ω(k) (Hz)*	*Φ(k) rad*	*k*	*A(k) (deg)*	*ω(k) (Hz)*	*Φ(k) rad*
1	1	0.1953	0.7254	7	0.352	2.7344	1.409
2	1	0.4883	-0.0631	8	0.263	3.2227	1.4172
3	1	0.8789	0.7147	9	0.212	3.5156	0.6715
4	0.949	1.3672	-0.205	10	0.201	4.4922	-1.2075
5	0.635	1.7578	-0.1241	11	0.16	7.0313	0.7172
6	0.483	2.2461	1.4897	12	0.17	10.0586	1.6302

The tests results are shown in Fig. 4.8. It can be seen that the low frequency detail is not recognized well with a window length of $2.56s$. As the low frequency is about $0.2 \sim 4Hz$, the period is up to $3.3s$ while the sampling time is only $2.56s$, the peak of the signal may be missed at this window length.

By comparing the window lengths of $10.24s$ and $5.12s$, low frequency content of the signal could be represented. The longer window length would increase the frequency resolution so that the lower frequency details could be distinguished better. However, considering the real time detection demand, $5.12s$ length was selected to improve the simulation speed and an overlap of $4.8s$ was selected. The change of this overlap was to increase the time resolution to $0.32s$, which indicated that the framed data was updated every $0.32s$. As shown in Fig. 4.8, Bartlett and Hann window are better than other two windowing functions. In consideration of this window length test and the window type selection test, a $5.12s$ Bartlett window with an overlap of $4.8s$ was selected.

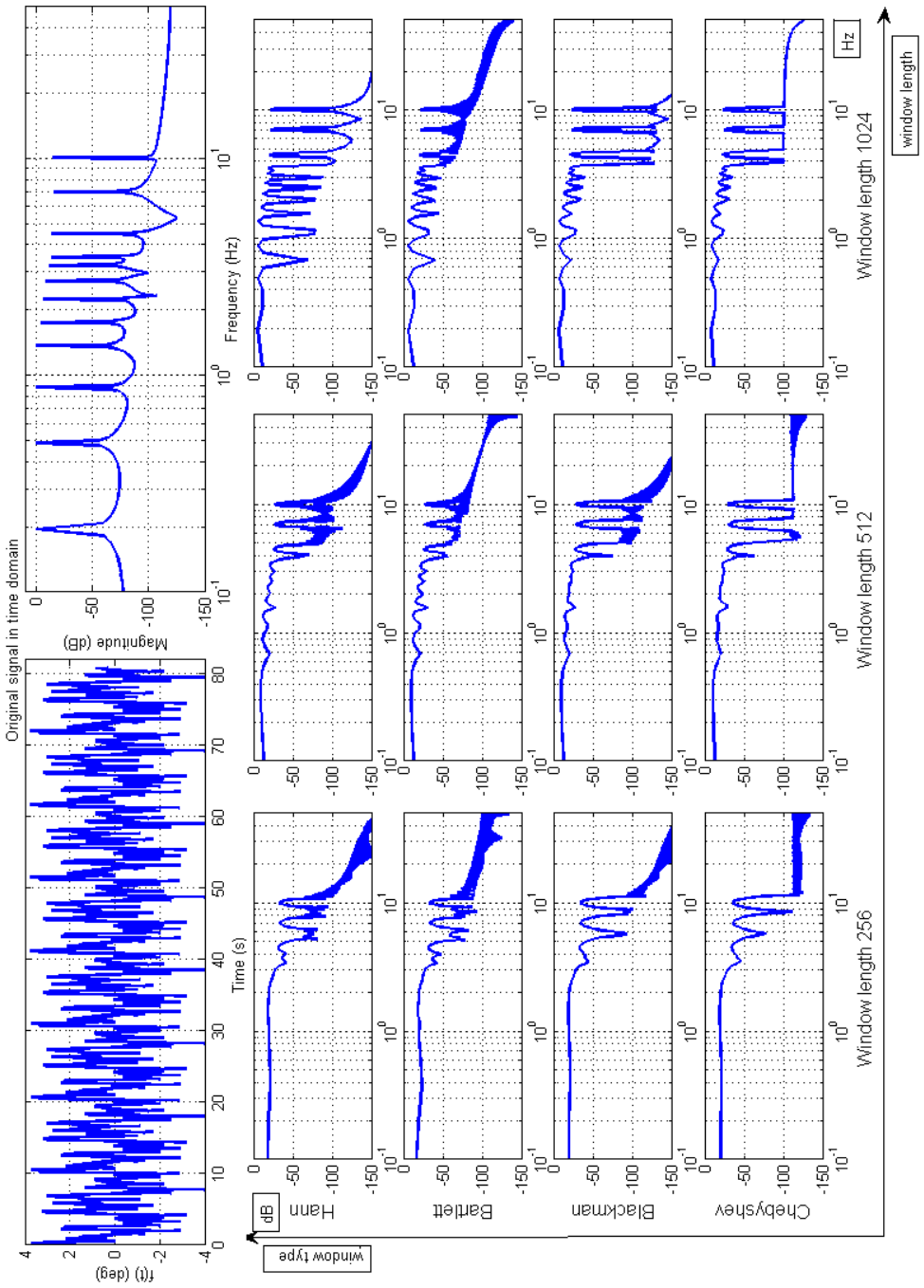

Figure 4.8: Comparison between Different Window types and Different Window lengths

Procedure of STFT calculation

The processing flow chart of STFT calculator is shown in Fig. 4.9. The dominant frequency of pilot control action and aircraft movement and the relationship between pilot and aircraft can be detected by STFT analysis over an observation time. The STFT calculator includes a buffer and STFT based processor. The buffer is adapted to receive windowed data of stick input and pitch rate and output the data to the STFT processor. The STFT processor is coupled to get the stored data and output main frequency and phase difference to the indicator.

4.2 Tendencies indicator

The tendencies indicator receives the six feature parameters and makes a judgment based on the review of existing data and experience. Judgment logic is based on criteria from the ROVER system and the Bandwidth Criterion. Finally, PIO cues are displayed on the PFD to give visual warning and the judgment result is output to the compensator. The PIO tendencies prediction flow chart is shown in Fig. 4.10, where $th(i)$ means the number i threshold.

Thresholds

The most significant and difficult item is to determine the tendency thresholds. The threshold were initialized as described in Table 4.3. These thresholds should be modified for different aircraft.

Table 4.3: Thresholds of PIO feature Parameters

Parameters	Symbles	Thresholds
main frequency	th1L, th1U	0.2 Hz, 3 Hz
Magnitude of pitch rate	th2	5 deg/s
Magnitude of stick input	th3	15% maximum stick deflection
Phase difference	th4	60 deg
Rate-limiting	th5	5% of rate limit
The rate of change in crossover frequency	th6	0.02 Hz/s

Weighting factors, sum function and PIO tendencies

The magnitude of pitch rate shows the degree of aircraft oscillations. The magnitude of stick input indicates the contribution of pilot control. The main frequency shows whether the oscillation is in a PIO frequency range. Phase difference exceeds the threshold during PIO events. When PIO occurs, all these four parameters will exceed the thresholds. The rate of change in crossover frequency shows the pilot effort during the oscillation and the r_{RL} directly discloses whether the actuator rate-limiting is exceeded. These two parameters give a further proof of PIO events. Based on the understanding of these PIO knowledge, different weighting factors are designed and applied to these parameters. The weighting factors function is shown in Fig. 4.11. Adding these weighting factors to the

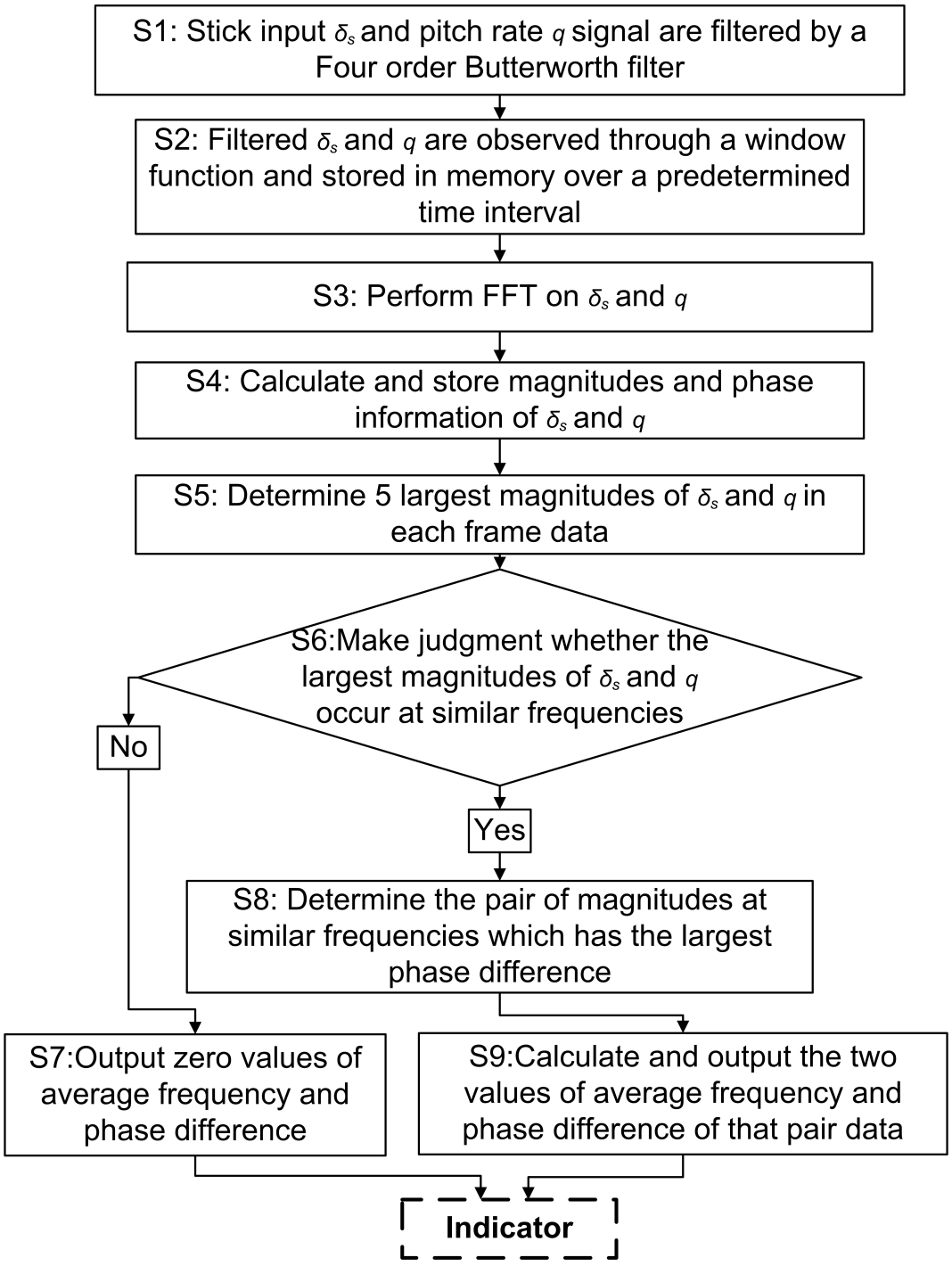

Figure 4.9: Procedure of STFT calculation

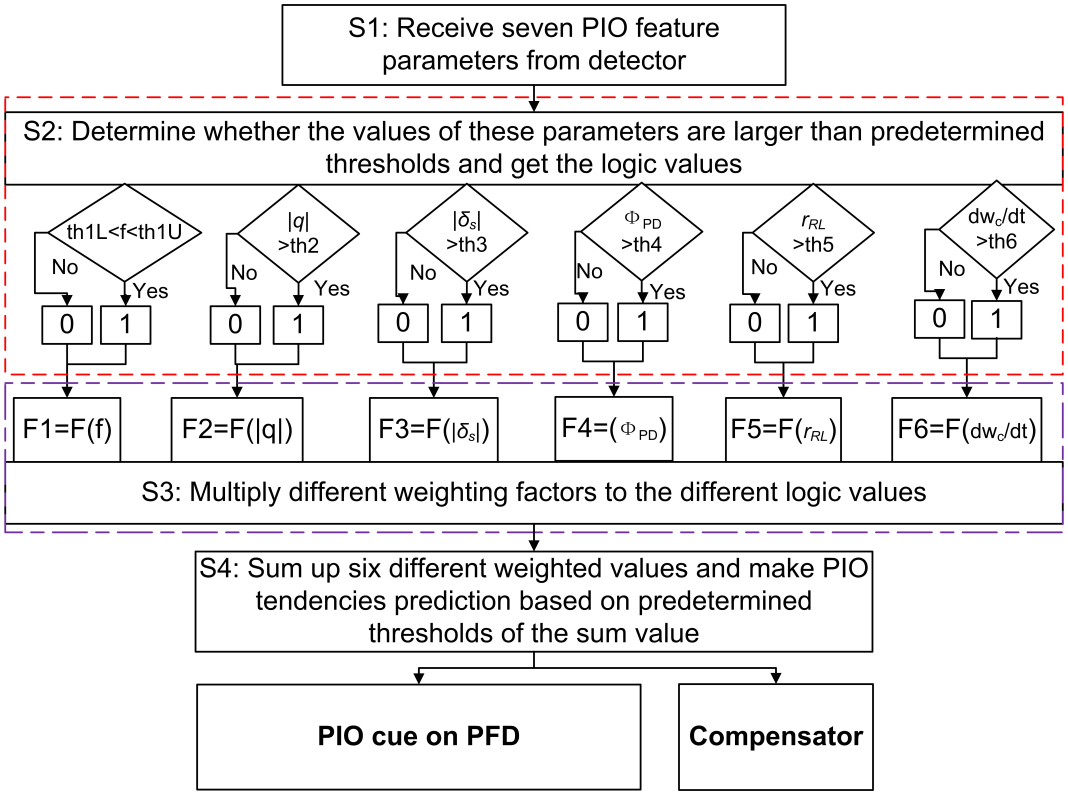

Figure 4.10: Procedure of tendencies indicator

feature parameter can help to differentiate the rate of change in crossover frequency and r_{RL} from other PIO feature parameters. When the four traditional PIO features are satisfied, just like ROVER, a PIO may happen. At the same time if the rate of change in crossover frequency is increasing or rate-limiting occurs, then the PIO tendency is becoming stronger.

The sum function and PIO tendencies are described by Eq. 4.4. If the value is equal to or larger than 4, a PIO warning will be given and the compensator will be activated.

$$\psi = \sum_{i=1}^{6} F_i L_i,$$
$$\textbf{PIO tendencies} \begin{cases} \textbf{No PIO} & 0 \leq \psi \leq 3.5 \\ \textbf{PIO} & \psi = 4 \\ \textbf{Strong PIO} & \psi = 4.5 \\ \textbf{Severe PIO} & \psi = 5 \end{cases} \tag{4.4}$$

where L_i is he flag value of 0 or 1, F_i is the weighting factor.

PFD interface

The original PFD was supplied by in-house code[47]. It is used as visual interface for pilot control. Fig. 4.12 shows the main features of the PFD. At the beginning, three different lights were designed as warning cues. Different lights were illuminated according to

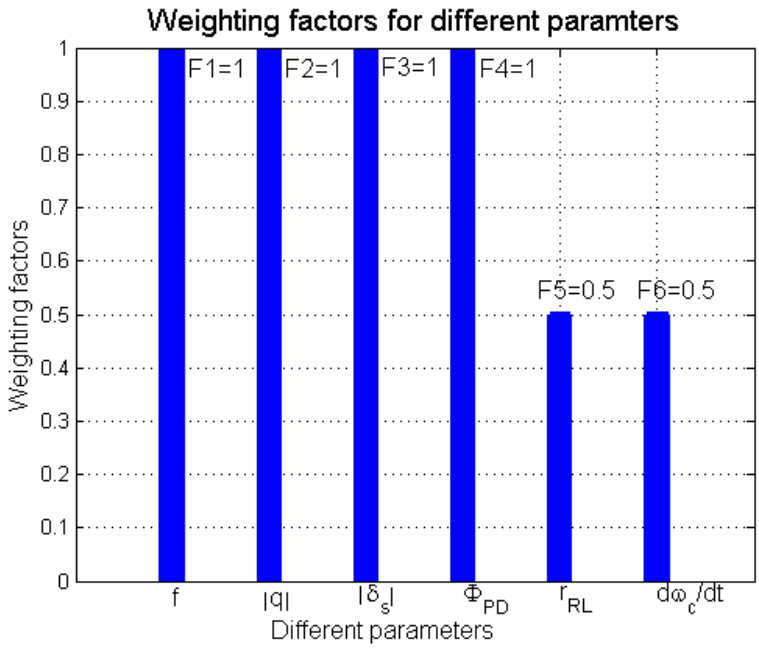

Figure 4.11: Weighting factors function

different levels of the sum function value. However, these flashing lights affected pilot control too much. Thus, only the red light was used to warn if $\psi \geq 4$. This warning can be helpful for the pilot to avoid PIO actively.

4.3 Compensator

A scheduled gain controller was coupled to the system. The structure of the compensator is shown in Fig. 4.13. If $\psi \geq 4$, the compensator will be activated and the stick input will be multiplied by scheduled gains. Thus, the PIO tendencies can be suppressed. The scheduled gains are shown in Eq. 4.5.

$$K(\psi) = \begin{cases} 1 & 0 \leq \psi \leq 3.5 \\ 0.3 & \psi = 4 \\ 0.1 & \psi = 4.5 \\ 0 & \psi = 5 \end{cases} \tag{4.5}$$

4.4 Off-line tests

4.4.1 Time error during real-time detection

The sampled data has to be buffered into frame data before STFT and ARX signal processing. The frame length is determined by the window length. In order to detect the

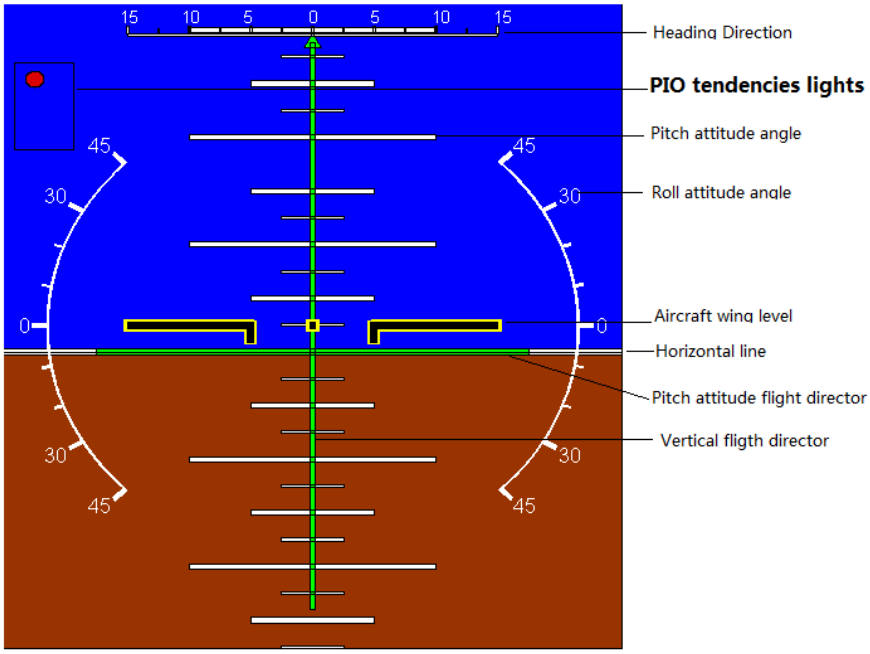

Figure 4.12: Primary Flight Display

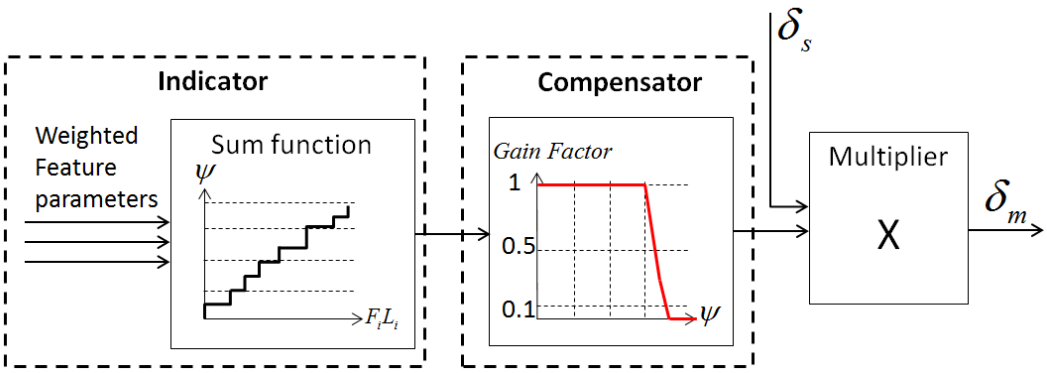

Figure 4.13: The structure of compensator

signal in real time, the frame data has to be updated quickly. A time error test was performed to identify the updated interval. The updated interval means the frame data will be updated every "interval" samples. The time step of the test was $0.01s$, the test laptop has a configuration of Intel Core i5-2520M, $4GB$ RAM. The results are shown in Table 4.4. The time error decreases as the interval increases. Consider the time error and the reaction time of pilot, the updated interval was selected to be 32 samples to give a time resolution of $0.32s$.

Table 4.4: System Time Error test

STFT updated interval	ARX updated interval	Time Error (RMS)	Time Error (Largest Error)
8	8	3.6	-6.3
16	16	0.017	-0.06
32	32	0.014	-0.05
64	64	0.012	-0.05

4.4.2 Off-line tests

Off-line tests were performed to tune the thresholds of the feature parameters and tune the structure of the detection and mitigation system. One case using tracking data from Boeing-747 simulation tests is introduced in this section. The thresholds of the four matured feature parameters: magnitudes of stick is 15% of maximum stick deflection, magnitude of pitch rate is $5deg/s$, $60deg$ of phase difference and $0.2 \sim 3Hz$ of main frequency. The thresholds of the other two parameters : the rate of change in crossover frequency is $0.02Hz/s$, r_{RL} is 5% of rate limit. It can be seen from Fig. 4.14 that the detection and mitigation system can detect small oscillations, as the results shown in $44s$, $77s$, $87s$, $95s$ and $118s$.

4.4.3 Limit cycle avoidance

The PVS may go into a limit cycle situation when the input magnitude is too large, as discussed earlier. One simple way to solve this problem is to reset the integrator to the initial state when such a situation occurs. In this thesis, when the PIO detection is true, the compensator will be activated to suppress the stick input gain and the integrator of the PI controller will be reset. This method will add another nonlinear element acts as a switch in the system, but it can solve the limit cycle problem during piloted test. An off-line test shown in Fig. 4.15 shows the effect of this integrator reset.

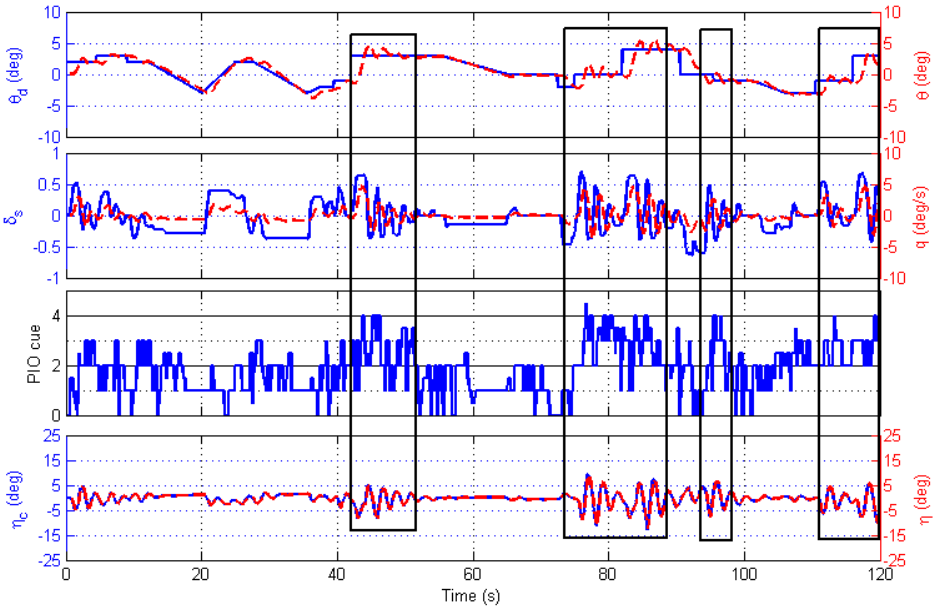

Figure 4.14: Off-line test

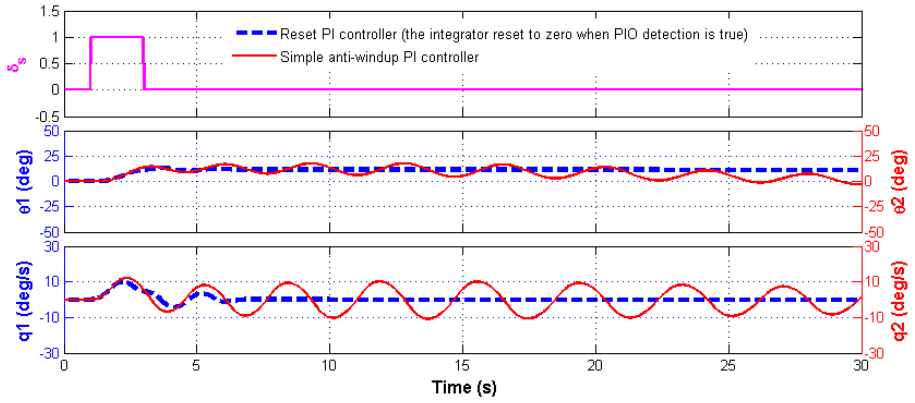

Figure 4.15: Comparison between simple anti-windup PI controller and reset PI controller

Chapter 5

Pilot-in-the-loop experiments

5.1 Experiment aims

The aims of these experiments were to investigate handling quality ratings, PIO ratings[28] and PIO detection and mitigation system evaluation on a Boeing-747 aircraft model. All experiments were conducted by subjects with different levels of flying experience. Data was collected in two stages. The first stage was compensatory training and discrete tracking training tests conducted by engineering students to achieve the following:

1. Design proper simulation model for the piloted tests and proper tasks for piloted tests.
2. Design analytical Matlab functions to cope with the test data.
3. Design suitable test procedures for piloted tests.
4. Get off-line data to tune the detection and mitigation system.
5. Draw conclusions from compensatory and tracking training tasks.

The second stage involved subjects with different flight experience to achieve the following:

1. Flight control quality and PIO tendency evaluation.
2. PIO detection system evaluation.
3. PIO mitigation system evaluation.
4. Draw conclusions from piloted tests.

5.2 Compensatory and tracking training

5.2.1 Compensatory training

The compensatory training was performed to do some research on pilot operation pattern under a certain range of disturbance frequencies and a duration of training time. The test subject was required to minimize the error between actual pitch attitude and horizon. The diagram of compensatory task is shown in Fig. 2.26. It consists of a joystick, an inceptor gain, a linearized Boeing-747 aircraft model with SAS at $0.5M$ and $20000ft$[51], an elevator actuator, a sum-of-sine disturbance function, a PFD, and a test subject closing the system. The open loop transfer function from elevator input to pitch rate of the aircraft was the same as described by Eq. 3.7. The actuator was the same as described by Eq. 3.5. The inceptor gain could be tuned to change the pilot's control feeling by enlarging or reducing the stick input.

The training task was conducted by five subjects with different flight experience. A great deal of training tests have been done in [55]. The results from [55] showed that if each compensatory training lasted for one minute, the control performance of compensatory training would stay similar after six or seven runs. The reason was that the test subjects tended to get familiar with the control law and the disturbance level after six or seven runs. The results also showed that the pilot would suffer from fatigue after five or six runs. Increasing test time in each run may enhance the pilot's fatigue easily since people would get tired in long duration events. In consideration of these factors, in this thesis, each subject performed seven test runs, each run lasted one minute. There was a two minute rest after the six run. The root mean square(RMS) of pitch angle was used to evaluate subject performance. Lower RMS implies better performance. After each run, RMS of pitch angle and stick input were shown to encourage the subject to reduce the compensatory error. The parameters of sum-of-sine disturbance signal were the same as used in ARX tests described by Table A.1.

The inceptor gain was set to be -1.5 for the subjects to get satisfactory control quality. This gain setting should make sure that the pilot can control the aircraft safely without exceeding the stick distance. On the other hand, the gain setting should not make the control too light that it would take exceptional skill to control the aircraft without over-stressing losing control. A record of the disturbance signal, stick input and pitch attitude of the fourth subjects on the third run is shown in Fig. 5.1. The disturbance and pitch angle were within the range of $\pm 5deg$ and no saturations happened in stick deflection. The average control deflection is about 0.25, which indicated that the inceptor gain was suitable for the piloted tests.

The RMS of disturbance, stick inputs and pitch error signal of five subjects in seven runs are shown in Fig. 5.2. It shows that the RMS of pitch angle error and stick input increased at the fifth and sixth runs. This may due to the subject fatigue in doing continual tasks as shown in [55].

The frequency domain response of the tests were analyzed by FCM. One sample of the

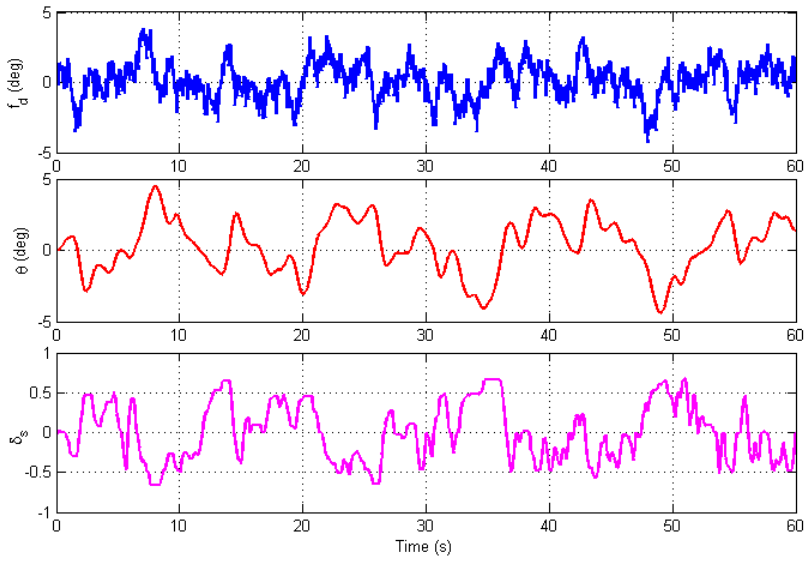

Figure 5.1: Time domain plots of compensatory training

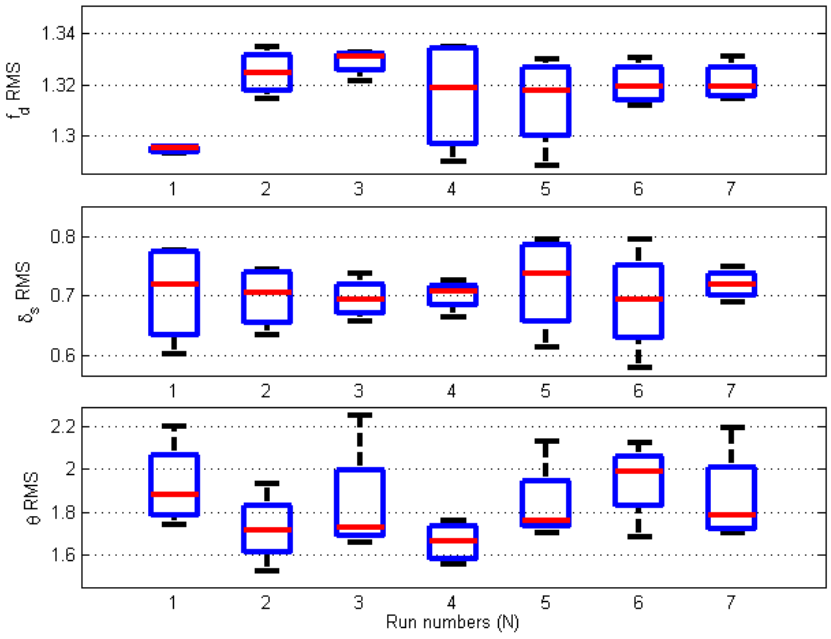

Figure 5.2: RMS plot of disturbance, stick input and pitch angle

pitch angle and stick input frequency response of the third subject in fourth run is shown in Fig. 5.3. The frequencies of response peaks on the figure are those particular frequencies of the sum-of-sine function. The spectrum of pilot model transfer function Yp can be calculated from pitch angle to stick outputs using FFT. The aircraft frequency response can be calculated by using bode function on the linear transfer function Yc. The spectrum of PVS open loop transfer function can be obtained by combining Yp and Yc. The spectrum of Yp, Yc and YpYc in particular frequencies is shown in Fig. 5.4. As can be seen from the figure, the crossover frequency is a little low at $0.5rad/s$, the reasons are: (1) aircraft model was at a configuration of $0.5M$ and $20000ft$ with SAS, (2) the test subject was not aggressive enough in the simulation tests.

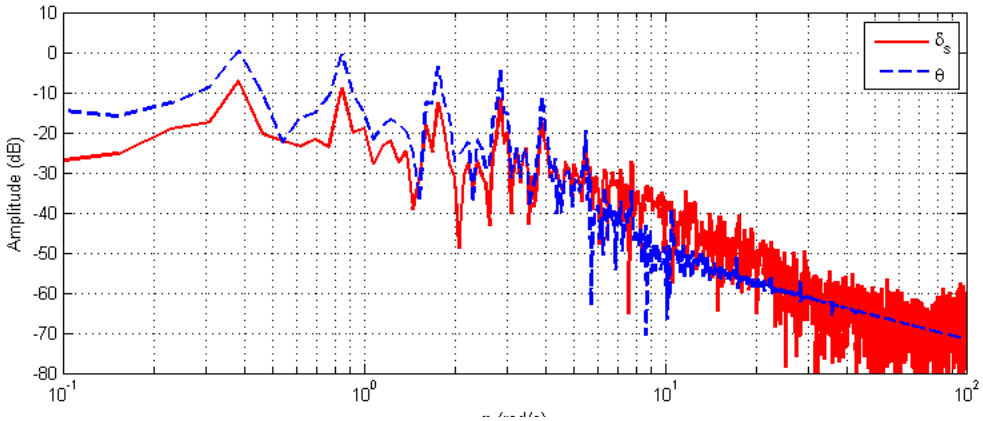

Figure 5.3: Frequency domain plots of stick input and pitch angle

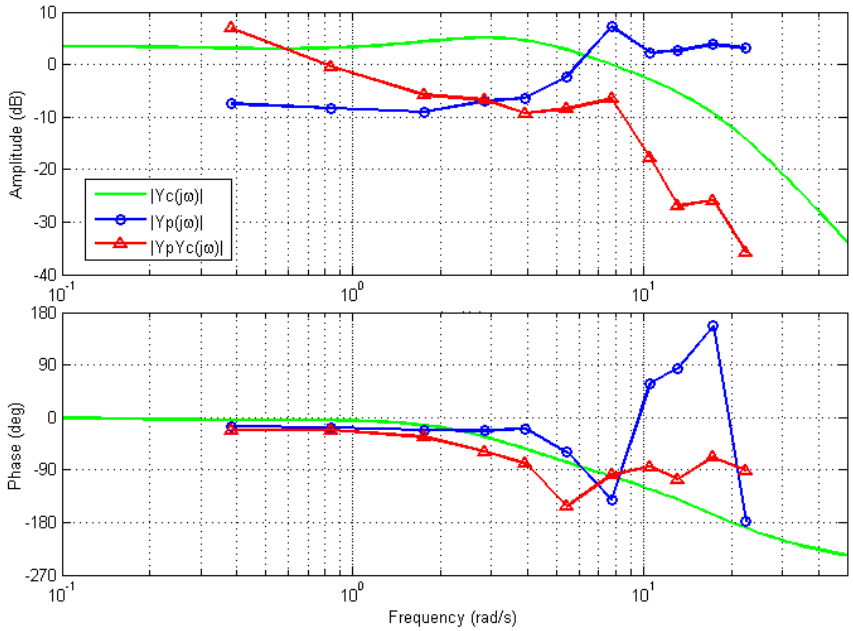

Figure 5.4: Frequency domain plots of Yp, Yc and YpYc

5.2.2 Discrete tracking training

A discrete tracking training was performed to get off-line data for the thresholds tuning of PIO feature parameters and to design suitable tasks for piloted tests. The aircraft configuration was the same as that used in the compensatory task. The diagram of tracking task is shown in Fig. 2.27. The tracking signal is a two minute task demonstrated in Fig. 2.28. Three different rate limits for elevator actuator were 37, 30 and $25deg/s$. These were selected in an attempt to induce category II PIO during the training. Two subjects attended the training. Each subject performed twelve runs, every three runs for one actuator rate limit, each run lasted two minutes. After six runs there would be twenty minutes rest to prevent the pilot from learning the task. After each run, the subject gave a Cooper Harper Rating[56] evaluation. Detailed evaluation data are attached in Appendix E. The author do not have enough time to do more tests. More test subjects should be involved to give a more accurate test result in the future.

Fig. 5.5 shows the training results. It is can be seen that the handing quality ratings were oscillatory at the beginning, then the rating experienced a general decreasing trend as the training runs increasing. This can be attributed to three factors: (1) the subjects learned from the former tests that abrupt stick input would trigger the limit cycle problem, (2) the subjects got familiar with the tracking task and, (3) the subjects were told that the actuator rate limits were decreased, which made the subjects operated more carefully to avoid PIO. Both the tracking error and handling rating show that the system went into catastrophic oscillations at runs $2, 4, 5, 6$. The reason was that the control law was modified using PI controller. The aircraft was more PIO prone. Therefore, abrupt input may trigger the windup effect of the integrator, resulting in the limit cycle phenomenon, as shown in Appendix E. The tracking error and handling quality rating increased at runs 6 and 12. It was probably fatigue effect. It can be learned from this tracking training that the tracking task should be divided into different series and tested in different days to avoid fatigue and learning effect. The information which will affect the subject's real operation should not be presented to the subject.

5.3 Piloted trials

5.3.1 Experimental setup

Experimental setup

The completely experimental setup and display is shown in Fig. 5.6. In the piloted tests, only the pure disturbance-rejection compensatory task and pure tracking task were carried out. For compensatory task, the pilot command function f_t equals to zero. For tracking task, the sum-of-sine function f_d equals to zero. The experimental sample time step is 0.01 seconds. The disturbance-rejection signal f_d was designed as a quasi-random sum-of-sine, and the tracking task is a discrete signal formed by a combination of steps and ramps over a period of 120 seconds, as discussed in Chapter 2, Section 2.3.2.

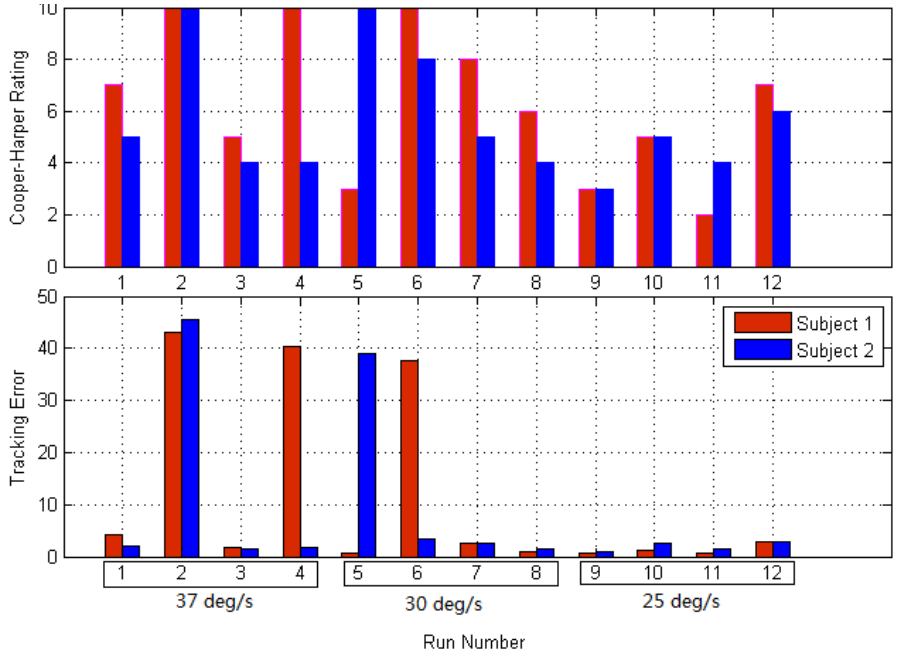

Figure 5.5: Handling quality rating and tracking error results of Tracking training test

The HotasWarthog® joystick is used for this experiment. Normally, the pilot controls the aircraft based on the stick feel and perceived aircraft dynamics. However, this joystick does not have as realistic feedback as real aircraft controls. In order to make the simulation test more like flying in a cockpit, the author visited simulators in CAE Ltd.(Burgess Hill, London), and was kindly allowed time in Airbus-320 level D simulator. The joystick was located to be as realistic as on the aircraft, shown in Fig. 5.7. The test pilot elbow leaned on the armrest to reduce unexpected movement. The configuration of the laptop using in the test was Intel Core i5-2520M, CPU 2.5GHz, RAM 4GB. It was located in front of the pilot on a desk with proper altitude. The task setup is shown in Fig. 5.8. The rate-limiting of the actuator is $37deg/s$ and the saturation is $25deg$.

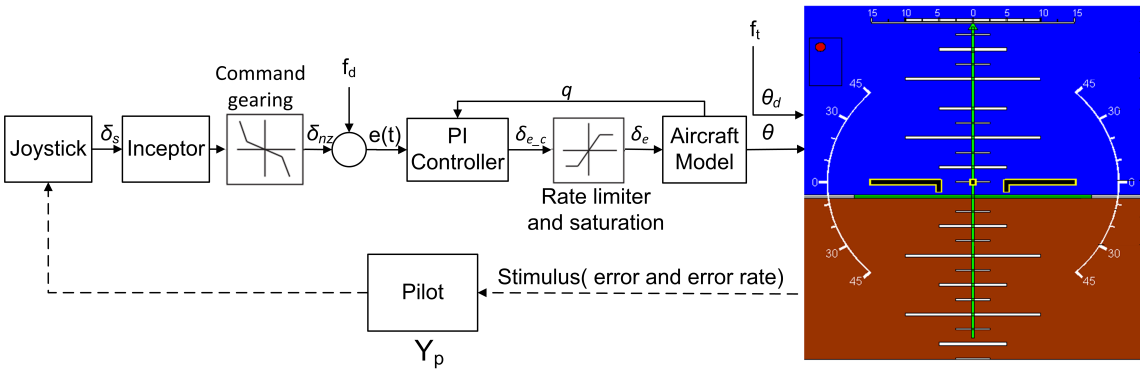

Figure 5.6: Structure of experimental setup and display (modified from [19])

Experimental procedures

Figure 5.7: Joystick and display setup

Test		Run No.	Forcing Function	Controller	Nonlinear component		
					Command gearing	Actuator rate-limiting	Actuator saturation
Compensatory task		1	Sum-of-sine	C2	Yes		
		2	Sum-of-sine	C2			
		3	Sum-of-sine	C2			
		4	Sum-of-sine	C2			
		5	Sum-of-sine	C2			
Tracking task	No PIO cue	1	Discrete	C1			
		2	Discrete	C2			
		3	Discrete	C3			
		4	Discrete	bare aircraft			
	PIO cue	1	Discrete	C1			
		2	Discrete	C2			
		3	Discrete	C3			
		4	Discrete	bare aircraft			
	PIO cue & Mitigation	1	Discrete	C1			
		2	Discrete	C2			
		3	Discrete	C3			
		4	Discrete	bare aircraft			

Figure 5.8: Experimental tasks setup

The tracking tests were divided into three series and tested in different day to inhibit learning effect and fatigue. The experimental procedures are designed as following:

- A briefing about the configuration and aims of the tests, Cooper-Harper rating and PIO rating criteria is given.
- Five training runs are conducted to familiarize the subject with the simulation and control, each lasts 1 minute.
- Four runs of the tracking task without any PIO cue are conducted, each lasts for 2 minutes, 30 seconds rest time between every two runs. Test in the morning.
- Four runs of the tracking task with PIO cue are conducted, each lasts for 2 minutes, 30 seconds rest time between every two runs. Test in the afternoon.
- Four runs of the tracking task with PIO cue and mitigation system are conducted, each lasts for 2 minutes, 30 seconds rest time between every two runs. Test in the next morning.

Information of test subjects

This test was conducted by subject with different flight experience. The information of test subjects is given in Table 5.1.

Table 5.1: Test subject information

Subject	Gender	Age	Flying hours	Aircraft types
A	M	29	3	/
B	M	27	10	/
C	M	28	67	C152
D	M	49	7200	Nimrod/Business Jets/Piston Engine

5.3.2 Training runs data analysis

These training runs were conducted to ensure the pilot had reached good control performance during the tests. Each test subject conducted 5 runs. All the data from 4 test subjects had a similar trend. Hence, only one sampled data is presented. The intensity of the disturbance for all test runs are similar except a randomize phase difference. A sample of time domain plots from fifth training run of the fourth subject is shown in Fig. 5.9. It can be seen that the general trend of pitch angle is similar as the disturbance but without high frequencies parts. This means that the test subject did not adapt high gain to compensate the disturbance. The stick movement was inside ± 0.5 most of the time. The test subject tended to move the stick in a regression strategy. The RMS of pitch error of all test subjects and all training runs are shown in Fig. 5.10. The descend trend of the RMS shows that the test subject got better control performance after five runs of training.

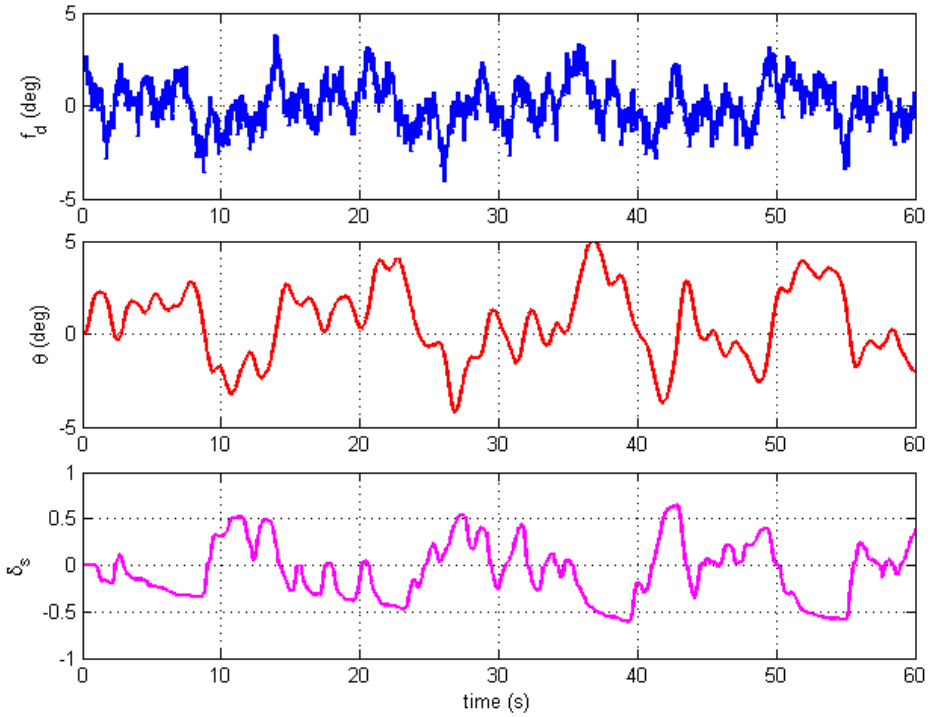

Figure 5.9: Compensatory task time domain plot of the fourth subject, the fifth run

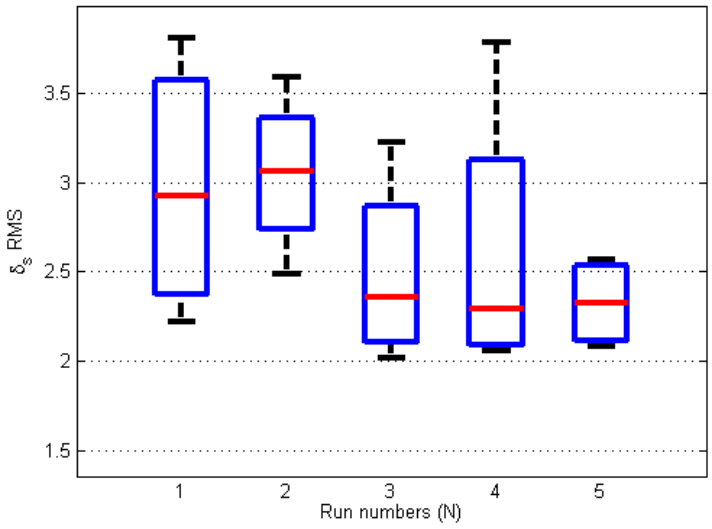

Figure 5.10: Pitch error RMS of compensatory training in piloted test

5.3.3 Tracking runs data analysis

In the tracking tasks, each test subject conducted twelve runs to evaluate the handling quality and PIO ratings. These twelve runs were separated into three series. Each series contains four runs tested in the system integrated with different controllers. During each series of test, the handling quality was varied by integrating controller C1, C2, C3 and no controller to the aircraft model. The aim of this test setting was to deteriorate handling quality and trigger PIOs. The tests of the first series were conducted without any PIO cues. The second series were conducted with PIO warning cue on the PFD. The third series were conducted with PIO visual cue and mitigation system. The mitigation system would be activated when the detection was true. This setting intended to evaluate the detection and mitigation system by comparing the handling quality and PIO rating results between different series.

A. Pilot handling quality rating and PIO rating

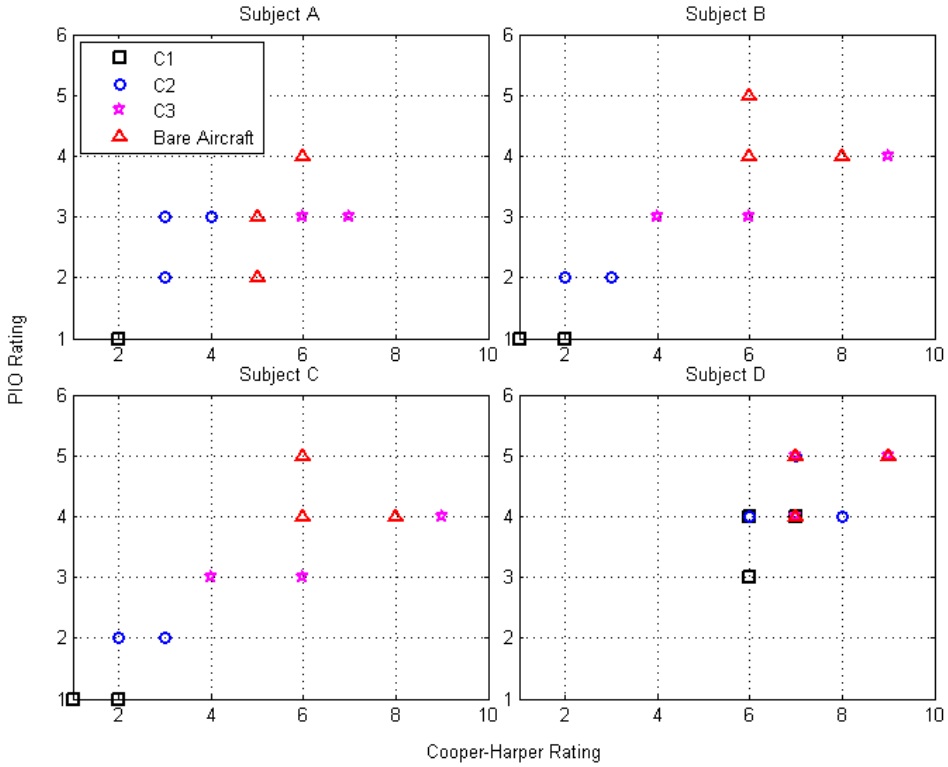

Figure 5.11: Cooper-Harper and PIO rating evaluation of PVS with different controllers

It can be seen from Fig. 5.11 that the handling quality rating and PIO rating increased as the control system changed from C1, C2, C3 to bare aircraft. PIO rating was related to the handling qualities. Most of the handling quality rating of bare aircraft and aircraft integrated with C3 were larger than 5. The PIO rating for these two configurations were larger than 3. These rating results were identical to the control law design. The evaluation results of subject A, B and C are similar while the evaluation of subject D was more severe. The reason was that the subject D was an experienced business jet pilot. He

compared the handling quality of the model with real business jets and suggested that the model was not stable enough. The whole control system was required to be faster, more stable and more precise.

Fig. 5.12 shows the pilot Cooper-Harper rating and PIO rating of PVS in different controllers and PIO detection and mitigation modes. It can be seen from the figure that the handling quality and PIO rating almost remain the same for aircraft with C1 and C2 controllers. It is evident that PIO detection system can improve the handling quality and PIO rating by giving a PIO visual cue for bare aircraft and aircraft with C3 controller. Most of the test runs show that the mitigation system can help to alleviate the PIO tendency. However, the mitigation system sometimes made the PIO tendency and handling quality worse since it affected the pilot's active control, such as the tests with C3 of subject A and the bare aircraft tests of subject B. The mitigation system reduced the pilot gain and reset the integrator in PI controller. Such sudden gain changes and nonlinear resetting made the aggressive pilot feel hard to control the aircraft. It is clear from the pilot evaluation that the PIO detection and mitigation system can detect undesirable oscillations. More data were required to verify the mitigation system.

B. PIO cue effects, results of calculators and indicators

The PIO detection system was evaluated through the discrete tracking tasks. Fig. 5.13 shows the test results of the second run(with PIO cue) of subject A. It can be seen from Fig. 5.13 that oscillations occurred from 45s to 52s and from 75s to 100s. The detection system gave PIO cue from 47s to 52s and from 77s to 100s most of the time. The detection time lag for the oscillations varies from 1 to 2 seconds. This delay was found to be due to the STFT block. Since the signal was processed and updated frame by frame while the window of STFT was fixed. When the oscillation occurred, the detector cannot detect it immediately. After two or three frame, enough oscillation data moved into the window, then the oscillation can be detected by the STFT method. It can be seen from the figure that the test subject reduced the stick input or even let go of the stick when the PIO cue was given on the PFD. The oscillation was alleviated after that. The PIO cue can help pilot to take active action to avoid PIO events.

Fig. 5.14 shows the detected values and flags for six parameters. It can be seen that these six parameters can be detected by ARX, STFT and time domain calculator respectively. It is evident that the time domain calculator can detect the magnitudes of stick and pitch rate and r_{RL} in real time. The predetermined thresholds of these three parameters in the indicator were suitable for oscillations detection. The STFT calculator can detect the main frequency and phase difference during the oscillations. However, the detection results were affected by the spectrum leakage effect, as can be seen from the spikes. The ARX calculator can calculate the crossover frequency. The crossover frequency increased when oscillations occurred. More PIO data was required to tune the predetermined threshold for this parameter.

C. PIO detection results and the rate of change in crossover frequency

The rate of change in crossover frequency shows the change in pilot control gain, as shown in Fig. 5.15, a close up to the event between 42s to 52s and 75s to 100s of the second

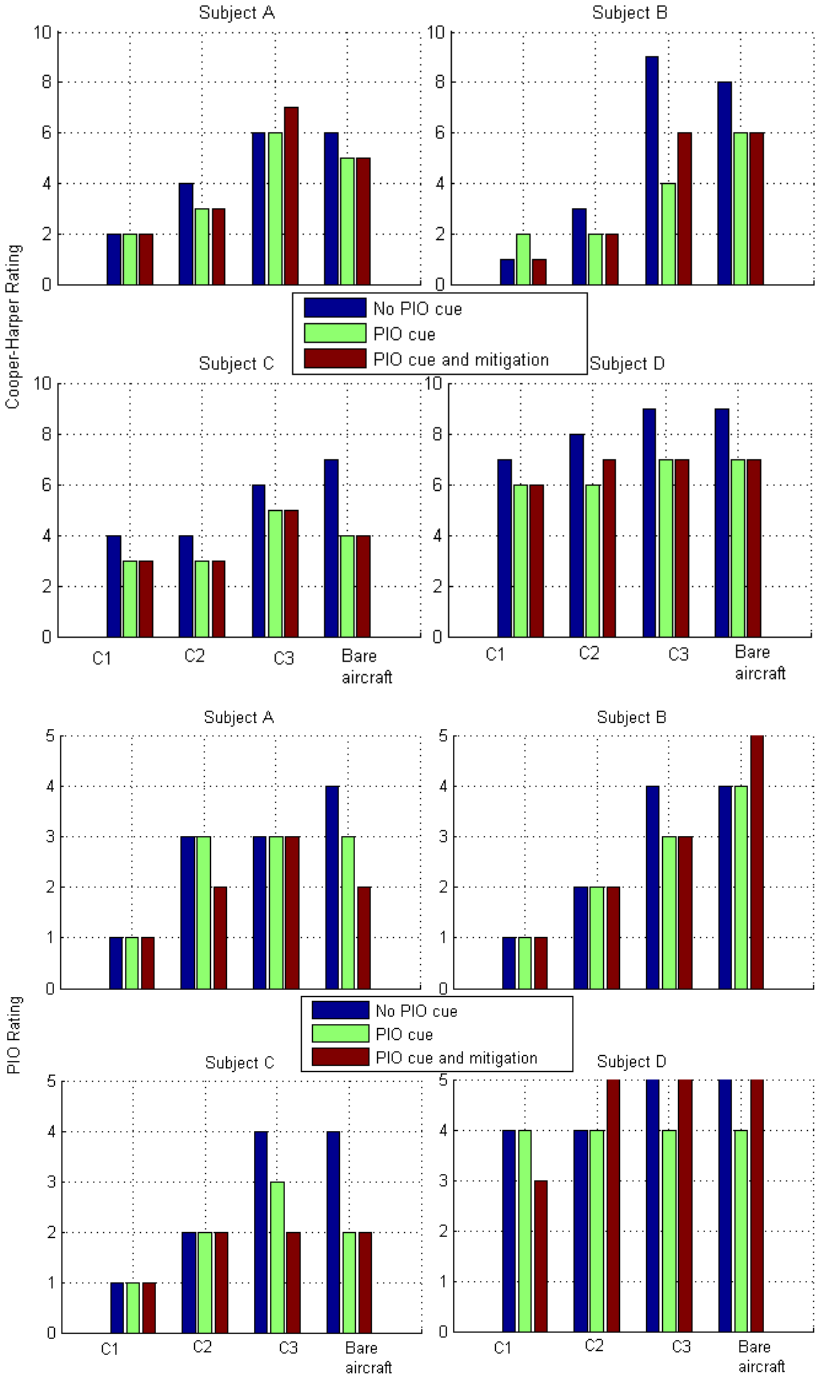

Figure 5.12: Cooper-Harper and PIO rating evaluation for PVS in different PIO detection and mitigation mode

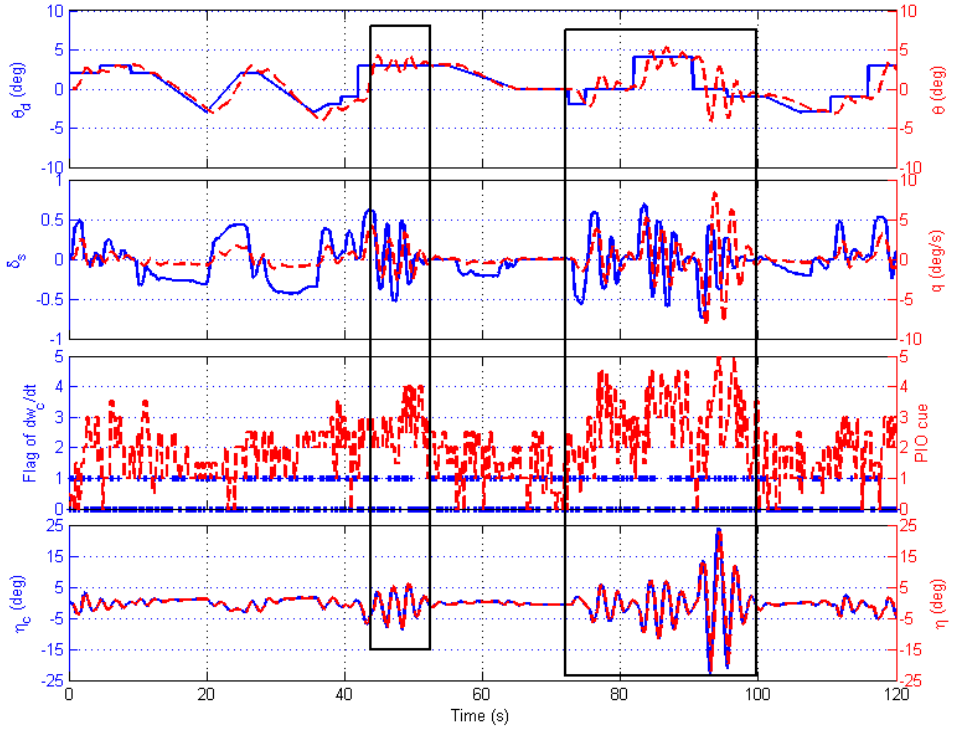

Figure 5.13: PIO detection results - the second run (with PIO cue) of subject A

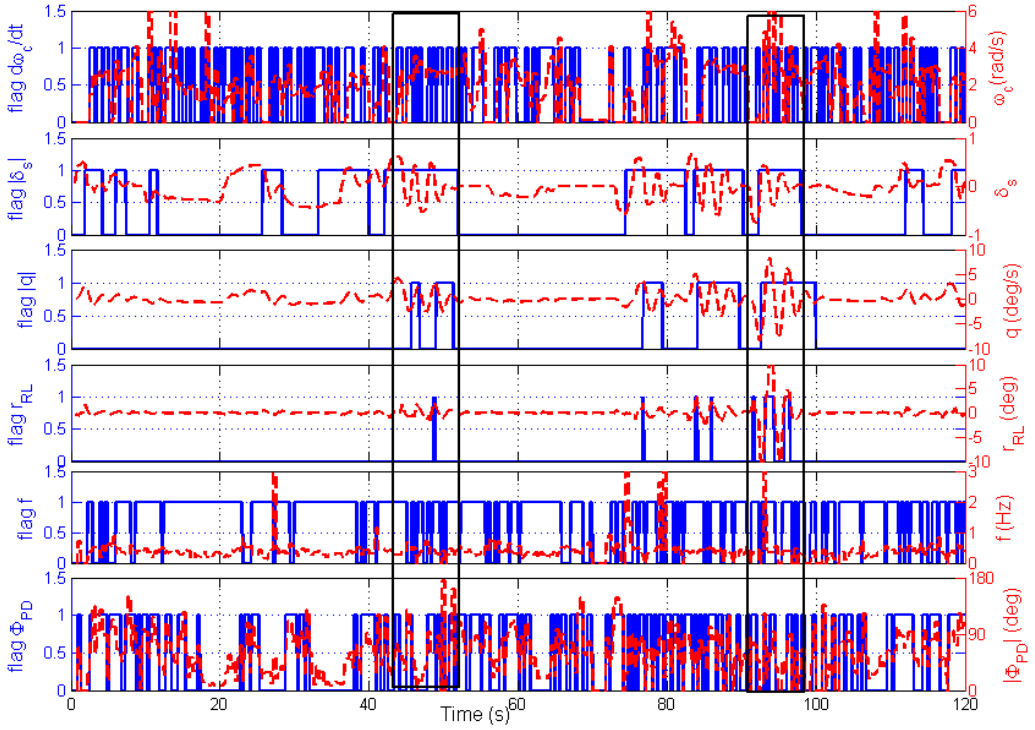

Figure 5.14: PIO detection six flags - the second run (with PIO cue) of subject A

run(with PIO cue) of subject A. It can be seen that the PIO events always occurred after an abrupt step input. The abrupt input caused over control. The test subject tried to readjust the attitude and catch up the reference signal by increasing his control gain. Such abrupt gain changing may trigger the rate-limiting. The rate of change in crossover frequency can be selected as a sign of pilot aggressiveness and PIO tendency during oscillations. However, the test subject would reduce his gain as soon as he realized that his input amplified the oscillation. This regression control feature can be seen after 50s and at the time of 85s, 90s and 95s in the figure. These results were identical to the theory introduced in ARX model design. Since the inputs of the ARX model are 256 samples per frame, the current detection results would be affected by the data in the past few seconds. It is a natural defect of ARX model since it needs enough data to do the system identification. Another two test runs showed similar results, as shown in Appendix E.

D. Detection results compared with ROVER

The time history plot of the fourth run(no PIO cue) of subject B was shown in Fig. E.11. It shows that the detection and mitigation system was more sensitive than ROVER when the thresholds were the same. As shown in Fig. E.11, the new system detected the oscillations at 9s, 24s, 48s 95s, 113s and 118s while the ROVER only detected the oscillations at 95s and 118s. The other test runs showed similar detection results. The new system can help the pilot to avoid getting into PIO events, but the flashing red PIO cue and the mitigation system sometimes interrupted pilot normal control because the system was too sensitive. According to the evaluation of test subjects, the handling quality rating and PIO rating decreased when the system was coupled. The new PIO detection system works, but more pilot tests and PIO data are required to improve the accuracy of this system.

The time history plot of the fourth run(no PIO cue) of subject D was shown in Fig. E.12. It can be obtained From Fig. E.11 and E.12 that the subject B went into PIO more than subject D. The reason was that subject B did not have much flight experience. He tried to follow the task by moving the stick with large amplitude and high frequency. Such abrupt input triggered the PIO events easily during the tracking task, especially when large step occurred at 95s and 118s. The stick input of subject B was near ± 0.5 when the reference signal jumped, the highest stick input reached -0.8 at $95s$. The test subject D was an experienced business jet pilot. He always kept in mind the comfort of passenger and did not try to follow the step and ramp reference signal accurately. Instead, he regressively followed the trend of the reference signal using gentle stick input. The stick input was always smaller than 0.3. Such moderate control was not likely to trigger PIO events.

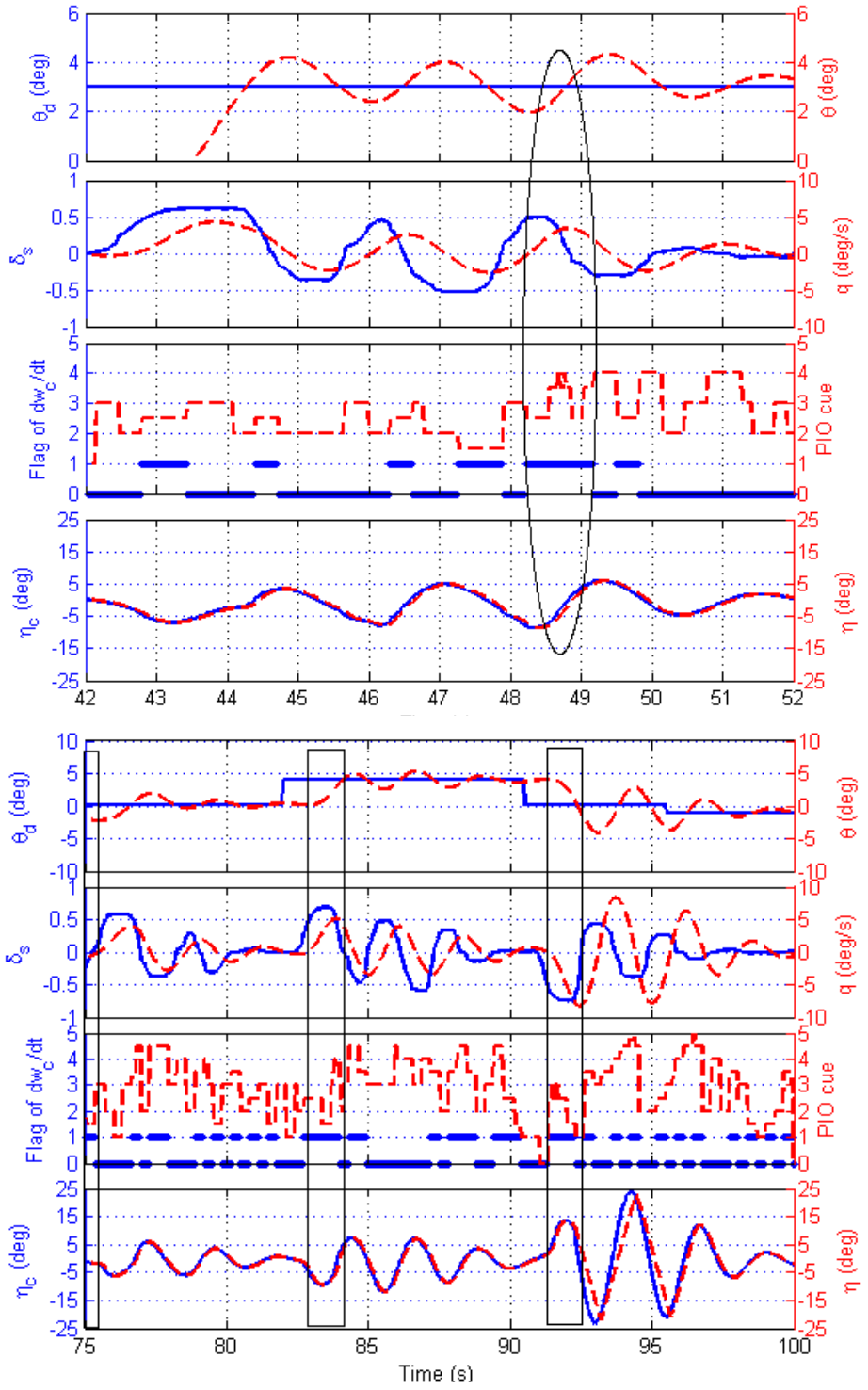

Figure 5.15: Relationship between PIO events and the rate of change in crossover frequency - the second run (with PIO cue) of subject A

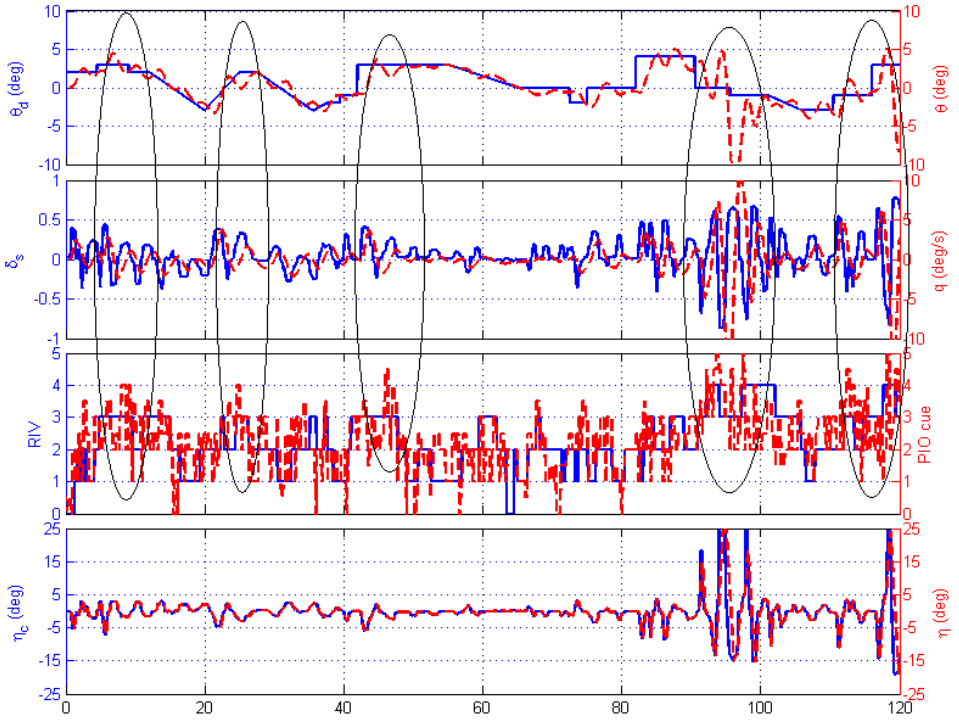

Figure 5.16: The fourth run(No PIO cue) of subject B

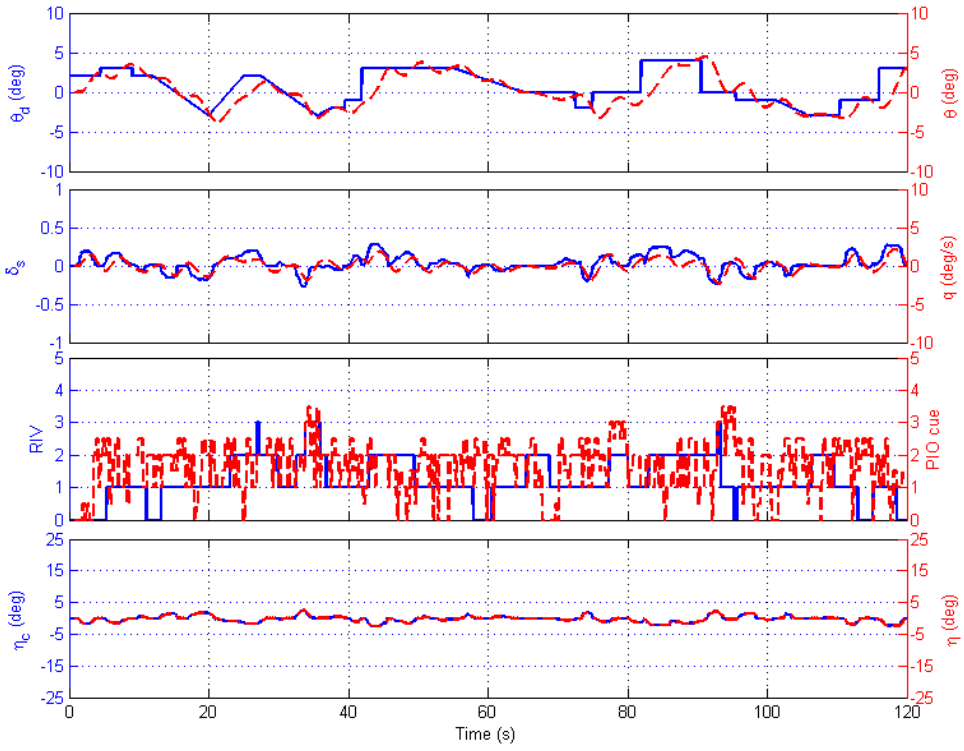

Figure 5.17: The fourth run of(No PIO cue) of subject D

E. Mitigation results compared with ROVER

The detection and mitigation system and ROVER were applied to the data of the fourth run(no PIO cue) of subject B. The Fig. 5.18 and 5.20 show that after the system, the stick control input was suppressed when PIO occurred. Such gain adjustment can help to suppress the oscillation, as can be seen from Fig.5.18 and 5.20 that the oscillation amplitude of pitch angle and pitch rate were suppressed from 86.5s to 88.5s and at 95s. The Fig. 5.19 and 5.21 show the stick modification after ROVER. It can be seen that the ROVER filtered the sitck input from 88.2s to 91s and from 94s to 95s. The new detection and mitigation system can detect and mitigate the PIO tendency earlier than ROVER.

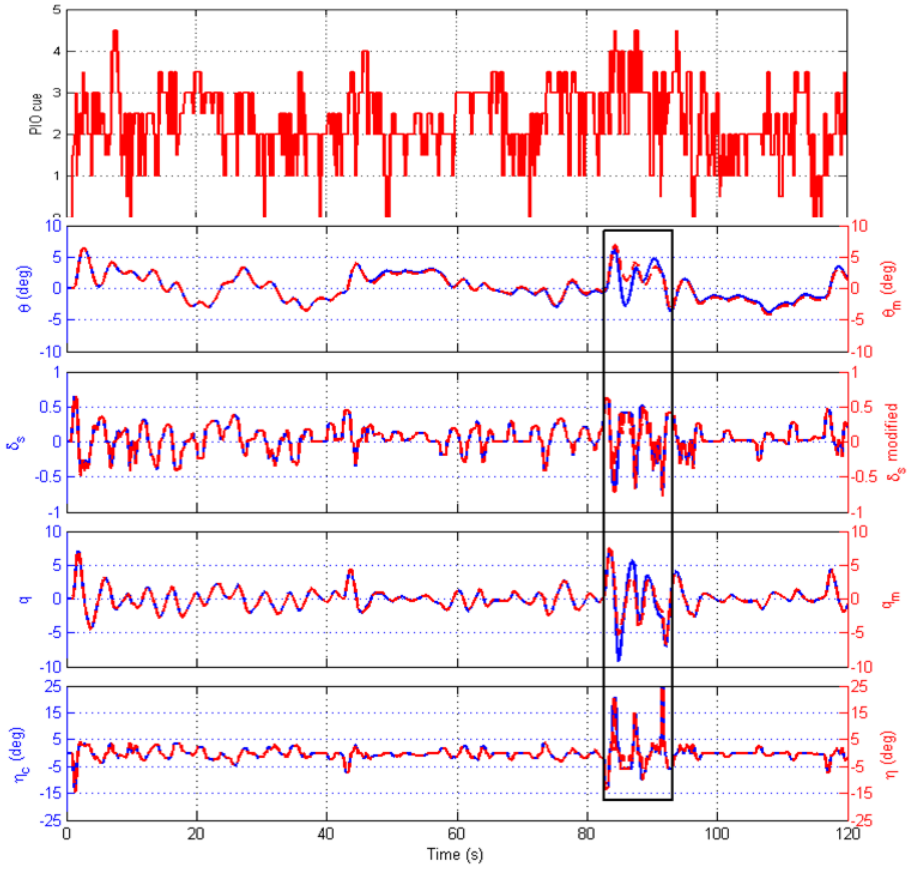

Figure 5.18: Stick input modification after mitigation for the fourth run of series one of subject B (The whole time history)

The five runs of compensatory tasks ensure that the test subject reached a proper control performance before doing the tracking tasks. The results of tracking results showed four major information: (1) the PIO detection and mitigation system can reduce the handling quality rating and PIO rating during the tests, (2) the rate of change in crossover frequency shows the intensity of pilot control and indicates the trend of PIO tendency, it can be calculated by the ARX model through the open loop system identification, (3) the detection and mitigation system can detect the PIO as ROVER does, but it is more sensitive than ROVER, the thresholds of the system needs to be modified to improve the performance of the system, (4) the mitigation system is activated to suppress the PIO tendency when the detection is true.

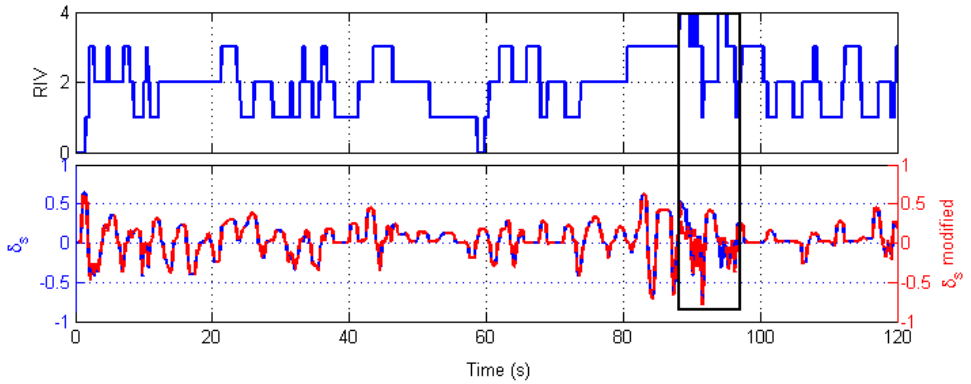

Figure 5.19: Stick input modification after ROVER for the fourth run of series one of subject B (The whole time history)

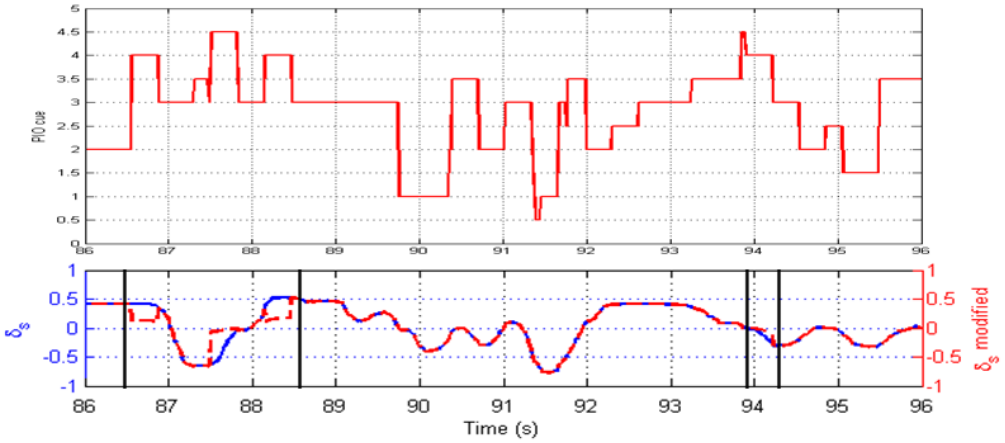

Figure 5.20: Stick input modification after mitigation system for the fourth run of series one of subject B (86s to 96s)

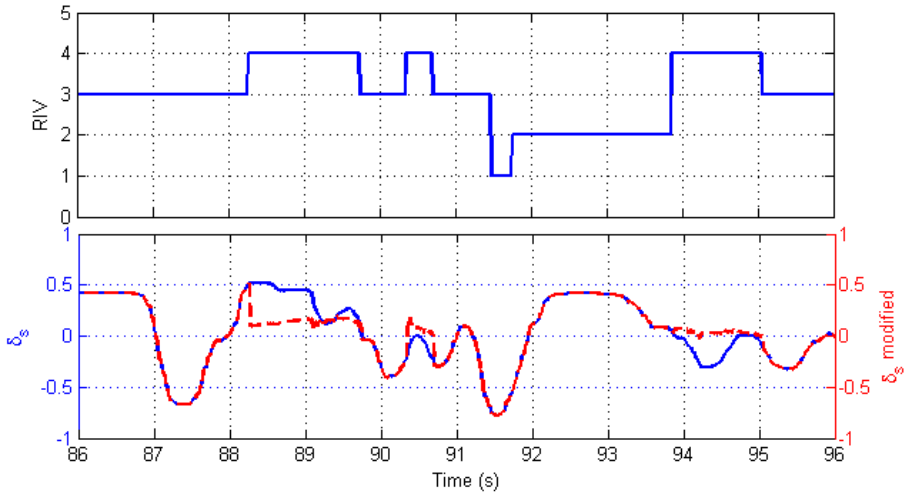

Figure 5.21: Stick input modification after ROVER for the fourth run of series one of subject B (86s to 96s)

Chapter 6

Conclusions and future work

6.1 Summary

The aim of this thesis is to design a PIO detection and mitigation system which consists of a detector based on STFT and ARX model, together with an adaptive controller based mitigation system. It has been realized through the following steps:

1. Review of a synopsis of PIO theory, detection and mitigation methods. After the review, an idea of using the rate of change in crossover frequency as a PIO feature parameter is proposed. This rate of change in crossover frequency indicates the moving trend of pilot during oscillations. A simple scheduled gain controller is selected to form the PIO mitigation system since it will not induce any phase distortion to the input signals.

2. Design control laws to make the aircraft PIO prone. PI controllers are used to place the poles and zeros of the vehicle system to put the vehicle dynamics in different PIO regions according to Bandwidth and Gibson criteria.

3. Design detection system using STFT, ARX and time domain peak-to-peak calculation methods. In the STFT calculator, the signals of pilot control and pitch rate are assumed to be stationary during a time interval of $5.12s$. Thus, the frequency resolution of the STFT is $0.2Hz$. This frequency resolution is high enough to detect the PIO frequencies from $0.2Hz$ to $3.5Hz$. Data overlapping is performed to make the data update every $0.32s$. A Bartlett window is coupled to distinguish the frequency components within the PIO frequency range. The reason for selecting Bartlett window is that it has a relative narrow main lobe. Thus, it can distinguish the PIO frequency components better. A linear ARX model is used to estimate the PVS. Therefore, the rate of change in crossover frequency can be obtained. The reason of using linear ARX model is to improve the real time detection speed without introducing complicated pilot modelling.

4. Design mitigation system using scheduled gain controller. In order to avoid limit

cycle problem, the PIO mitigation system is designed to give a signal to reset the PI integrator to zero when PIO detection is true.

5. Design test tasks and perform piloted tests. The single-loop compensatory system with visual stimulus is used to perform the piloted tests. It is reasonable to do this simplification because the joystick does not have a force feedback and no other motion cues are provided to the pilot. The only visual cue is the compensatory/tracking error displayed on the PFD. It should be noticed that the error signal contains information about error and error rate.

6. Perform system evaluation and comparison with results obtained by implementing ROVER model.

6.2 Conclusions

The value of crossover frequency indicates the effort of pilot operations during oscillations. Nevertheless, the crossover frequency itself cannot provide an indication of changes in pilot aggressiveness during an oscillation. The rate of change in crossover frequency on the other hand, can be used to monitor changes in aggression. The merit of this rate of change detection method is that it focuses on pilot moving trend. The false PIO detection can be reduced by this method. The rate of change is assumed to reflect the trend of the pilot gain during oscillations. The pilot control gain is not high enough during the piloted trials. Thus, only some of the existing test data reflected this assumption, as shown in 5.3.3. More test data are required to further prove it. Besides, the rate of change in crossover frequency during oscillations is related to the value of crossover frequency. The relationship between these two parameters needs to be identified to give more accurate PIO prediction.

The rate of change in the crossover frequency can be obtained by system identification using a linear ARX model in real time. This was shown in 4.1.1. It can be seen that the linear ARX model can represent the PVS system after structure optimization with off-line data. The correlation between the simulation model and the experimental outputs is up to 76%. The crossover frequency can be calculated after PVS identification. The rate of change in crossover frequency can be obtained by dividing the difference of the crossover frequency over the updating time interval.

The STFT method can detect the main oscillatory frequency and phase difference between the signal of pilot input and aircraft states. The tests analysis in 5.3.3 show the detection results. However, the detection results are easily affected by spectrum leakage. Moreover, no boundary noise is added to test the detector's sensitivity against noise.

The real time calculation speed is constrained by the computer and the calculation algorithm. The time error of the detection and mitigation increases if the time resolution of the STFT and ARX model increases. With a time resolution of $0.32s$, there is only a 0.05s error during real time detection. This time lag is acceptable during the PIO detection.

The magnitudes of pilot input and pitch rate can be calculated by time domain peak-to-peak method. However, the peak-to-peak method is sensitive to noise. A low pass filter should be added to filter the input signals.

PIO tendencies can be alleviated by reducing the stick gain with scheduled gains but the gains setting need to be tuned with more PIO test data.

6.3 Future work

1. Program the Matlab PIO detection and mitigation system using C language to improve the real time detection speed.

2. Do more piloted trials to identify the relationship between the value of crossover frequency and the rate of chnage in crossover frequency.

3. Develop experimental tests including combined compensatory and tracking tasks. The reason is that the pilot always performs the combined compensatory and tracking tasks at the same time in real flight, especially in approaching and landing phase. Perform the piloted tests in the Boeing-747 simulator since the simulator can give a more real cockpit visual and control feeling.

4. Add boundary noise to the input signals of PIO detector to identify the detector's sensitivity against noise.

5. Apply wavelet transform method to get the information of main frequency and phase difference. The window length in STFT calculator is fixed during the whole time history. The wavelet transform can adapt its window length according to the signal frequency. It can give more accurate results but requires more complicated calculation.

6. Develop a fuzzy logic PIO indicator to receive PIO feature parameters from the detector and compare the results with those obtained from the weighting function method.

References

[1] Oliver Brieger. Investigating the PIO-susceptibility of the F-4C. Technical Report CO/COA-2000/0004, College of Aeronautics,Cranfield University, June, 2000.

[2] National Research Council. *Aviation safety and pilot control: understanding and preventing unfavorable pilot-vehicle interactions*. Washington, DC, The National Academies Press, 1997.

[3] Airbus. Delivering the future: Airbus global market forecast 2011-2030. *Airbus S.A.S. 31707 Blagnac Cedex, France*, 2011.

[4] R.A. Hess. Multi-axis pilot modelling: Models and methods for wake vortex encounter simulations. *Presentation to WakeNet-3 Europe Safety Workshop*, 2010.

[5] D.G. Mitchell and D.H. Klyde. Identifying a PIO signature- new techniques applied to an old problem. *AIAA Atmospheric Flight Mechanics Conference and Exhibit, Keystone, Colorado, August*, 2006.

[6] D.A. Johnson. *Suppression of Pilot-Induced Oscillation(PIO)*. PhD thesis, Air Force Institute of Technology, Air University, March, 2002.

[7] G.J. Jeram and J.V.R. Prasad. Fuzzy logic detector for aircraft pilot coupling and Pilot-Induced Oscillation (PIO). In *Proceedings of the 59th American Helicopter Society Annual Forum, Phoenix, Arizona, USA*, 2003.

[8] C.J. Cox and C.E. Lewis. Pilot-induced oscillation detection and compensation apparatus and method. *US Patent 5935177*, 1999.

[9] C.J. Cox, C.E. Lewis, and C. Suchomel. A neural network based, real-time algorithm for detection and mitigation of pilot induced oscillations. *2000 IEEE International Conference on Systems, Man & Cyberbetics - "Cyberbetics Evolving to Systems, Humans, Organizations, and their Complex Interactions" , Nashville, Tennessee, USA, October*, 2000.

[10] H. Duda. Effects of rate limiting elements in flight control systems-a new PIO criterion. *In Proceedings of the AIAA Guidance, Navigation and Control Conference and Exhibit, Baltimore, Maryland, August 7-10, 1995.*

[11] Xiaohong Li. Real time prevention of Aircraft-Pilot Coupling using multi-model adaptive control. *AIAA Guidance, Navigation, and Control Conference and Exhibit, San Francisco, California, August*, 2005.

[12] D.H. Klyde, Chiying Liang, and D.J. Alvarez. Mitigating unfavorable pilot interactions with adaptive controllers in the presence of failures/damage. *AIAA Atmospheric Flight Mechanics Conference and Exhibit, Boston, Massachusetts, Portland, Oregon, August*, 2011.

[13] T.J.J. Lombaerts, G.H.N. Looye, Q.P. Chu, and J.A. Mulder. Pseudo control hedging and its application for safe flight envelope protection. *AIAA Guidance, Navigation, and Control Conference and Exhibit, Toronto, Ontario, Canada, August*, 2010.

[14] D.H. Klyde and Chiying Liang. Approach and landing flight evaluation of smart-cue and smart-gain concepts. *AIAA Atmospheric Flight Mechanics Conference and Exhibit, Honolulu, Hawaii, August*, 2008.

[15] Anon. *Military Standard: Flying Qualities of Piloted Aircraft, MIL-STD-1797A*. U.S. Department of Defense, 1990.

[16] D.G. Mitchell and R.H. Hoh. Development of methods and devices to predict and prevent Pilot-Induced Oscillations. Technical Report AFRL-VA-WP-TR-2000-3046, Air Force Research Laboratory, 2000.

[17] D.T. McRuer. Pilot-induced oscillations and human dynamic behavior. Technical Report NASA Contractor Report 4683, National Aeronautics and Space Administration, 1995.

[18] I.L. Ashkenas, H.R. Jex, and D.T. McRuer. Pilot-Induced Oscillations: Their cause and analysis. Technical Report NCR-64-143, National Technical Information Service, US, 1964.

[19] M.M. Lone. Introduction to flight dynamics and control, course notes, presented at the University of Leicester as part of the aircraft navigation and guidance course. 2012.

[20] C. Fielding and P.K. Flux. Non-linearities in flight control systems. *The Aeronautical Journal, Vol. 107, Pages 673-696, November*, 2003.

[21] D.T. McRuer, W.F. Clement, P.M. Thompson, and R.E. Magdaleno. Minimum flying qualities. Volume II: Pilot modeling for flying qualities applications. Technical Report WRDC-TR-89-3125, Wright Research and Development Center, January, 1990.

[22] D.G. Mitchell and D.H. Klyde. A critical examination of PIO prediction criteria. *AIAA Atmospheric Flight Mechanics Conference and Exhibit, Boston, Massachusetts, August*, 1998.

[23] W.J. Norton. Aero-elastic pilot-in-the-loop oscillations. *Flight Vehicle Integration Powel Workshop on Pilot Induced Oscillations*, 1994.

[24] R.E. Bailey and T.J. Bidlack. A quantitative criterion for Pilot-Induced Oscillations - Time domain Neal-Smith criterion. *AIAA Atmospheric Flight Mechanics Conference and Exhibit, San Diego, CA, July 29-31,1996, Technical Papers, Reston, VA, American Institute of Aeronautics and Astronautics*, 1996.

[25] M.V. Cook. Lectures in flying qualities and flight control, Cranfield University. 2012.

[26] L.A. Foringer and D.B. Leggett. An analysis of the Time-domain Neal-Smith criterion. *AIAA Atmospheric Flight Mechanics Conference and Exhibit, Boston, Massachusetts*, 1998.

[27] R.E. Bailey and T.J. Bidlack. Unified Pilot-Induced-Oscillation theory.Volume IV:Time-domain Neal-Smith Criterion. Technical Report WL-TR-96-3031, Wright Laboratory, December, 1995.

[28] J.C. Gibson. *The definition, understanding and design of aircraft handling qualities*. Delft University Press, 1997.

[29] E.J. Field, K.F. Rossitto, and D.G. Mitchell. Landing approach flying qualities criteria for active control transport aircraft. *Active Control Technology for Enhanced Performance Operational Capabilities of Military Aircraft, Land Vehicles and Sea Vehicles, RTO-MP-051, Paper No. 33, June*, 2001.

[30] H.A. Mooij. *Criteria for low-speed longitudinal handling qualities of transport aircraft with closed-loop flight control systems*. Publisher: Dordrecht, Boston, M. Nijhoff for Nationaal Lucht- en Ruimtevaartlaboratorium, National Aerospace Laboratory, NLR, The Netherlands, 1985.

[31] J.E. Gautrey. *Flying qualities and flight control system design for a fly-by-wire transport aircraft*. PhD thesis, Cranfield University, March, 1998.

[32] D.G. Mitchell, A.J. Arencibia, and S. Munoz. Real-time detection of pilot-induced oscillations. *AIAA Atmospheric Flight Mechanics Conference and Exhibit, Providence, Rhode Island, August*, 2004.

[33] D.G. Mitchell and D.H. Klyde. Testing for pilot-induced oscillations. *AIAA Atmospheric Flight Mechanics Conference and Exhibit, San Francisco, California, August*, 2005.

[34] J.G. Hanley. A comparison of nonlinear algorithms to prevent pilot-induced oscillations caused by actuator rate limiting. *Master thesis, Air Force Institute of Technology, Air University, Wright-Patterson Air Force Base, Ohio, March*, 2003.

[35] G.P. Gilbreath. Prediction of Pilot-Induced Oscillations(PIO) due to actuator rate limiting using the Open-Loop Onset Point(OLOP) criterion. *Master thesis, Air Force Institute of Technology, Air University, Wright-Patterson Air Force Base, Ohio, March*, 2001.

[36] P.M. Thompson, D.H. Klyde, and E.N. Bachelder. Development of wavelet-based techniques for detecting loss of control. *AIAA Atmospheric Flight Mechanics Conference and Exhibit, Providence, Rhode Island*, 2004.

[37] N. Raimbault and P. Fabre. Probabilistic neural detector of Pilot-Induced Oscillations(PIO). *AIAA Guidance, Navigation and Control Conference and Exhibit, Montreal, Canada, August*, 2001.

[38] R.A. Hess and P.W. Stout. Assessing aircraft susceptibility to nonlinear Aircraft-Pilot Coupling/Pilot-Induced Oscillations. *Journal of Guidance, Control, and Dynamics, Vol.21, No.6, November-December*, 1998.

[39] M.R. Anderson. Pilot-Induced Oscillations involving multiple nonlinearities. *Journal of Guidance, Control, and Dynamics, Vol.21, No.5, Pages 786-791, September-October*, 1998.

[40] Meng Jie, Haojun Xu, and Jiankang Zhang. A comparison of rate-limit phase compensator to prevent category II pilot induced oscillations. *Proceedings of the 8th World Congress on Intelligent Control and Automation, Jinan, China, July*, 2010.

[41] A.V. Oppenheim, R.W. Schafer, and J.R. Buck. *Discrete-time signal processing*. Publisher: Prentice-Hall, Inc. Upper Saddle River, NJ, USA, second edition, 1999.

[42] E.A. Morelli. High accuracy evaluation of the finite Fourier transform using sampled data. *NASA Technical Memorandum 110340, National Aeronautics and Space Administration, June*, 1997.

[43] P.M.T. Zaal, D.M. Pool, M. Mulder, and M.M. van Paassen. New types of target inputs for multi-modal pilot model identification. *AIAA Modeling and Simulation Technologies Conference and Exhibit, Honolulu, Hawaii, August*, 2008.

[44] D.T. McRuer and E.S. Krendel. Dynamic response of human operators. Technical Report WADC 56-524, Wright Air Development Center, Air Research and Development Command, United States Air Force, 1957.

[45] D.T. McRuer and E.S. Krendel. Mathematical models of human pilot behavior. Technical Report AGARD-AG-188, Advisory Group for Aerospace Research and Development, 1974.

[46] D.T. McRuer and H.R. Jex. A review of quasi-linear pilot models. *IEEE Transactions on Human Factors in Electronics, Vol.8, No.3, Pages 231-249, September*, 1967.

[47] M.M. Lone and A.K. Cooke. Effects of nonlinear flight control system elements on aircraft manual control. Technical Report CU/COA-2011/01, College of Aeronautics, Cranfield University, September, 2011.

[48] D.G. Mitchell, B.A. Kish, and J.S. Seo. A flight investigation of pilot-induced oscillation due to rate limiting. *IEEE 1998 Aerospace Conference Proceedings, Paper 270, Snowmass, CO, March*, 1998.

[49] N. Ruseno. Effects of electronic flight control systems nonlinearities on manual control. *Msc thesis, School of Engineering, Cranfield University, June*, 2011.

[50] M.M. Lone, N. Ruseno, and A.K. Cooke. Towards understanding effects of nonlinear flight control system elements on inexperienced pilots. *Royal Aeronautical Society*, 2012.

[51] R.K. Heffley and W.F. Jewell. Aircraft handling qualities data. Technical Report NASA CR-2144, National Aeronautics and Space Administration, Washingtong, DC, 1972.

[52] D.P. Davies. Handling the big jets. *Civil Aviation Authority*, 2006.

[53] L. Rundqwist. *Anti-reset windup for PID controllers*. PhD thesis, Lund Institute of Technology, 1991.

[54] C. Lohner, M. Mulder, and R. van Paassen. Multi-loop identification of pilot central visual and vestibular motion perception processes. *AIAA Modeling and Simulation Technologies Conference and Exhibit, SanFrancisco, California, August*, 2005.

[55] Yingchun Shen. Effect of flight control system mode switching on pilot dynamics. *Msc thesis, School of Engineering, Cranfield University, January*, 2012.

[56] M.V. Cook. *Flight dynamics principles*. Elsevier Ltd., second edition, 2007.

[57] F. Amato, R. Iervolino, M. Pandit, S. Scala, and L. Verde. Analysis of pilot-in-the-loop oscillations due to position and rate saturations. *Proceedings of the 39th IEEE Conference on Decision and Control*, 2000.

Appendix A

Review test examples

A1. ROVER example

The test results of using ROVER during a tracking task in Boeing-747 model. The thresholds of the four flags were pitch rate of $5deg/s$, 10% stick deflection, $60deg$ phase delay and $1{\sim}8$ rad/s frequency of pitch rate.

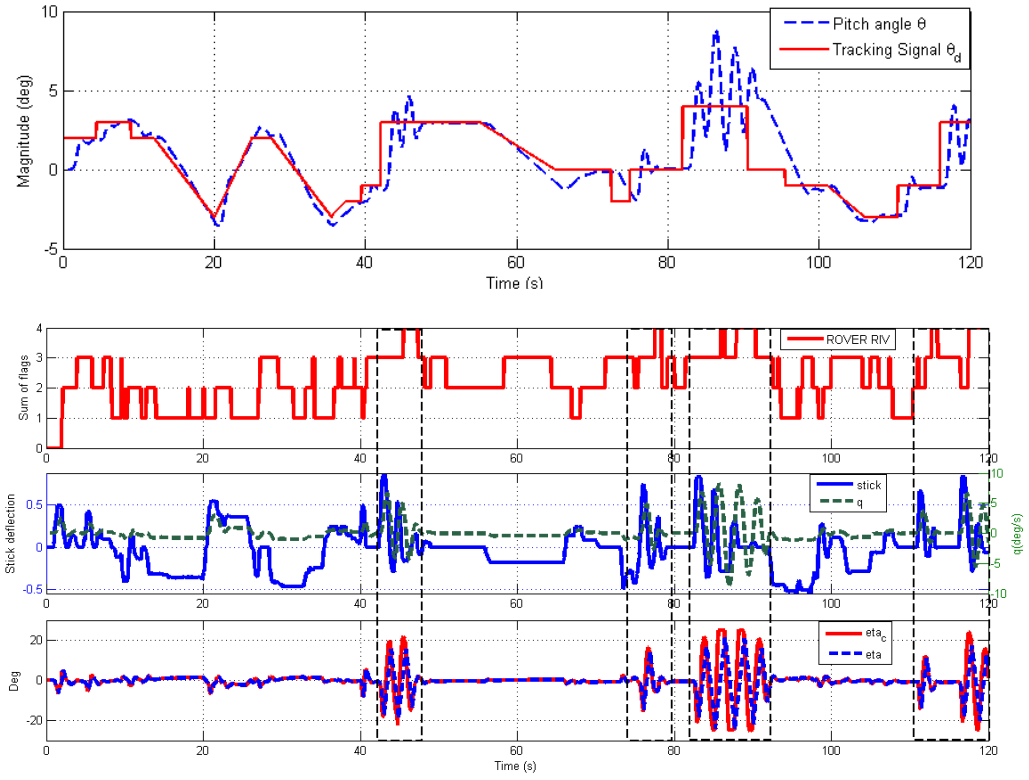

Figure A.1: ROVER detection example

A2. Fuzzy logic detector example

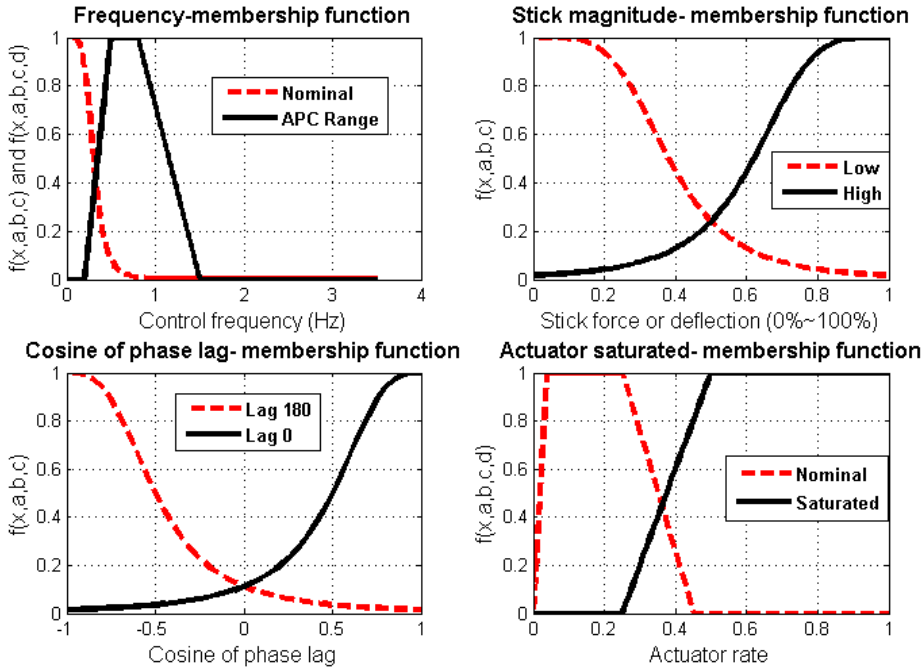

Figure A.2: Fuzzy variables descript membership function

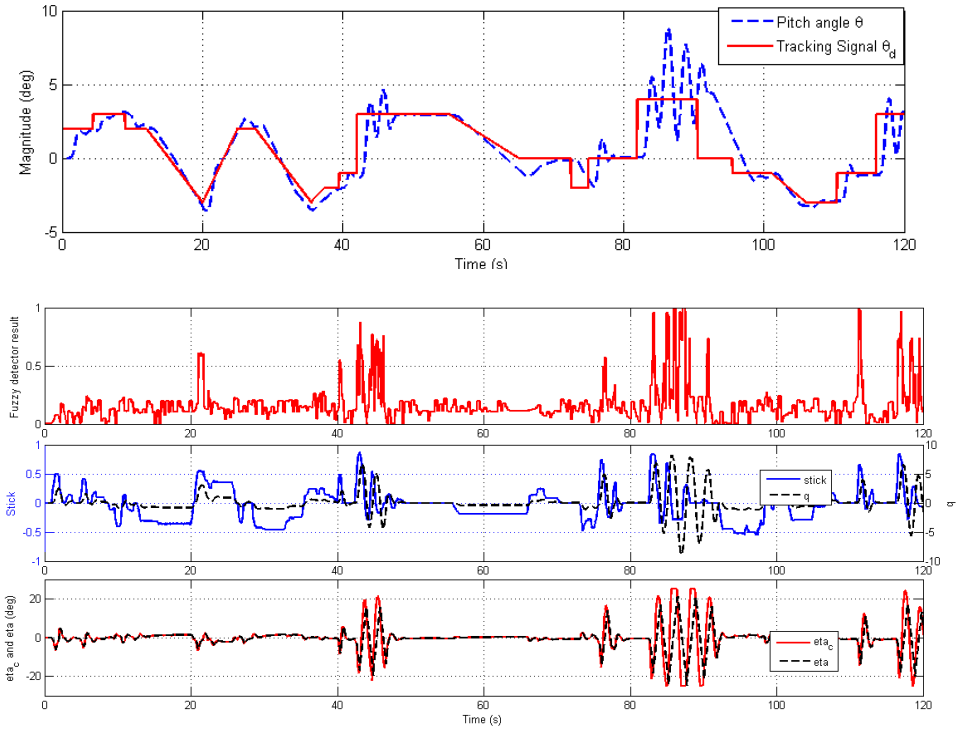

Figure A.3: Example of fuzzy logic detection for Boeing-747 model

A3. OLOP detector example

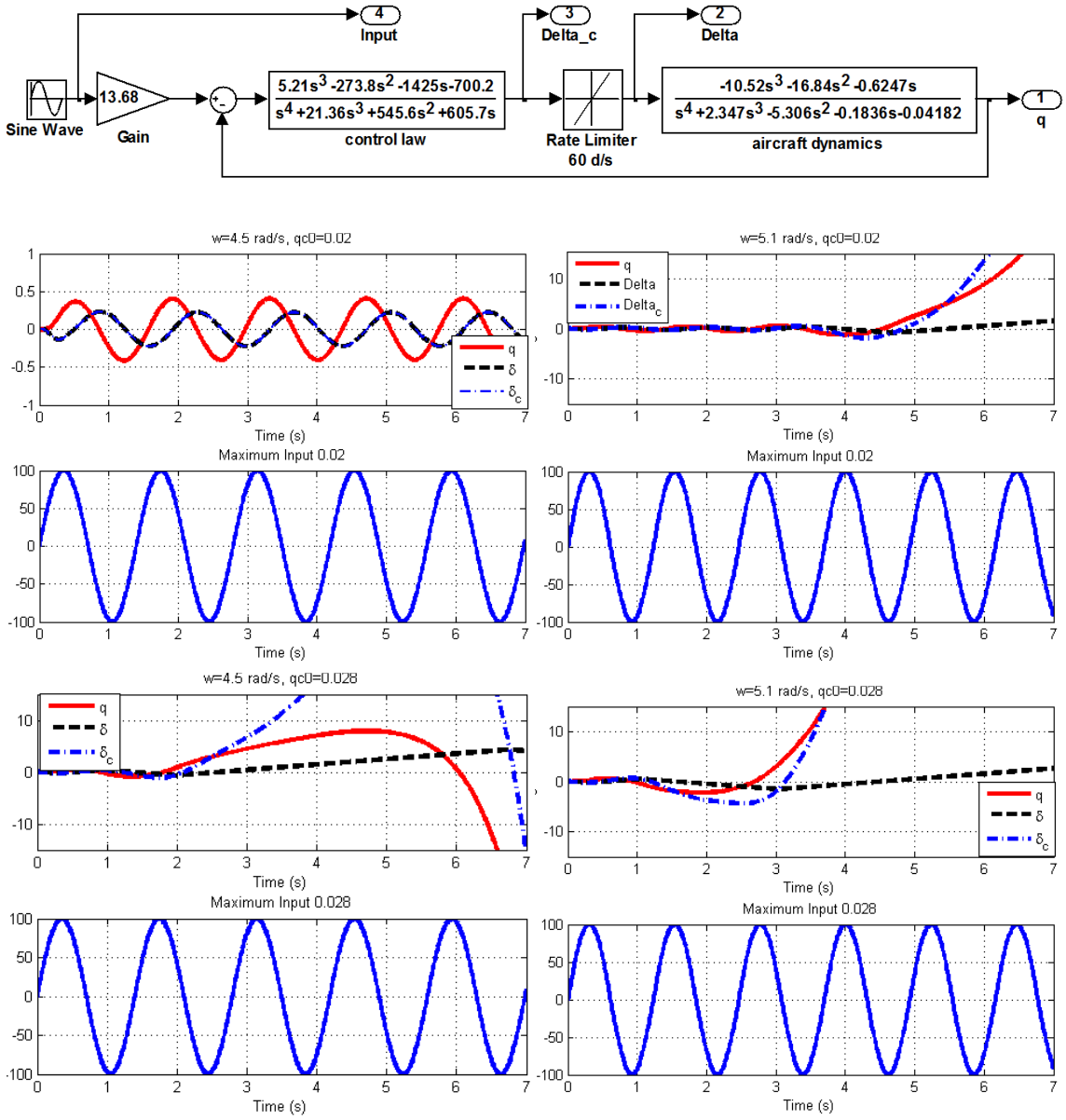

Figure A.4: OLOP test model and test results

A4. System identification case study

One system estimation study case for the full order longitudinal model of F-4C linearized at $0.8M$ at sea level[51] is performed using the FFT and ARX function in Matlab. The transfer function of the test model is described by Eq. A.1.

$$\frac{\theta(s)}{\delta_e(s)} = \frac{-32.2(s+0.0162)(s+1.46)}{(s^2-0.039s+0.0031)(s^2+3.4898s+19.7136)} \tag{A.1}$$

The input of the system is a sum-of-sine signal. The parameters of the signal are shown

in Tab. A.1 with random phases. The inputs of the ARX model are disturbance signal and the system output signal. FCM method was also applied by calculating the Fourier coefficients to make a comparison. The result is shown in Fig. A.5. It can be seen that the ARX model and Fourier coefficients fit the real system quite well. The system here was known, so it was easy to choose proper numerator and denominator orders of the ARX model to get good results for the system identification. The zeros and poles order of the ARX model were [43] in this test. System identification results would be affected by the orders of ARX model. Thus, before real time detection, the ARX orders have to be optimized to obtain reasonable system identification result because the system is unknown. It is clear from this case that one way to perform the ARX model optimization is to use FCM by using a predetermined disturbance signal.

Table A.1: parameters of ARX model test forcing function

k	*nd*	*ωd (rad/s)*	*Ad (deg)*	*k*	*nd*	*ωd (rad/s)*	*Ad (deg)*
1	5	0.383	1	9	171	13.116	0.212
2	11	0.844	1	10	226	17.334	0.201
3	23	1.764	1	11	293	22.456	0.308
4	37	2.838	0.949	12	367	28.123	0.505
5	51	3.912	0.635	13	468	35.875	0.385
6	71	5.446	0.483	14	558	42.784	0.2
7	101	7.747	0.352	15	664	50.962	0.2
8	137	10.508	0.263				

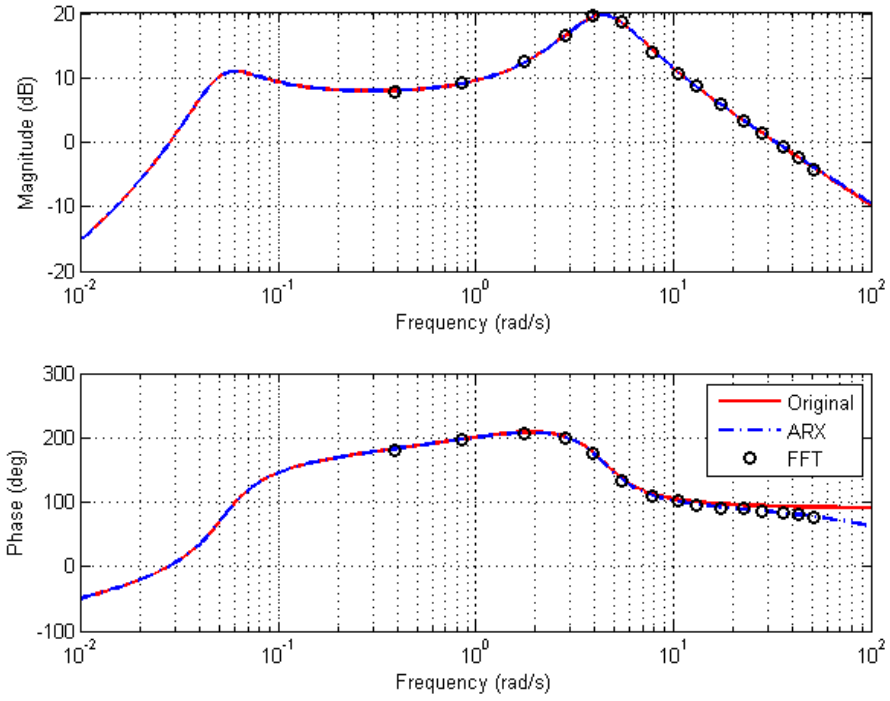

Figure A.5: Disturbance open loop full order system estimation using ARX and FCM

Appendix B

Boeing-747 model

The following equations show the longitudinal flight dynamics of quasi-linear B747 model linearized at the airspeed of $0.5M$ and at the altitude of $20000ft$. The scheduling parameters ρ described in 3.2$\sim$3.4 are frozen at the state of $0.5M$ and $20000ft$. The linearized aircraft model is shown in B.1.

$$\begin{bmatrix} \dot{u} \\ \dot{w} \\ \dot{q} \\ \dot{\theta} \end{bmatrix} = \begin{bmatrix} -0.0025 & 0.0782 & -72.4958 & -31.8989 \\ -0.0690 & -0.4399 & 563.1382 & -3.8650 \\ 0.0003 & -0.0016 & -0.4914 & 0.0005 \\ 0 & 0 & 1 & 0 \end{bmatrix} \begin{bmatrix} u \\ w \\ q \\ \theta \end{bmatrix} + \begin{bmatrix} 2.02 & 0.0001 \\ -17.1696 & 0 \\ -1.0879 & 0 \\ 0 & 0 \end{bmatrix} \begin{bmatrix} \delta_e \\ \delta_\tau \end{bmatrix} \tag{B.1}$$

$$\begin{bmatrix} u \\ w \\ q \\ \theta \\ a_z \\ a_{z_p} \\ C^* \\ \dot{h} \\ \dot{h}_p \end{bmatrix} = \begin{bmatrix} 1 & 0 & 0 & 0 \\ 0 & 1 & 0 & 0 \\ 0 & 0 & 1 & 0 \\ 0 & 0 & 0 & 1 \\ -0.0690 & -0.4399 & 8.8411 & -0.0607 \\ -0.0905 & -0.3017 & 50.1181 & -0.1013 \\ -0.0905 & -0.3017 & 47.1181 & -0.1013 \\ 0.1184 & -0.9930 & 0 & 558.2250 \\ 0.1184 & -0.9930 & 83.4089 & 558.2250 \end{bmatrix} \begin{bmatrix} u \\ w \\ q \\ \theta \end{bmatrix} + \begin{bmatrix} 0 & 0 \\ 0 & 0 \\ 0 & 0 \\ 0 & 0 \\ -17.1696 & 0 \\ 74.2102 & 0 \\ 74.2102 & 0 \\ 0 & 0 \\ 0 & 0 \end{bmatrix} \begin{bmatrix} \delta_e \\ \delta_\tau \end{bmatrix} \tag{B.2}$$

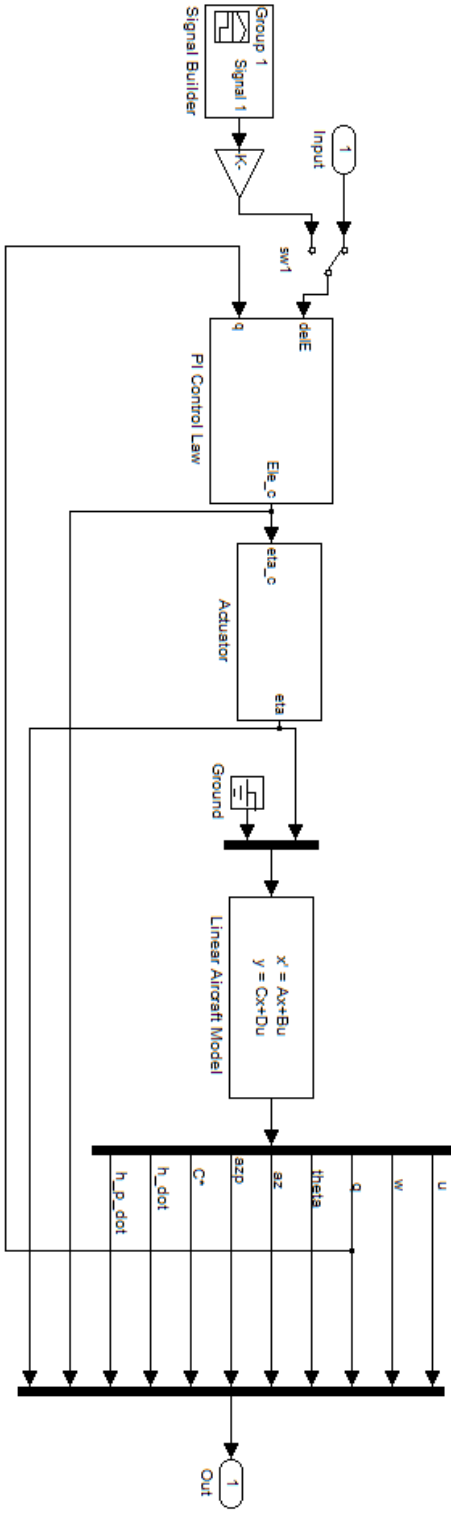

Figure B.1: Linear Boeing-747 aircraft model

Appendix C

Limit cycle analysis

It can be seen from 3.13 that the rate-limiting signal has fully developed to triangle wave during the limit cycle. A single input sinusoid describing function was used to analyze the influence of the rate-limiting. The describing function for this rate-limiting can be described by Eq. C.1 and the saturation can be described by Eq. C.2[57]. To simplify the analysis, the saturation and rate-limiting were separated. As can be seen in Fig. C.1, the control law transfer function can be moved behind the nonlinearities since it is linear. Use the describing function to describe the nonlinearities and solve the Eq.C.3, the limit cycle point can be predicted by the intersection of the $G_c(j\omega)G_c(j\omega)$ and $\frac{-1}{NL(j\omega)}$ in the Nyquist chart, as shown in the Fig. C.2. The input δ_s varied from 0.1, 0.3, 0.5, 0.7, 0.9 to 1, the limit cycle frequency caused by the rate-limiting decreased from $9.02rad/s$ to $6.523rad/s$. The saturation has two intersection with the system transfer function, one is at frequency $0.1rad/s$, the relevant input amplitude is $0.5rad$. Another one is at frequency $16.6rad/s$, the relevant input amplitude is $0.05rad$. This limit cycle point will not triggered as the input frequency is too high. The actual limit cycle frequency is $1.8rad/s$. This may caused by the rate-limiting and saturation together. Detailed analysis of this limit cycle problem is beyond the scope of this thesis. In order to avoid the limit cycle problem, the integrator will be reset to initial state When the PIO detector detects the oscillation.

$$N_{RL}(j\omega, A) = \frac{4R}{\pi A\omega} e^{-j\cos^{-1}(\frac{\pi R}{2A\omega})} \qquad \omega \geq 1.862\frac{R}{A} \tag{C.1}$$

where A is the maximum input amplitude, R is the rate limit.

$$N(U) = \begin{cases} k & U \leq \frac{M}{k} \\ \frac{2k}{\pi}\left[\arcsin(\frac{M}{kU}) + (\frac{M}{kU})\sqrt{1-\left(\frac{M}{kU}\right)^2}\right] & U > \frac{M}{k} \end{cases} \tag{C.2}$$

where U is the input, M is the saturation threshold and k is the slope.

$$G_c(j\omega)G_c(j\omega)NL(j\omega) + 1 = 0 \tag{C.3}$$

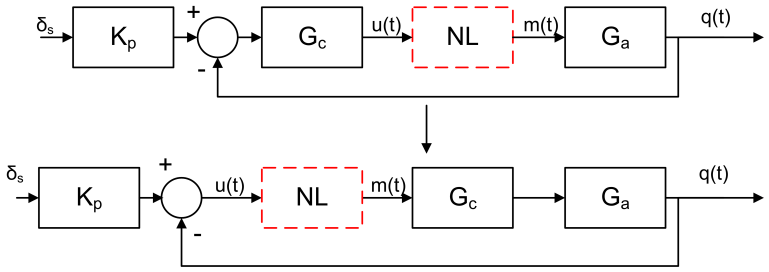

Figure C.1: The nonlinear actuator rate limiting and saturation

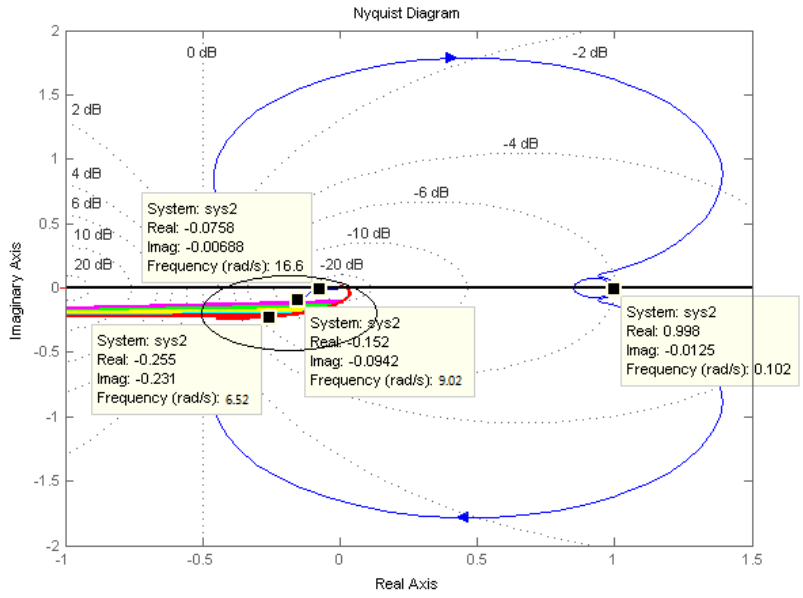

Figure C.2: The describing function tests of rate-limiting and saturation

Appendix D

ARX structure optimization results

The following figures show the ARX structure optimization results of runs number *3, 4, 5*.

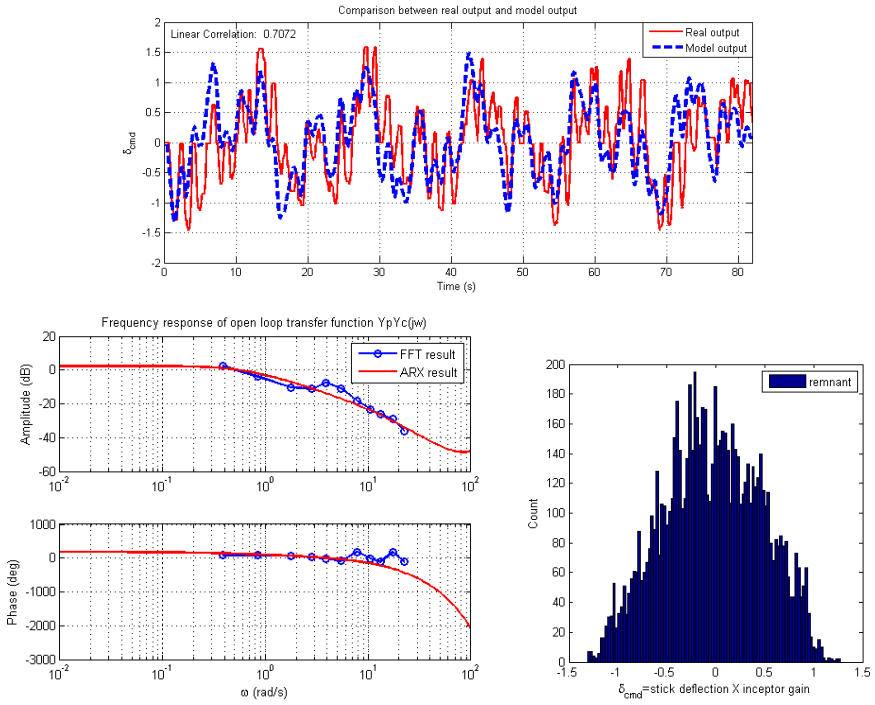

Figure D.1: ARX structure optimization Run No.3

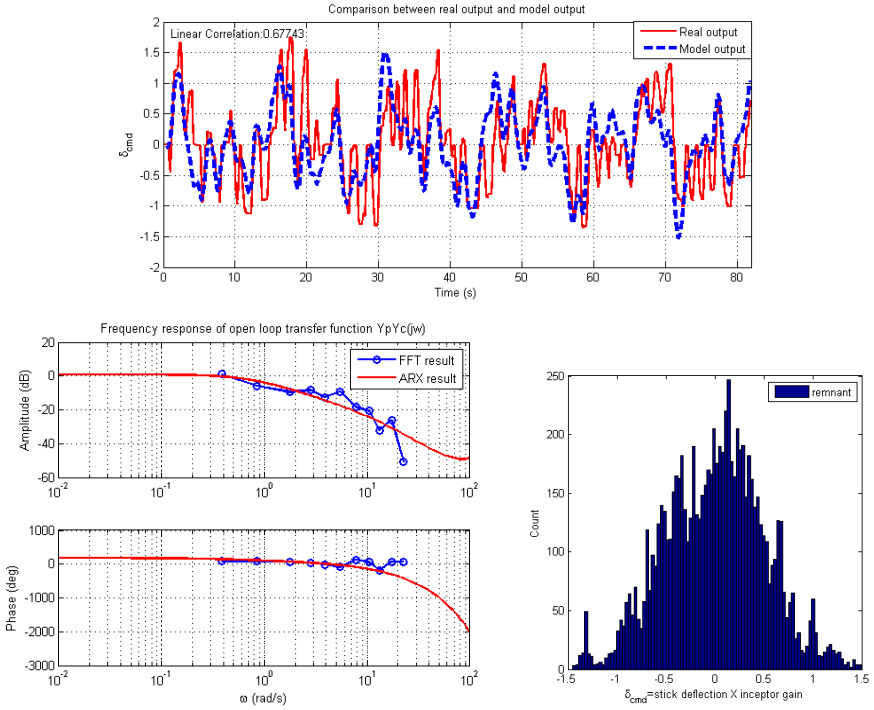

Figure D.2: ARX structure optimization Run No.4

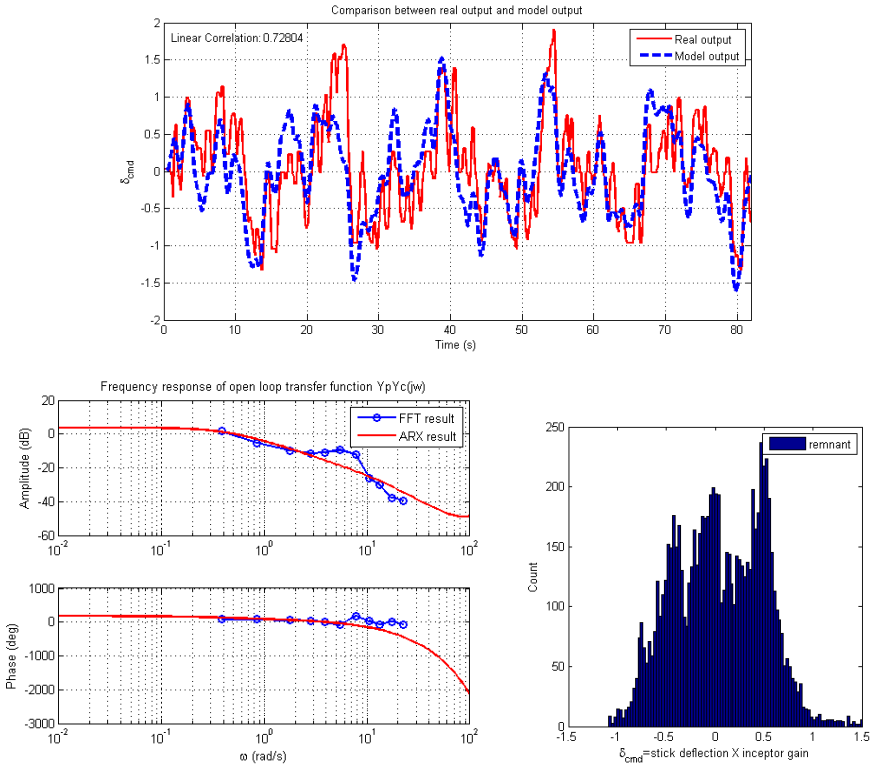

Figure D.3: ARX structure optimization Run No.5

Appendix E

Experiment data

E1. Tracking training data

Subject 1	37 deg			30 deg			25 deg		
	Run No.	Pilot Rating	error	Run No.	Pilot Rating	error	Run No.	Pilot Rating	error
Without Rover	1	7	4.165	5	3	0.74	9	3	0.797
ROVER(PA=70)	2	10	42.98	6	10	37.68	10	5	1.219
ROVER(PA=60)	3	5	1.693	7	8	2.66	11	2	0.8
ROVER(PA=45)	4	10	40.34	8	6	1.08	12	7	2.958
Subject 2	37 deg			30 deg			25 deg		
	Run No.	Pilot Rating	error	Run No.	Pilot Rating	error	Run No.	Pilot Rating	error
Without Rover	1	5	2.127	5	10	38.88	9	3	0.984
ROVER(PA=70)	2	10	45.64	6	8	3.29	10	5	2.469
ROVER(PA=60)	3	4	1.63	7	5	2.474	11	4	1.51
ROVER(PA=45)	4	4	1.634	8	4	1.609	12	6	2.774

Figure E.1: Evaluation results of tracking training

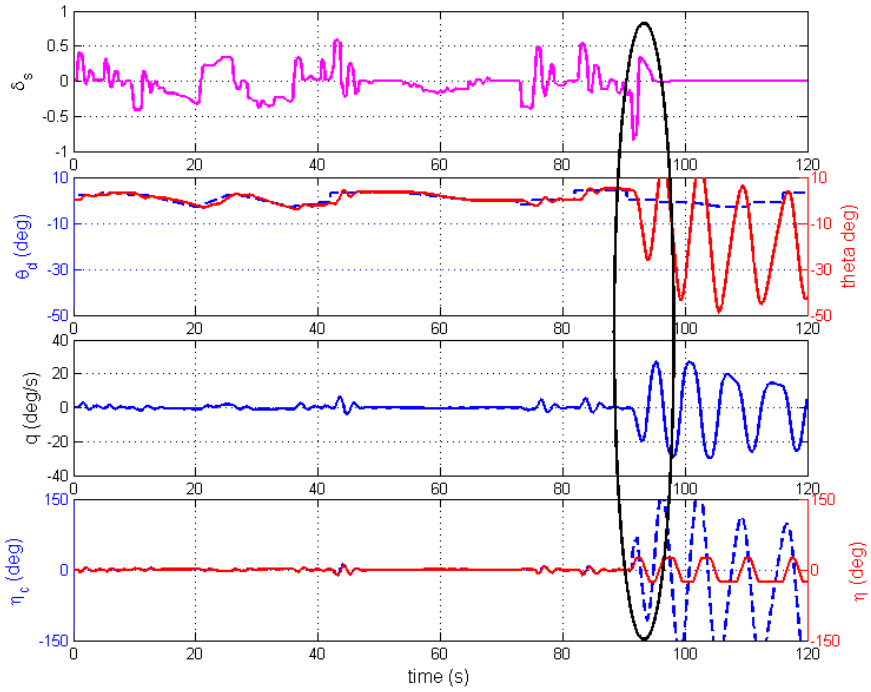

Figure E.2: Time history plot - the second run of subject 1 in tracking training task

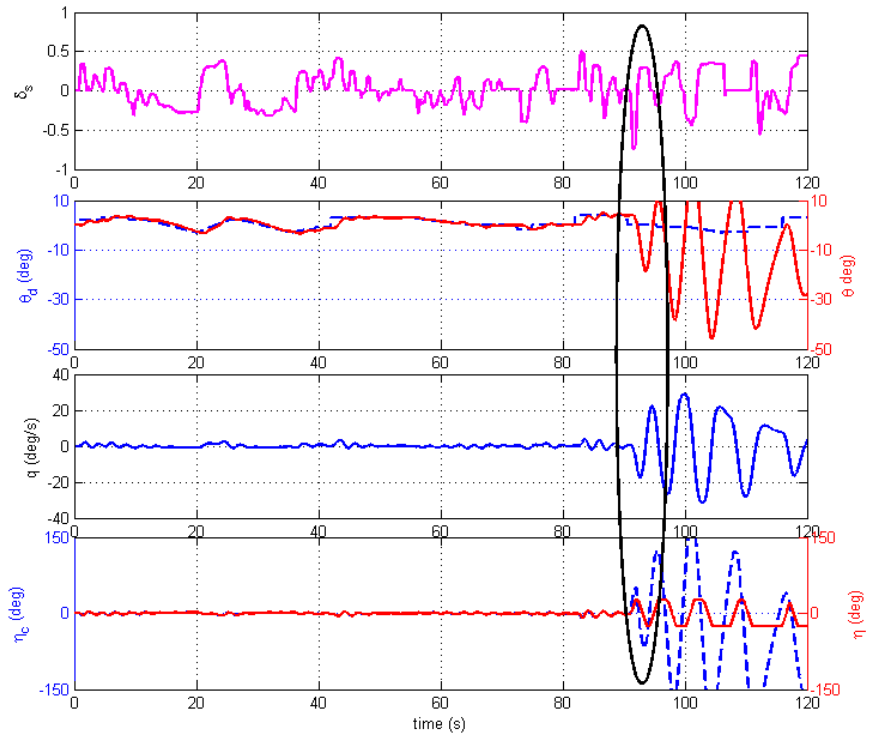

Figure E.3: Time history plot - the second run of subject 2 in tracking training task

E2. Piloted trials questionnaire

Rating Information and Comment Card

The objective of this questionnaire is to collect information concerning your flight experience. This information will be used only for experimental purpose. Information for all subject pilots will be reported in summary form only. No information that identifies the training school and specific pilots will be released.

Personal Information: (Subject pilot No._____)

Name : _____ Age : _____ Gender : M / F

Flying hours : _____ Aircraft Types : _____

Test comments:

How is the handling quality of the system during tracking tasks? Please use the ratings suggested to answer to each run:

Test		Run No.	Cooper-Harper Rating	PIO Rating	RMS (tracking error)	RMS (Stick input)
Compensatory task		1	\	\		
		2	\	\		
		3	\	\		
		4	\	\		
		5	\	\		
Tracking task	Serial A	1				
		2				
		3				
		4				
	Serial B	1				
		2				
		3				
		4				
	Serial C	1				
		2				
		3				
		4				

Figure E.4: Pilot trials questionnaire

E3. Pilot tracking data - detection results and $\frac{d\omega_c}{dt}$

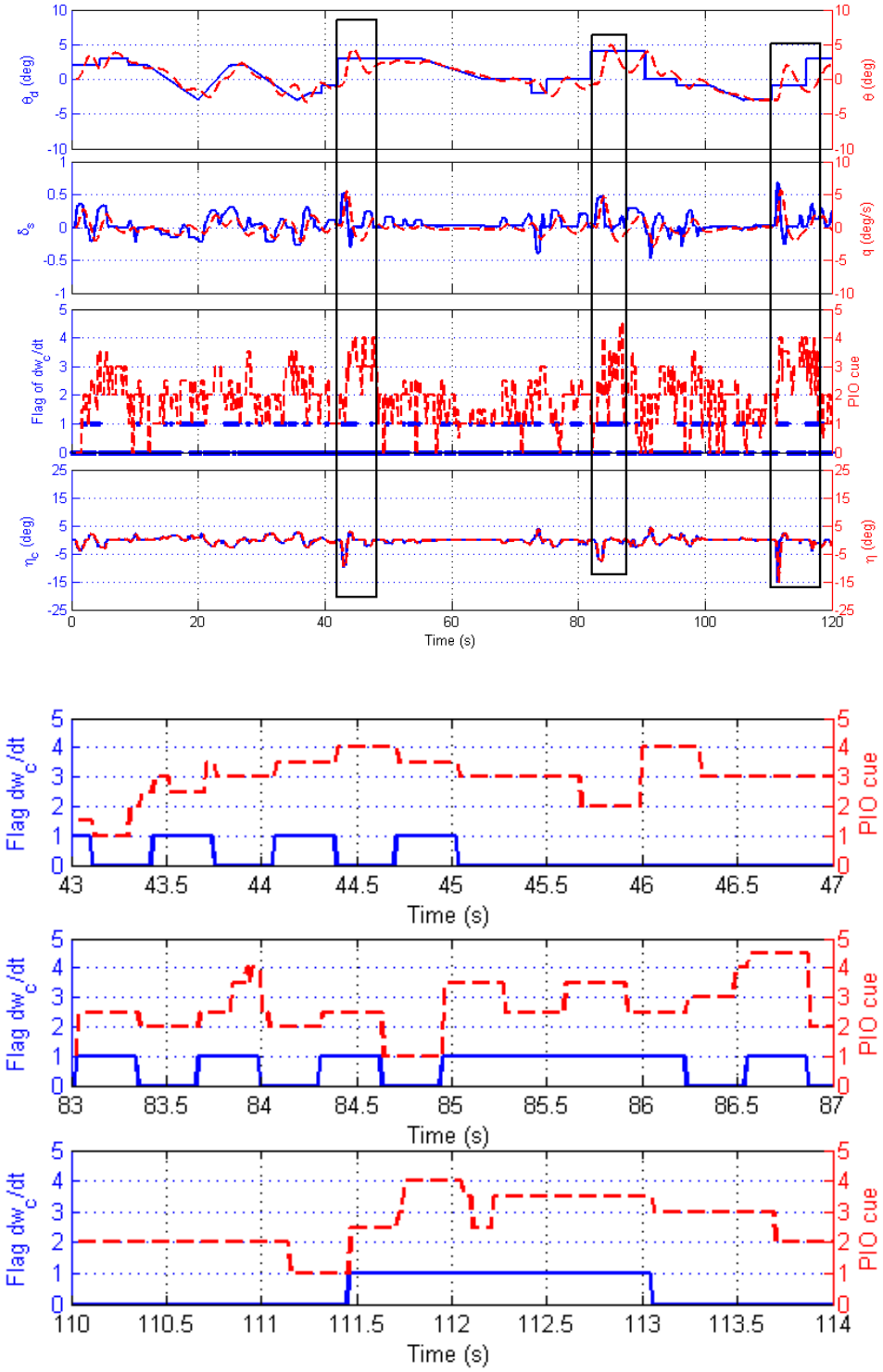

Figure E.5: Relationship between PIO events and the rate of change in crossover frequency - the fourth run(with PIO cue and mitigation) of subject B

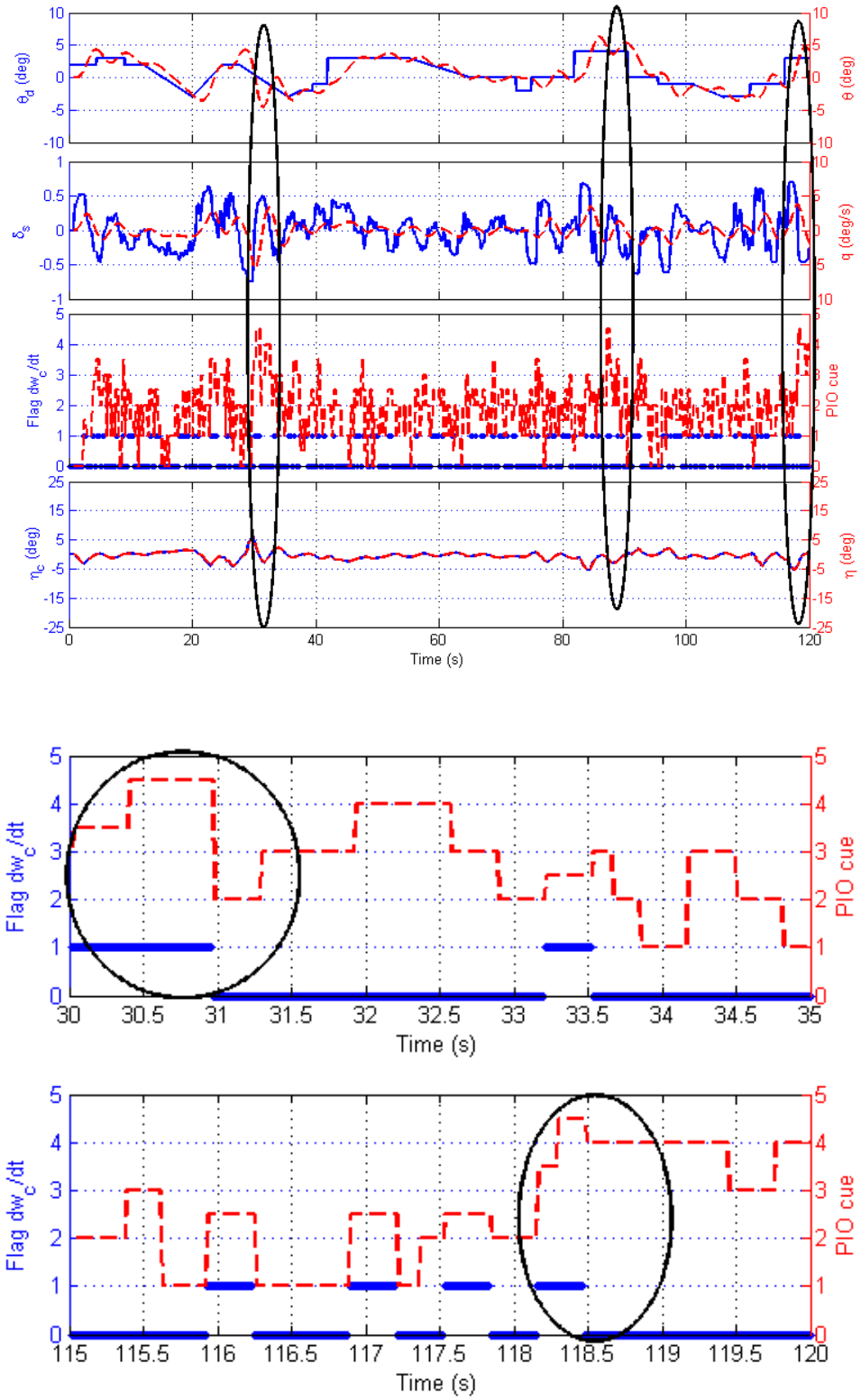

Figure E.6: Relationship between PIO events and the rate of change in crossover frequency - the third run (with PIO cue) of subject C

E4. Pilot tracking data - detection results compared with ROVER

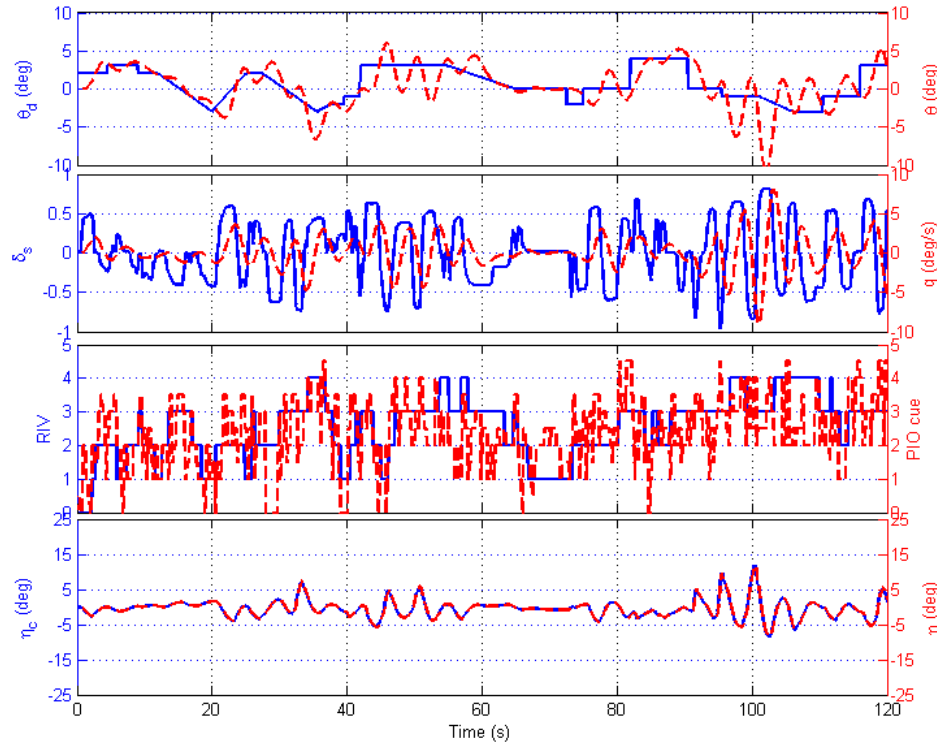

Figure E.7: The third run of subject B(No PIO cue)

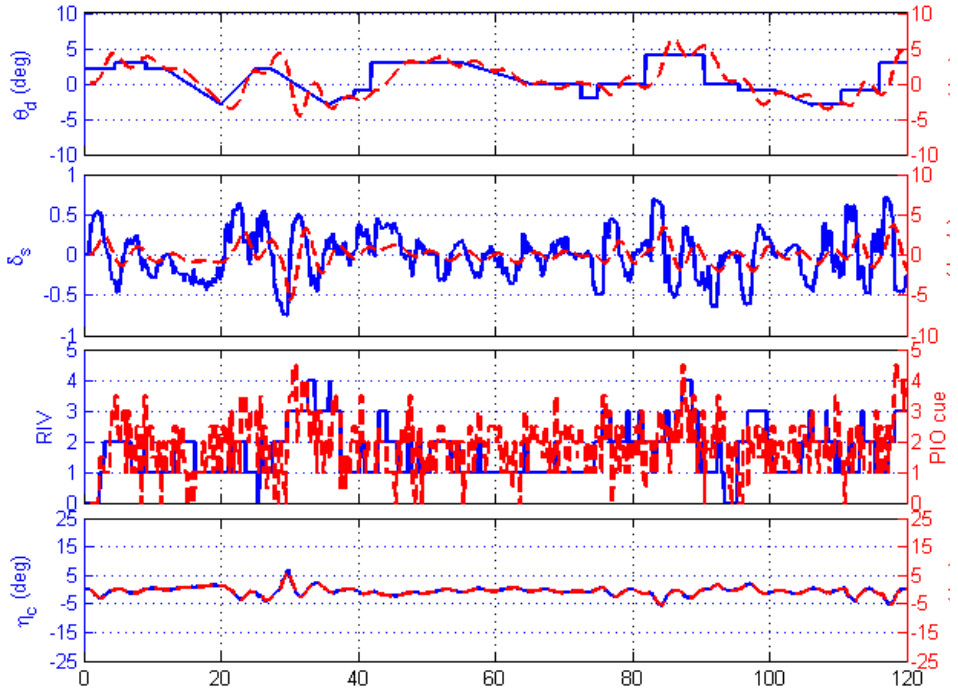

Figure E.8: The third run of subject D(No PIO cue)

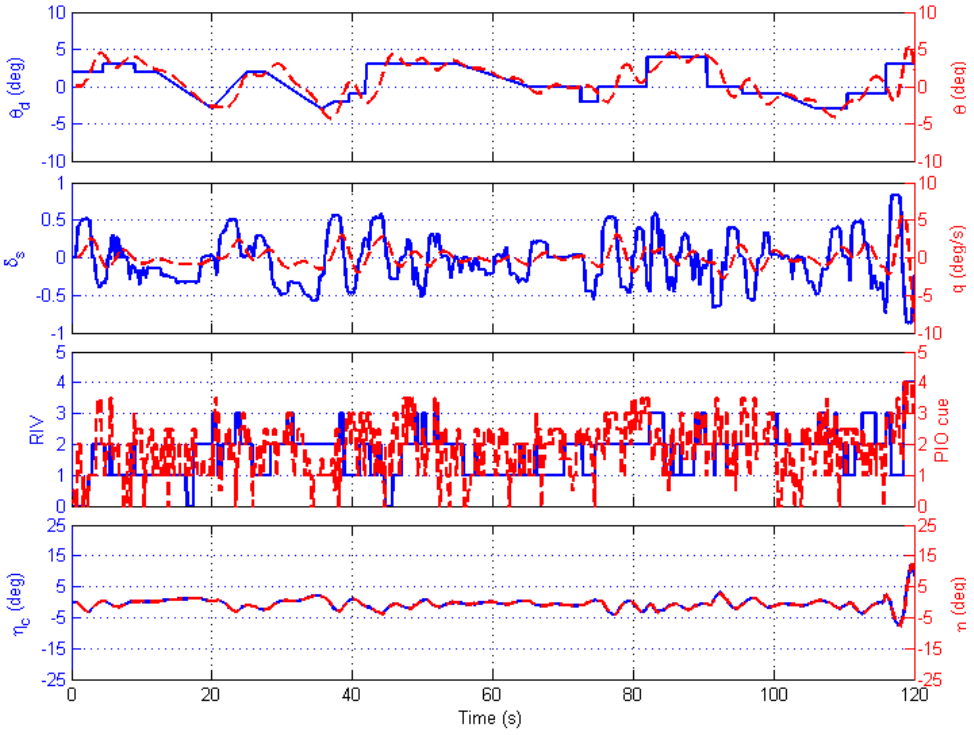

Figure E.9: The third run of subject B(PIO cue)

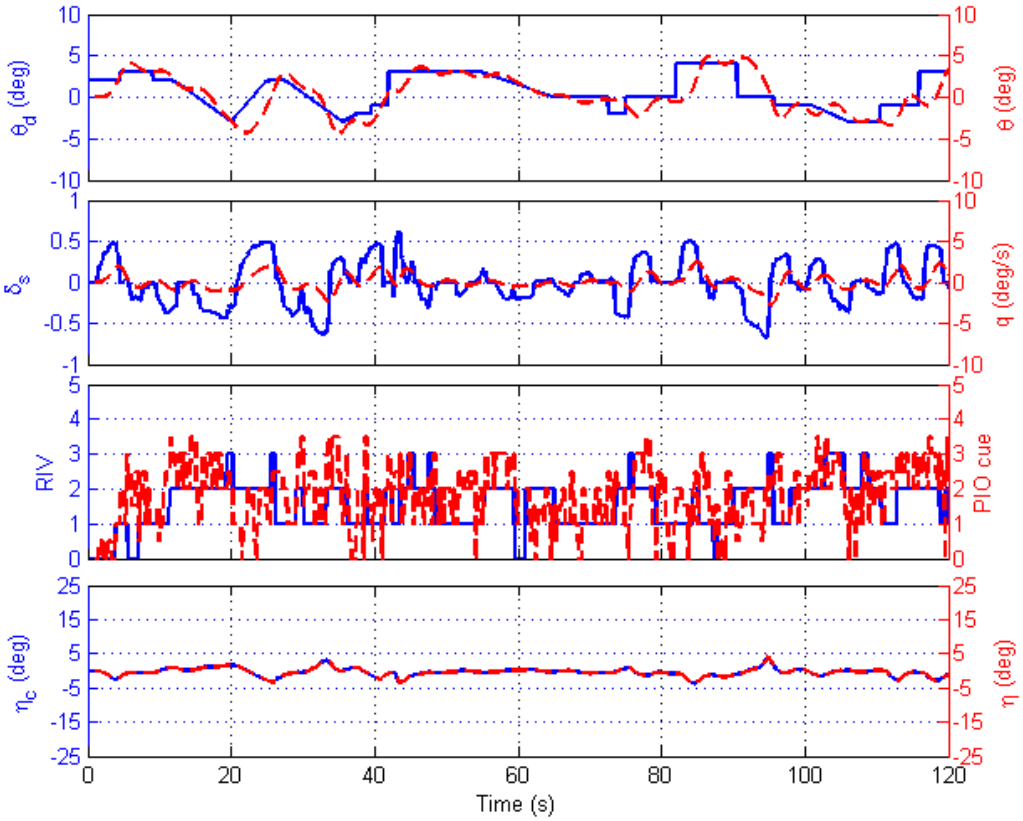

Figure E.10: The third run of subject D(PIO cue)

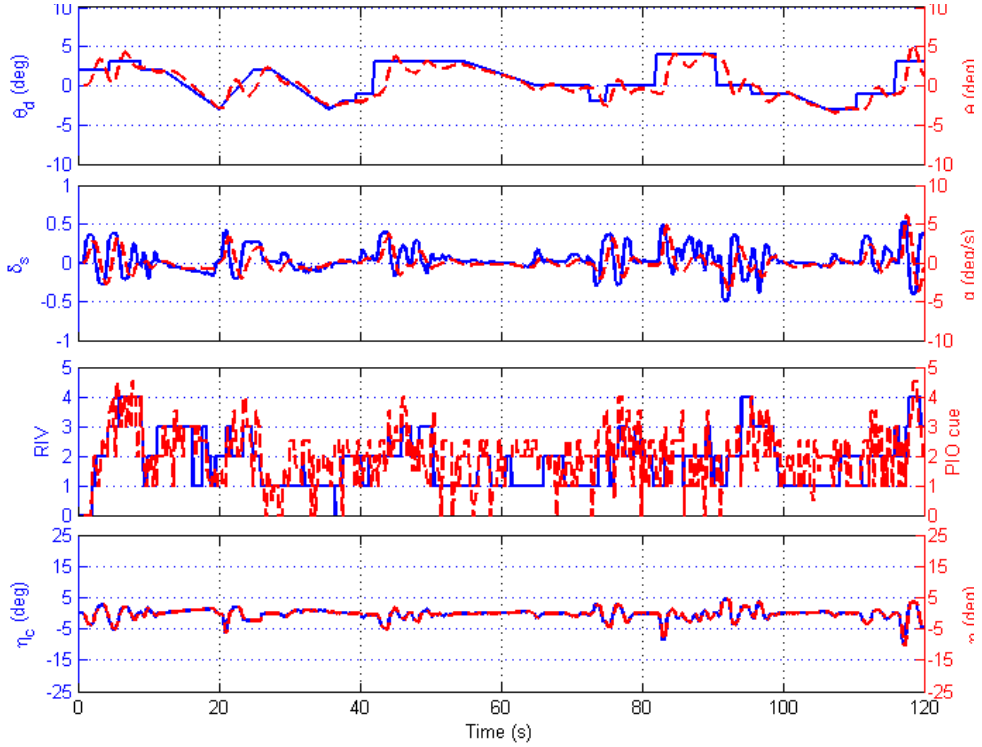

Figure E.11: The fourth run of subject B(PIO cue)

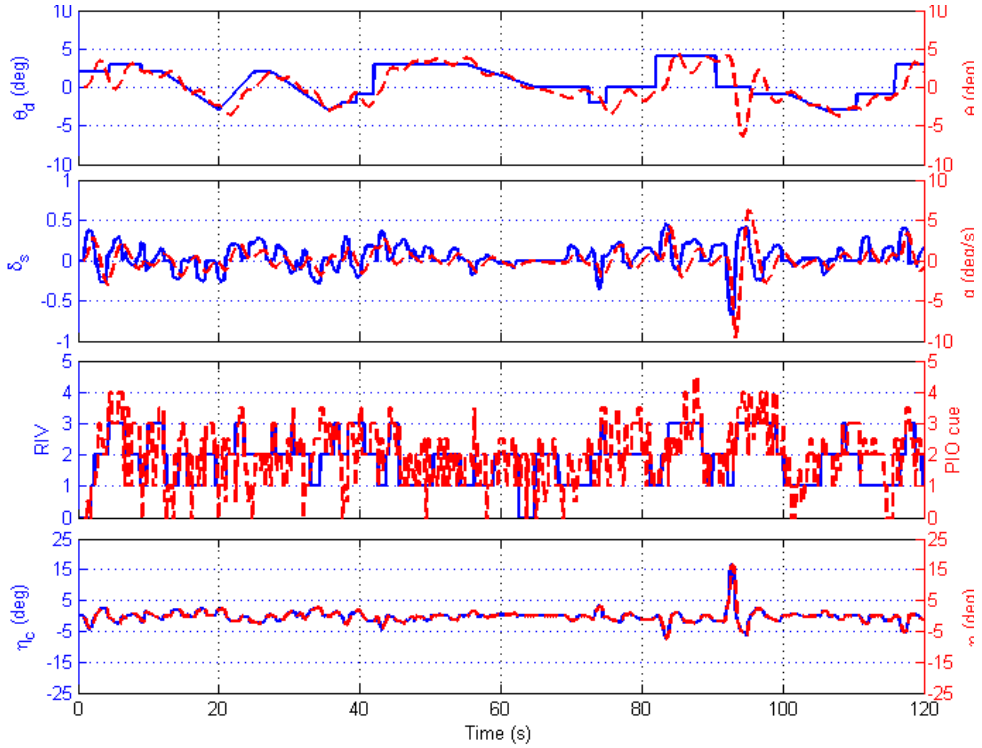

Figure E.12: The fourth run of subject D(PIO cue)